# EARTH OBSERVATION FOR QUANTIFYING ECOHYDROLOGICAL FLUXES AND INTER-RELATIONS:

## A REGIONAL CASE – THE KONYA CLOSED BASIN, TURKEY

Mustafa Gökmen

**Examining committee:**

| | |
|---|---|
| Prof.dr. A. Verhoef | University of Reading |
| Prof.dr. M. Menenti | Delft University of Technology |
| Assoc. Prof. O. L. Sen | Istanbul Technical University |
| Prof. Dr. V.G. Jetten | University of Twente |
| Prof. dr. Z. Su | University of Twente |

Paranymphs:

| | |
|---|---|
| Mireia Romaguera | University of Twente |
| Tolga Görüm | University of Twente |

ITC dissertation number 238
ITC, P.O. Box 217, 7500 AE Enschede, The Netherlands

ISBN 978-90-6164-366-1
Cover designed by Mustafa Gökmen (MODIS and LANDSAT images of NASA were used in the in the front cover)
Printed by ITC Printing Department


# EARTH OBSERVATION FOR QUANTIFYING ECOHYDROLOGICAL FLUXES AND INTER-RELATIONS:
## A REGIONAL CASE – THE KONYA CLOSED BASIN, TURKEY

DISSERTATION

to obtain
the degree of doctor at the University of Twente,
on the authority of the rector magnificus,
prof.dr. H. Brinksma,
on account of the decision of the graduation committee,
to be publicly defended
on 26 November 2013 at 14:45 hrs

by

Mustafa Gökmen

born on 19/02/1978

in Karaşar, Ankara, Turkey

This thesis is approved by
**Prof dr. ing. Wouter Verhoef**, promoter
**Dr. Zoltan Vekerdy**, assistant promoter
**Prof Okke Batelaan**, assistant promoter

Dedicated to my mother (Sultan Gökmen),
to my father (Ali Gökmen),
and also to all the hard working people of Konya plain.

*"Çumra kanalının suları Beyşehir kanalından çıkarken su rengindedir,*
*Konya ovasında kan renginde.*
*Siz buna, ovanın kırmızı toprağının rengidir diyeceksiniz;*
*ben, Dedemköylü Mehmet'le kardeşinin kanlarının rengidir diyeceğim.*
*Konya Ovası'nın ufukları mavi değil, sarıdır, sapsarıdır.*
*Siz bunun, rüzgarın kaldırdığı tozlardan böyle olduğunu söyleyeceksiniz;*
*ben, Konya hapishanesinde yatan Zağar Mehmet'in benzinin sarılığından*
*diyeceğim..."*
Kanal (1934), Sabahattin Ali

# Acknowledgements

From my own experience I can tell that a PhD thesis needs a lot of hard work for sure, but that is not enough at all. You need also not only luck and good coincidences but also a lot of support, cooperation and good company of course. I was really lucky, I could get plenty of them during this so called “journey”.

To start with, I’m grateful to HSP-Huygens Scholarship by Nuffic and to the Dutch Ministry of Education, Culture & Science for financing the first two years of my PhD research. All the rest of this research could build up on it. It is really pity HSP-Huygens scholarship is discontinued as of January 2012. I’m also grateful to ITC Faculty (and Twente University) for providing me the PhD opportunity and for financing the last two years of it. Lucky me that I could have Master and PhD experiences in one of the unique international study environments of the world.

Coming to the people, Zoltan was the person that I had first mentioned about the scholarship possibility. If he didn't encourage and supported the idea, it would not even start at all. From that moment till the end, he has helped me basically in everything: shaping the research, making out a team, a close monitoring (every week in principle), discussing the scientific part, facilitating the practical things whenever needed. If I ever get a chance for supervising students, the experience I had with him will be guiding me for sure. More importantly, I’m very happy to be part of the Vekerdy family and thank to both Zoltan and Marcsi for everything.

Zoltan had known me from my Master study, but we had not met with Wout at that time. Still, he has taken the responsibility of the scholarship application and I’m really grateful for that. Just before my qualifier, Wout had come up with an animation he made about the vegetation dynamics in Turkey. I was happily surprised with his enthusiasm for my research, and I’m glad he has always been during this research. He not only truly promoted to make a good quality research but also has approached it with interest and support. I could not imagine a better team.

Well, that was the core starting team, and it has expanded greatly within time. And the first person to mention is Okke. I’m glad that Okke has accepted to be the external supervisor. From the research proposal stage throughout all the papers, he has contributed greatly with an external eye despite all the distances. And I’m thankful for the inspiring discussions on every occasion we had.

At this point, I also have to mention the key local person, Hasan Z. Sarikaya. He not only facilitated my leave from the job at the ministry but also greatly supported for obtaining the local data and realizing the necessary fieldwork, which were indispensable part of this research. I'm grateful for all his support.

As part of the expanded team, I thank to all the members of WRS department, and particularly to Maciek, Christian and Joris. Christian gave great ideas at the initial stage for designing the field setup. He has also contributed a lot to the first paper, which has been both the most challenging stage and achievement in this research I think. He also introduced me Anne Verhoef, who has been an important contributor for the first paper. By this occasion, I'm also grateful to Anne for sparing her time and making some critical contributions. Maciek was always available for any advice and discussion from the beginning, and I consider him as an additional co-supervisor of this research. He has not only greatly contributed to the second paper, but also always pushed for improving the quality of it. I'm grateful for all his support and contributions. And Joris, as much as he does for the department (or possibly more) he did contribute in this thesis. He has been the programing advisor, problem solver, paper contributor, and a good friend as well. It was great to share the Tiger workshop experience we held in South Africa. Besides these established collaborations, I also benefited a lot from spontaneous supports in the department. Most importantly, Bob was always there available whenever I wanted ask his feedback and ideas, and they have always been inspiring, especially at the first paper stage. Also, I thank to Gabriel, Wim, Lichun, and Murat for always helping and sharing their expertise whenever I need. And big thanks to Anke, Tina of course, the department and the PhDs are lucky to have such friendly support from them.

I also thank to our MSc students Obie, Jay and Zizawar. It has been a great experience for me the fieldworks we organized together in Konya, and I thank for all your help in the field and contributions through your MSc. theses.

Before passing to the PhD life other than the research, I must also mention all the great support I got for realizing the fieldwork locally. Without the support of Regional Water Authority (DSI Konya Bölge Müdürlüğü) and its staff, the quality of fieldwork would never be the same. I'm deeply thankful to Mehmet Demirel, who has been the key person for arranging the installation of BR stations, solving any practical problem and arranging me all the contacts. I'm also grateful to Kemal Olgun for his support related with groundwater data, and Adnan Basaran for his help establishing the BR stations and providing hydro-meteorological data.

And I thank to Bayram Oyman, Serhan Pocan, Bulent Ilgin, Necati Simsek (and to Konya Soil and Water Investigation Institute) and Ramazan Turgut (and Sekersut company) for their support establishing the BR stations and maintaining them.

My other biggest luck with the PhD was Tolga. We both got the same scholarship, and we even arrived with the same flight to the Netherlands thanks to the introducing by our common friend Fusun, who is also an ITC alumni. That nice coincidence had already helped me to overcome some of the doubts to start the long the PhD adventure. I still remember the welcoming by Patrick at ITC-Hotel reception and telling us “oh long stayers”. Well, great that I never had the worry about the passing the time and Enschede could be a home thanks to the great friends like Tolga, later on the whole Gorum family with Hale, and my dear nephew Aral. And together with the PhD, I could gain life-long friends.

Music is as important as research in my life. What a great surprise it was to meet Mireia, Yiannis (well, he was already a close friend from Master time, and it was great to find him back in Enschede!), Ozgun, Enrico and Mauro (and our special fan and manager Diana of course), with whom we could have our beloved band Ken Lee. A dream came true that we could share listening, playing, rehearsing, staging (well ok only once but that doesn't reduce its specialty) of music together. Thank you for all the good time, and despite any distances from New Zeeland to Colombia, Netherlands to Turkey, friends will be friends!

Another surprise meeting happened in a concert in Enschede, when I met Oktay and Banu. They are one of those special couples, with each and both you can be best friends. I’m very happy to have met you.

During Master time, I was really keen on making international friends. This time, I was rather relaxed about it, benefited from meeting great Turkish friends in Enschede. Cuneyt, Sedef, Gul, Bengu, Mehmet, Damla, Devrim, Metehan, Serkan, Derya, Aytac and Zeynep. Thank you for sharing a lot of great moments.

Probably everyone see his/her term of fellows as the most special term and group of people, but I think this time was really true for the PhD group of WRS. Just the example of PhD-WPW meetings and drinks (with the support of Bob and Wout) can prove it I think, which has been the longest standing PhD activity at ITC. I’m very happy to have met all the special friends in our department: Mireia, Enrico, Chandra, Alain, Leonardo, Yijian, Guido, Mariela, Laura, Fouad, Joris, Syarif,

Jahanzeb, Xin, Xuelong, Kitsiri, Lal, Donghai, Tanvir, Ying, Haris, Vincent, Jenifer and Marcel. Thank you each and all for the times we shared.

In the meeting pot of ITC, you come across many friends from all over the world. You meet, become great friends, sometimes they stay quite long but mostly they leave in too short. It's hard but you get used to it somehow. I had many of them, hope I didn't forget any friend: (grande) Mauro, Andre, Blanca & Freek, Arta, Maria Fernanda (MaFeCo), Rafa, (Don) Juan, Nuria, Maitreyi, Divyani, Valentina, Jean Pascal, Byron, Flavia, Michal, Meisam, Nelly, Simona, Maria Fernanda (MaFeBo), Diana Lucia, Juan Pablo, Xuanmei, Paco, Pinar, Ulanbek, Dimo, Sahnaz, Marshall, Irena, Ivo, Ali, Christine, Clarisse and all other friends that I forget the names from my poor memory.

Apart from the people and the life in Enschede, my family and friends at home had also big share in this thesis. Without the recharge and motivations you get from them, things can get very hard going. I'm grateful for all the love and support I get from my big family, from my mother, father, sisters, brother, sister/brother-in-laws to nephews, nieces and cousins.

And I thank to my dear friends Kutay, Boray, Ugras and Omer, besides their great friendship, they directly contributed in the thesis through joining my fieldtrips, offering any possible help and also bearing to listen the PhD stories sometimes too much.

The extended 5$^{th}$ and last year of my PhD has been away from ITC, back home in Turkey. A period when PhDs can get easily distract away. I'm thankful to my bosses in the ministry to Cengiz T. Baykara and Zumrut Ozbahar for their understanding and support whenever I needed. I also thank to my colleagues and friends Nihan, Neslihan, Ali, Gulsun, Cemre, Canay, Baran and Erhan for their support and friendship.

And finally, my dearest thank to her who inspired me the will and thought to go for the adventurous PhD. Otherwise, it would not start at all.

# Table of Contents

# List of Acronyms

| | |
|---|---|
| **AMSR-E** | Advanced Microwave Scanning Radiometer - Earth Observing System |
| **BR** | Bowen Ratio |
| **CORINE** | Coordinate Information on Environment |
| **DEM** | Digital Elevation Model |
| **DSI** | State Hydraulic Works of Turkey |
| **ECMWF** | The European Centre for Medium-Range Weather Forecasts |
| **GIS** | Geographic Information System |
| **GRACE** | Gravity Recovery and Climate Experiment |
| **GW** | Groundwater |
| **LSA-SAF** | Land Surface Analysis - Satellite Application Facility |
| **MODIS** | Moderate Resolution Imaging Spectroradiometer |
| **MSG** | Meteosat Second Generation |
| **RGB** | Red, Green and Blue (colour) image |
| **RMSE** | Root Mean Square Error |
| **rRMSE** | Relative Root Mean Square Error |
| **RS** | Remote Sensing |
| **SEBS** | Surface Energy Balance System |
| **SEBS-SM** | Soil Moisture integrated SEBS |
| **TRMM** | Tropical Rainfall Measuring Mission |

# Chapter 1

## General introduction

## 1.1 Background

Arid, semi-arid and sub humid regions (sometimes collectively called dry lands) occupy approximately 50% of the global land area (Parsons and Abrahams, 1994). Because of the low annual precipitation input (with extreme temporal variability and extended periods of no precipitation) compared to high potential evapotranspiration demand, these regions are considered as water-limited environments (Newman et al., 2006). While in humid areas it is the climate (i.e. atmospheric demand) that controls the evapotranspiration, in semi-arid areas, it is the soil moisture that constraints evapotranspiration (Seneviratne et al., 2010).

In arid and semi-arid regions, groundwater is usually the only dependable water resource, which is available not only for human activities but also for use by groundwater-dependent ecosystems. It plays a central part in sustaining the irrigated agriculture and influences the health of many ecosystems (Giordano, 2009; Siebert et al., 2010). We can expect that the value of groundwater will increase in the coming decades, as the temporal variability in precipitation, soil moisture and surface water is projected to increase under more frequent and intense weather extremes associated with climate change (Taylor et al., 2012), and also along with the rising population and their food demands. According to Gleeson et al. (2012), about 1.7 billion people live in areas where groundwater resources and/or groundwater-dependent ecosystems are under threat. However, unsustainable depletion of groundwater has recently been documented on both regional (Famiglietti et al., 2011; Rodell et al., 2009) and global scales (Konikow, 2011; Wada et al., 2012; Wada et al., 2010).

Arid and semi-arid regions are highly vulnerable to anthropogenic and climate effects due to their scarce water resources, usually with a clear imbalance and a widening gap between the demand and the availability of water, mainly due to agricultural activities. The vulnerability of these regions can mainly be attributed to their high sensitivity to the changes in the hydrological fluxes. For example, even small changes in precipitation may lead to large changes in groundwater recharge (Woldeamlak et al., 2007), because the absolute quantities of the fluxes are generally low in these regions. Furthermore, when groundwater or surface water is used for irrigation, the increased evapotranspiration by crops may largely exceed the

input from precipitation, causing large deficits in the regional water balance. Therefore, acquiring accurate knowledge of both precipitation and evapotranspiration and their spatial distribution in arid and semi-arid regions are both considered important challenges in the scientific community and essential for a sustainable water and land resources management.

Estimating the water balance components over large spatial scales from ground-based measurements alone remains a challenge and is usually prone to large uncertainties. On the other hand, remote sensing (RS) data provides large-scale, spatiotemporally distributed, systematic land surface observations consistently over the globe, with spatial resolutions from meter- to kilometer-scales and temporal resolutions from half-hourly to bimonthly. Moreover, advancements in sensors, development of improved retrieval algorithms and tremendous increases in data distribution, storage and processing have greatly promoted the use of remote sensing data in hydrology (Pan et al., 2008). Besides these advancements, these RS datasets from different sources, resolution and coverage, are increasingly becoming freely accessible globally for relatively long timeframes.

Establishing the spatial and temporal distribution of hydrological fluxes using RS methods has been the focus of many recent researches (McCabe et al., 2008). Spatio-temporal evapotranspiration (*ET*) can be determined from RS-supported estimates of the surface energy balance (Su et al., 2005). Global *ET* products from the RS retrievals are becoming increasingly available (e.g., Ghilain et al., 2011; Su et al., 2010; Vinukollu et al., 2011). Precipitation is regularly retrieved from multi-sensor microwave and infrared data, using a variety of techniques (e.g., Huffman et al., 2007; Joyce et al., 2004). One of the most recent datasets comes from the Tropical Rainfall Measuring Mission (TRMM) Multi-satellite Precipitation Analysis (TMPA), which is designed to combine precipitation estimates from various satellite systems, as well as land surface precipitation gauge analyses when possible (Huffman et al. 2007). Although snow cover extent data is regularly provided by moderate resolution sensors like MODIS, RS measurements of snow water equivalent (*SWE*) at present are limited (Tang et al., 2010). The available RS products from microwave sensors are known to be less accurate in regions of complex terrain due to slope-aspect and the limitations from the instantaneous field of view of the sensors, which can cause underestimations on mountains of complex geometry (Muskett, 2012).

The capabilities of RS to look below the ground surface directly are extremely limited (Green et al., 2011). Nevertheless, radar and passive microwave RS techniques are widely used to obtain soil moisture information in a spatially and temporally distributed manner for large areas. Examples of soil moisture products available at global scale are passive microwave based (Owe et al., 2008), and active microwave based (Wagner et al., 2013 and Wagner et al., 2003). Together with the coarse spatial resolution (about 25 km), the main limitation of RS retrieval of soil moisture is the fact that it is only representative for the top few centimeters of the soil. On the other hand, changes in total surface and subsurface storage can be derived using gravity anomaly measurements using the satellite-based observations of earth's gravity field (Swenson and Wahr, 2002). Many recent studies (e.g. Famiglietti et al., 2011; Strassberg et al., 2007; Swenson et al., 2008; Swenson and Wahr, 2006; Yeh et al., 2006) used the satellite gravity data from the Gravity Recovery and Climate Experiment (GRACE) project to analyse groundwater storage changes from large basins to continental scales. However, it should be noted that GRACE can measure variations in equivalent height of water over regions of about 150,000 $km^2$ or higher (400-500 km spatial resolution) from 10-daily to monthly temporal frequency, with uncertainties in the order of a few centimeters (Wahr et al., 2006).

Besides the wide application of RS to retrieve and quantify hydrological variables, satellite-based vegetation indexes such as Normalized Difference Vegetation Index (*NDVI*) are commonly used to examine the dynamics of vegetation health, density, land cover and phenological changes. Many different studies (e.g. Elmore et al., 2000; Evans and Geerken, 2004; Fensholt et al., 2012; Fensholt and Rasmussen, 2011; Heumann et al., 2007; Julien et al., 2006; Lunetta et al., 2006; Pettorelli et al., 2005) have used *NDVI* time series data from different sensors to assess land cover changes, as well as trends and responses of vegetation greenness to changes in the climatic (e.g. rainfall or air temperature) or anthropogenic (e.g. irrigation and deforestation) drivers.

## *1.2 Problem statement*

Regional or basin scale studies are of particular importance for the assessment of the hydrological fluxes and ecological health of arid and semi-arid regions, because it is at the basin/region level where water management (*e.g.*, man-made reservoirs and irrigation water withdrawals) substantially affects the hydrological and ecological dynamics. In addition, the controlling

mechanisms of hydrological fluxes (especially evapotranspiration) change regionally, which necessitates the consideration of regional (and temporal) variations in the fluxes and the main drivers of them.

The Konya basin in central Anatolia (Turkey), which is one of the biggest endorheic basins in the world, is a characteristic example of a semi-arid region where groundwater resources are under strong anthropogenic pressure. Over the last few decades, the basin experienced huge non-renewable groundwater abstraction for irrigation, which caused approximately a head decline of 1 m/year (Bayari et al., 2009). Along with the groundwater head declines, the basin also experienced environmental degradations such as draining of a number of ecologically important wetlands, as these ecosystems are also mostly groundwater dependant. However, so far, hydrological and ecological variables (and the interaction between them) have not been quantified in a spatially and temporally distributed manner in order to get a holistic insight into the climate-human-hydrology-ecology dynamics in the basin.

Taking this prominent example of a semi-arid region, where scarce water resources and sensitive ecosystems are prone to strong anthropogenic and climate change effects, the research presented in this thesis aims at tackling the following problems:

**1. Quantification of the spatio-temporal hydrological fluxes, especially evapotranspiration in semi-arid regions.**
Conventional point monitoring methods, which are common practice among water managers, provide limited insight into the spatial distribution of hydrological and eco-environmental variables. Therefore, RS-based retrievals and methods are preferred over these conventional methods, considering their capabilities to provide spatially continuous measurements. However, it is still a challenge to achieve accurate quantification of hydrological fluxes in arid and semi-arid regions.

**2. Quantifying spatio-temporal distribution of groundwater storage changes using earth observation methods**
An alternative to the spatial low resolution GRACE estimated groundwater storage changes is to infer changes in the water storage ($\Delta S$) by estimating the difference between precipitation ($P$), evapotranspiration ($ET$) and runoff

($R$) (Brunner et al., 2004). However, estimating the water balance and its distribution over large spatial scales from ground based measurements or RS retrievals alone remains a challenge and is usually prone to large uncertainties. Furthermore, in arid and semi-arid regions with typically low intensities of water fluxes, a relatively small error in any component will translate to a large error in the resultant water balance.

**3. Building a harmonized and consistent time-series of ecohydrological fluxes, combining different sources of data with different spatial, spectral and temporal resolution to allow spatio-temporal analysis of trends, changes and inter-relations in the ecohydrology of a semi-arid region**

The subject of trend detection in hydrologic and vegetation data has received attention lately, especially in connection with the anticipated changes in global climate (Hamed, 2008), and increasing anthropogenic pressures along with the rising population and their food demands. The responses of water cycle components and vegetation to the changing climate and anthropogenic effects has been discussed and studied widely at global and regional scales by recent studies (e.g. Dorigo et al., 2012; Douville et al., 2012; Fensholt et al., 2012; Jung et al., 2010; Zhang et al., 2012). A variety of earth observation satellites provides large-scale, spatially and temporally continuous, systematic and periodical land surface observations over the globe, which make them ideal for using in time-series analysis. However, as they observe different land surface parameters, these different satellites provide data which differ largely in their spatial (from a few meters to kilometers) and temporal (from half-hourly to bimonthly) resolutions, and spectral characteristics. Therefore, an important challenge is not only building harmonized and consistent time-series of RS-based datasets, but also integrating them in a manner both to reveal the spatio-temporal trends/changes in the regional ecohydrology, and attributing them to climate and anthropogenic effects in an improved way, so that it could be used as a model for other semi-arid regions.

**4. Defining a quantitative framework for determining the sustainable water resources in connection with ecological water demands**

In water-limited regions, groundwater (GW) is often the only reliable water resource, which has been affected by a number of non-climatic forcings, primarily for irrigated agriculture (Green et al., 2011). Historically, it was

common practice by water managers to assume a "safe yield" term (Lee, 1915; Todd, 1959) with respect to groundwater resources, which used to be taken equal to the volume of recharge to an aquifer while ignoring the fact that over the long term and under natural conditions, natural recharge is balanced by discharge from the aquifer by evapotranspiration or into streams, springs, wetlands, or seeps (Sophocleous, 2000). Along with the changing view from the "safe yield" to "sustainable yield", regulations such as the Water Framework Directive by European Union redefined sustainable use of groundwater resources, stating that for good management, only that portion of the overall recharge can be abstracted, which is not needed by the ecology. However, because of uncertainties and spatio-temporal variability of key controlling variables (such as recharge and other water budget components), it is still a challenge to determine the limits and variations of sustainable water resources in connection with the quantity of ecological water demands.

## *1.3 Statement of objectives*

Main objective of this research study is to effectively utilize and integrate earth observation methods in assessing spatially and temporally the hydrological fluxes, ecosystem's health and the inter-relations between them in a semi-arid basin, with an emphasis on defining the quantification accuracies.

In accordance with the main objective, the specific objectives are:

1. To improve the surface energy balance model SEBS for better estimation of energy and water fluxes in water-stressed regions.

2. To construct and validate a spatiotemporally distributed water balance for assessing the water availability (i.e. surface runoff), consumptive water uses (i.e. irrigation), *GW* storage changes and *GW* discharges at large basin scale.

3. To develop and implement a framework for a RS-based and integrated assessment of ecohydrological trends and their causes at regional scale.

4. To develop a quantitative framework for assessing the limits and variations of sustainable water resources along with the ecological water demands annually and seasonally.

## 1.4 The proposed procedure

With these specific objectives in mind, the proposed procedure may be described as:

1. **Integration of soil moisture into SEBS: a new approach for the calculation of sensible heat**
   Remote sensing based models that estimate evapotranspiration, *ET*, from the energy balance with a single source approach (e.g. SEBS) do not take below-ground processes explicitly into account, assuming that the effects of soil moisture and other processes are all implicitly incorporated in the observable land surface temperature. We propose a new method that integrates soil moisture data explicitly in the calculation of sensible heat flux by introducing a soil moisture dependent scaling factor for the parameter $kB^{-1}$ that plays a role in the aerodynamic resistance.
2. **Quantifying spatiotemporal water balance with improved estimates of *ET* and *P***
   A conceptual model is proposed to build a spatially distributed water balance for assessing *GW* storage changes at large basin scales. The method relies on improved *ET* and *P* estimates for semi-arid conditions using the modified surface energy balance model (SEBS-SM) for calculating *ET* and integrating RS and ground data for calculating unbiased rainfall and *SWE* contribution to the total precipitation.
3. **Investigating spatio-temporal trends in the ecohydrological processes of a semi-arid basin**
   An integrated framework is proposed through trend analysis of evapotranspiration (actual and potential), vegetation greenness (i.e. *NDVI*) and precipitation using satellite-based observations to assess the human-induced changes in the hydrology and the associated ecological health of a semi-arid region. The spatio-temporal trend assessment will be implemented at a medium spatial resolution (i.e. 1 km) to reveal the inter-relations between hydrology and ecosystems in the region.
4. **An RS-based quantitative framework for assessing the limits and variations of sustainable water resources considering the ecological water demand**
   Sophocleous (2000) highlights that a wise management of water resources needs to recognize that yield should vary over time as environmental conditions vary because of the uncertainties and spatiotemporal variability of key controlling variables (such as recharge and other water budget components). Seasonal and yearly distributions of *P*, *ET* and *P-ET* will be

utilized for the spatio-temporal assessment of limits and variations of water availability for sustainable use and the quantities of ecological water demand in the water-limited Konya basin.

## 1.5 Structure of the thesis

This thesis consists in total of seven chapters. Three of the four core chapters have been published as peer-reviewed papers (Chapters 3, 4, and 5).

Chapter 2 provides the description of the study area.

Chapter 3 deals with improving the quantification of hydrological fluxes, particularly evapotranspiration, for continuously or seasonally water-stressed regions. An updated version of the SEBS model (SEBS-SM), that explicitly includes the effect of soil moisture availability on evapotranspiration, is introduced and validated by comparing the model outputs (both SEBS and SEBS-SM) with field observations from several Bowen Ratio stations installed in the semi-arid Konya basin in Turkey.

Chapter 4 presents an integrated method, which combines remote sensing based evapotranspiration and precipitation estimates with available ground data to establish each component of the water balance (i.e. rain, snow water equivalent, *ET*, runoff), in order to quantify and validate a spatially distributed water balance for analysing groundwater storage changes due to supplementary water uses.

Chapter 5 presents a regional framework for an integrated and spatio-temporally distributed assessment of human-induced trends in the hydrology and the associated ecological health of a semi-arid basin where both human activities (i.e. agriculture) and natural ecosystems are highly groundwater-dependent.

Chapter 6 describes an RS-based and quantitative framework for assessing the limits and variations of sustainable water resources and the ecological water demand in the water-limited Konya basin.

Chapter 7 presents a synthesis about the main contributions of the research to the state of the art and gives an outlook into the additional research aspects.

# Chapter 2

## Site description

The study area is the Konya basin, located in central Anatolia, Turkey, between 36.8° N 31.0° E and 39.5° N 35.1° E. The basin covers an area of about 54,000 km$^2$, with elevations ranging from 900 to 3,500 m above sea level (Figure 2.1). The Taurus Mountains border the basin from the south and southwest. There are extensive plains in the mid- and downstream areas, making the Konya basin one of the important agricultural regions of Turkey. Parts of the plains are occupied by two large lakes: the hyper-saline Tuz Lake in the downstream part and the freshwater Lake Beysehir in the upstream part. Numerous smaller fresh/brackish wetlands are present in the mid- and downstream areas, some of which have dried out in the last decades.

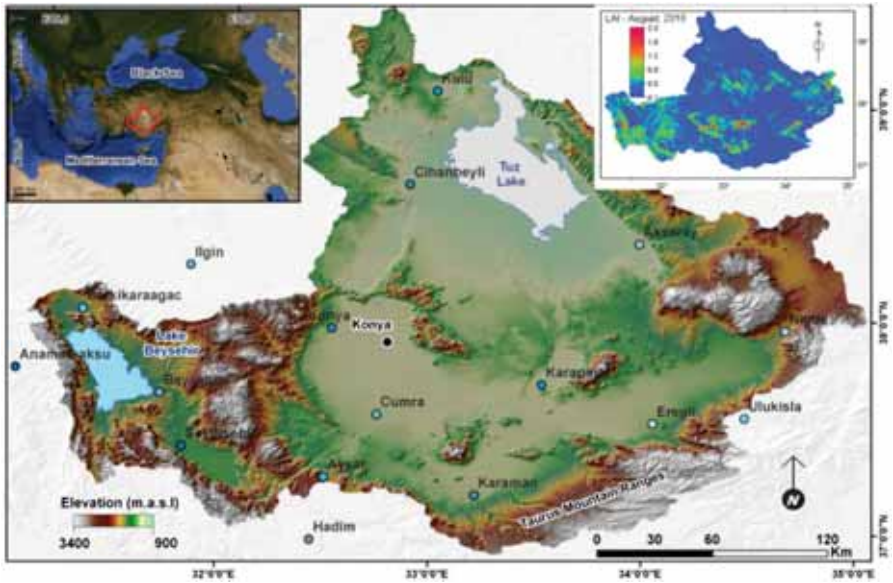


**Figure 2.1** The geographic location (top left), vegetation distribution (Leaf Area Index map, top right), and SRTM-based elevation map with the locations of the meteorological stations (main panel) of the study area.

The region has a typical arid to semi-arid climate with a long-term average yearly precipitation of 380 mm (unpublished data from State Hydraulic Works, DSI), spatially ranging from 250 mm in the plain parts to more than 1,000 mm in the mountainous areas (Chapter 4). The summers are hot and dry (with a maximum temperature reaching ~40 °C) whereas winters are cold and wet (the minimum temperature may go down to ~-20 °C). While the south-western upstream part shows a warmer and wetter Mediterranean

character, the rest of the basin has a drier, continental climate, isolated from the moderating effect of the sea by the Taurus Mountains in the south.

The land cover in the low-lying areas of the basin shows a strong contrast between intensively irrigated agricultural lands and the sparsely vegetated steppe areas covering the mid and downstream plains (Figure 2.2a). For example, as of August 2010, around 80% of the Konya basin had a leaf area index (LAI) value equal to or less than 0.5, while only around 5% had an LAI equal to or higher than 1.0 (top-right map in Figure 2.1). Natural vegetation is dominated by Artemisia grasses (Fontugne et al., 1999). Salt steppes were formed in the saline conditions surrounding the Tuz Lake, with the dominant halophytic species belonging to the Chenopodiaceae and Plumbaginaceae families. In the less saline areas in the midstream plains, Limonium anatolicum is the dominant species. (http://www.eoearth.org/article/Central_Anatolian_steppe). Generally, all these steppe vegetation types are formed by non-woody plants with a relatively small canopy height and shallow rooting depths. The adaptation methods of the natural vegetation to drought stress differ between the downstream area where the groundwater is shallow and soils are saline, and the rest of the region, where the groundwater table is located between 35 to 50 m depths. In the mountainous parts, forest and shrub lands form the dominant land cover. The distribution of agricultural crops (based on data from 2007) is as follows: 38% cereals, 28% sugar beet, 19% vegetables, 13% fruits and 2% other (unpublished data from State Hydraulic Works, DSI).

Although surface water is also utilized, groundwater is the main source of water for irrigation. It can be accessed almost anywhere in the flat areas of the basin by means of 50 to 250 m deep wells (Bayari et al., 2009), abstracting it from the Neogene aquifer. According to an unpublished inventory conducted by the regional water authority (DSI), there are more than 90,000 groundwater abstraction wells, around 75% of which are unregistered, in the Konya basin. The distribution of the groundwater abstraction wells is shown in Figure 2.2b. Most of the wetlands and the water bodies in the region can also be classified as groundwater-dependent ecosystems.

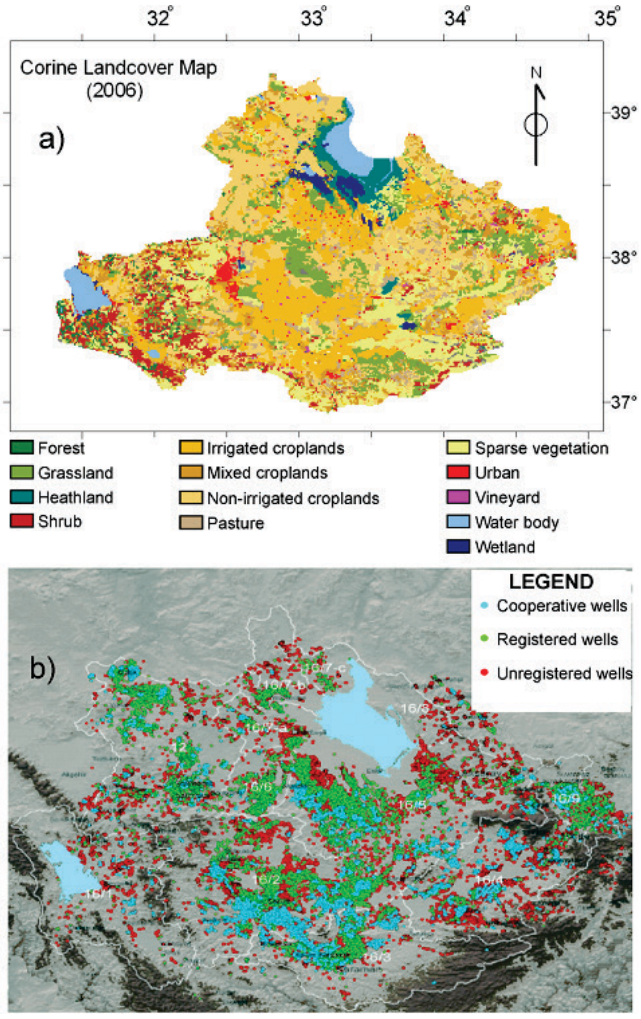


**Figure 2.2a** CORINE land cover classification map of the Konya basin (source: Ministry of Environment and Forestry); **b)** Distribution of the groundwater abstraction wells in and around the Konya basin (source: unpublished data by State Hydraulic Works, DSI).

Figure 2.3 presents the conceptual model of the hydrological fluxes in the Konya basin. The Taurus Mountains in the south and southwest are the main water source areas, where high rainfall and snowmelt feed the ephemeral rivers and recharge the aquifer. Due to a well-developed karst geology, the (semi-)arid climate and the huge plain areas in the mid- and downstream parts, the Konya basin has no well-established drainage network. The water from the ephemeral rivers is either stored in the reservoirs to facilitate

irrigation, or feeds the groundwater along the foot-slopes of the mountains. The basin is hydrologically closed, meaning that the horizontal fluxes of surface and groundwater are retained in the basin, terminating at the Tuz Lake in the north (Bayari et al., 2009). Evapotranspiration is the only out-flux from the basin and controls salinization of the surface water bodies such as the hyper-saline Tuz Lake (Bayari et al., 2009).

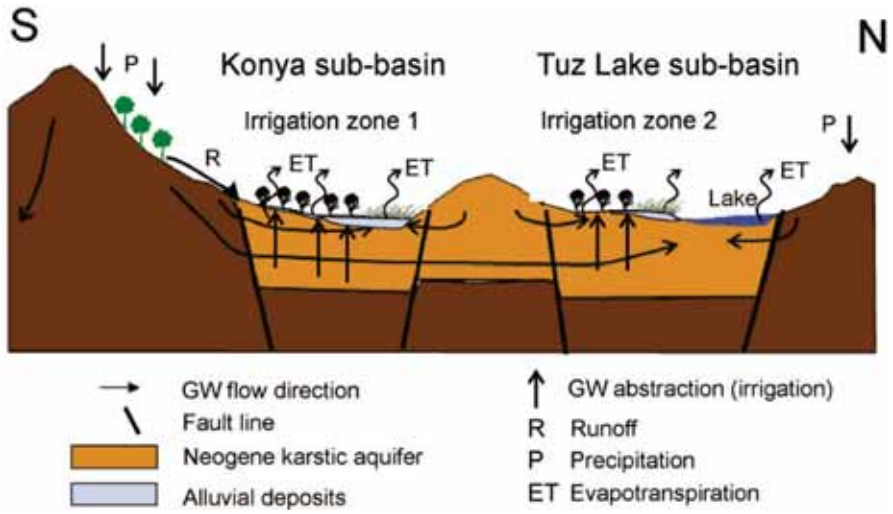


**Figure 2.3** Conceptual model of the Konya basin (modified after Bayari et al., 2009 and Naing, 2011)

# Chapter 3

# Improved estimation of evapotranspiration under water-stressed conditions

**Abstract**: In this chapter we integrate the information about water stress into SEBS, one of the surface energy balance models that employ remote sensing (RS) data. The level of water stress is taken into account in the calculation of sensible heat, through a modified definition of $kB^{-1}$, the parameter that summarizes the excess aerodynamic resistance to heat transfer compared to momentum transfer. Surface energy balance models are employed to obtain evapotranspiration as the remainder of available energy minus sensible heat flux ($H$). These models assume that information on the ratio of actual to potential evaporation is implicitly embedded in the land surface temperature. This assumption is usually adequate where available energy is the limiting factor for evapotranspiration ($ET$), but there is a problem when water availability becomes limiting for $ET$. In this case, the daily evapotranspiration is often overestimated, in particular for sparsely vegetated semiarid regions, because of an underestimation of sensible heat flux for these areas. Our method remedies this shortcoming by progressively decreasing $kB^{-1}$ with increasing levels of water stress. This decreases aerodynamic resistance, and hence increases H, leading to lower estimates of $ET$. The decrease of $kB^{-1}$ with a rise in plant water stress is based on general plant physiological observations related to vertical canopy stomatal conductance profiles, which affects the exchange of sensible and latent heat between the canopy and the atmosphere. The new approach was tested by comparing SEBS $H$ outputs with field observations from Bowen ratio stations distributed over the Konya basin in Turkey, and the results indicate a large improvement when soil moisture is integrated explicitly in the calculation of sensible heat flux by SEBS. More importantly, the new approach provides a considerable operational improvement for regional $ET$ mapping through integrating microwave soil moisture measurements into SEBS, as illustrated by our findings for this semi-arid region. Improved mapping of regional $ET$ by soil moisture integrated SEBS offers the opportunity to provide more accurate estimation of energy and water fluxes in regions where plant water stress is a recurrent feature.

This chapter is based on:

Gokmen, M., Vekerdy, Z., Verhoef, A., Verhoef, W., Batelaan, O., and van der Tol, C.: Integration of soil moisture in SEBS for improving evapotranspiration estimation under water stress conditions, Remote Sensing of Environment, 121, 261-274, 2012.

## 3.1 Introduction

Nowadays remote sensing (RS) techniques are widely used to determine the surface energy balance, i.e. the distribution of net radiation, $R_n$, over evapotranspiration, $ET$, sensible heat flux, $H$, and soil heat flux, $G_0$. In most cases, the emphasis is on the assessment of the spatio-temporal variability of evapotranspiration, by calculating $ET$ as the remainder of $R$n - $H$ - $G_0$, where $H$ is generally derived from the bulk transfer equation.

Many RS-based empirical relationships for the determination of $ET$ have been developed over the past few decades (Carlson et al., 1995; Jiang and Islam, 2001; Kustas et al., 1994; Rivas and Caselles, 2004; Wang et al., 2007), while other researchers have pursued semi-physical or physical approaches, since these are more generally applicable (Bastiaanssen et al., 1998; Kustas and Norman, 1997, 2000; Menenti and Choudhury, 1993; Roerink et al., 2000; Su, 2002). The focus of this chapter is on physically-based surface energy balance (SEB) models, specifically SEBS (Su, 2002). These models are usually less site-specific and, as stated by Kustas and Anderson (2009), they do not require subjective intervention by the model user, such as in techniques where selecting hot and cold end-members within the scene is required (e.g. SEBAL by Bastiaanssen et al., 1998; S-SEBI by Roerink et al., 2000; or METRIC by Allen et al., 2007). Also, physical models serve as a more consistent tool when time series of evapotranspiration are desired.

Physically-based SEB models can be divided into those that calculate $H$ using a single-source (e.g. SEBS by Su, 2002) and a multi-source (generally two-source, e.g. TSEB by Kustas and Norman, 1997) bulk transfer equation. There is considerable interest in the hydro-meteorological community in single source models due to their simplicity. In this regard, various researchers in land surface modelling and thermal remote sensing communities have focused on developing simple schemes to accommodate the inherent differences between the radiometric and aerodynamic surface temperature in the calculation of the sensible heat flux while using the bulk transfer equation (Kustas et al., 2007).

A number of validation studies indicate that both single-source and two-source models can provide good and comparable estimates of the surface energy budget partitioning at different scales (e.g., Anderson et al., 2007; Su

et al., 2001). This is mainly due to the fact that, instead of explicitly separating canopy and soil as different source terms (e.g. two-source models), the modified single-source models such as SEBS by Su et al. (2002) accommodate the differences between radiometric and aerodynamic surface temperatures in partial canopy covers by employing physical models of soil-canopy heat exchange (Kustas et al., 2007). Studies by French et al. (2005) and Timmermans et al. (2007) present detailed inter-comparisons of single and two-source models. Recent and thorough reviews of RS-based surface energy balance models can be found in the literature (Gowda et al., 2007; Kalma et al., 2008).

The ultimate aim of deriving the surface energy budget (and specifically evapotranspiration) by remote sensing methods is to reach good operational utility under different land surface conditions (Meijerink et al., 2005; Norman et al., 2006). However, estimates of surface energy budget partitioning by single and two-source models are not widely validated; most studies reported in the literature use field measurements obtained over a limited number of land cover and hydro-meteorological conditions (Kustas et al., 2007). Problems appear for RS-based surface energy balance models, especially for sparsely vegetated and (occasionally) dry areas: studies (Lubczynski and Gurwin, 2005; Timmermans and Meijerink, 1999; Van der Kwast et al., 2009) indicate that RS-based solutions of the surface energy balance overestimate $ET$ in such areas by 1.5-3.0 mm $day^{-1}$ due to an underestimation of the sensible heat flux.

The overestimation of $ET$ usually occurs in the hydrological regime where water availability is limiting $ET$. Seneviratne et al. (2010) provide a conceptual framework for defining soil moisture regimes and the corresponding evapotranspiration regimes (Figure 3.1), which was also highlighted before by other studies (Budyko, 1974; Koster et al., 2009; Parlange and Albertson, 1995; Seneviratne et al., 2006; Teuling et al., 2009). Although the relation between soil moisture, *SM*, and evapotranspiration depends on soil type, vegetation type, and vegetation adaptation to drought (Teuling et al., 2006), the role of near-surface soil moisture is significant, especially where the groundwater is relatively deep and shallow-rooted plants dominate the vegetation.

With the advances in active and passive microwave observations, it is possible to measure the near surface *SM* by remote sensing techniques, and

RS-based soil moisture data are increasingly used and assimilated in regional/global climate and hydrological models for improving prediction capabilities (Seneviratne et al., 2010). A study by Jung et al. (2010) looked at the recent global trends in land evapotranspiration by using microwave satellite observations of soil moisture. They conclude that soil-moisture limitations on evapotranspiration largely explain the recent decline of the global land-evapotranspiration trend.

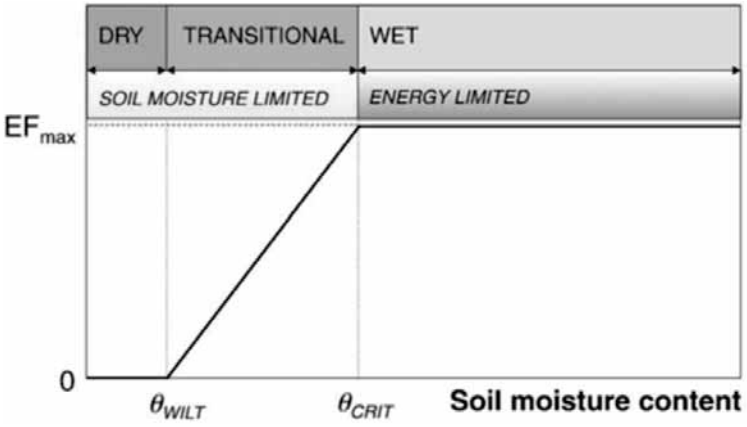


**Figure 3.1** A conceptual framework for the soil moisture dependent evapotranspiration regime. Adapted from Seneviratne et al. (2010). *EF* denotes the evaporative fraction ($EF = \lambda E / R_n$), while $\theta_{WILT}$ and $\theta_{CRIT}$ are the soil moisture values at wilting and critical points, respectively.

Surface energy balance models that determine $ET$ from $R_n - H - G_0$, do not explicitly consider soil moisture dependency for the calculation of $ET$. The individual effects of soil evaporation, soil moisture storage, stomatal regulation, transpiration and interception storage are all implicitly incorporated in the resulting land surface temperature variable. This approach is usually adequate where available energy is the factor limiting evapotranspiration, but there is a problem when water availability becomes the limiting factor for $ET$, which is often the case, especially in semi-arid regions. Therefore, while SEBS and other physical SEB models are found to work well for a range of crops and land covers, there is still a need to improve these models to make them more suitable for water-stressed conditions. In this chapter, we have developed an approach to take into account water stress through integration of soil moisture information into the SEBS bulk transfer equation for $H$ (via the parameter $kB^{-1}$), to allow for a more accurate

mapping of evapotranspiration under water-limited conditions. The new approach was first tested and validated by comparing the SEBS model output with field observations from Bowen Ratio ($BR \approx H/\lambda E$) stations installed in the semi-arid Konya basin in Turkey. Next, microwave soil moisture measurements were integrated into SEBS to achieve an operational improvement in regional $ET$ mapping for this semi-arid region.

The updated SEBS model (that will be called as SEBS-SM in the following) can be considered as an example of the next generation single-source SEB models, i.e. those that explicitly include the effect of soil moisture availability. SEBS-SM has a large potential in providing a more accurate estimation of energy and water fluxes in continuously or seasonally water-stressed regions. Hence, it can contribute to the development of improved global $ET$ products, an initiative which has already been started by studies, including that of Su et al. (2010) in the context of WACMOS (Water Cycle Multi-Mission Observation Strategy), a project supported by ESA, and Vinukollu et al. (2011) in the context of NASA's Energy and Water Systems (NEWS) study in cooperation with the global GEWEX Landflux initiative.

## *3.2 Field setup*

A total of five Bowen ratio stations were installed in the Konya basin following the recommendations of Pauwels and Samson (2006). Two sensors that measure both temperature and relative humidity (PASSRHT sensor by Decagon devices, WA, USA) were mounted at heights of around 0.5 and 2 m at each station. For the determination of the sensor heights, it was considered as a rule of thumb that the lower sensor had to be above the surrounding vegetation, while the upper sensor should be low enough not to sample the air coming from a different environment upwind. The fetch requirements described by Brutsaert (1982) and Shuttleworth (1992) were followed for each station, which state that the surface being measured should extend to a distance upwind that is at least 100 times the height of the sensors.

In addition, one 5TE sensor (Decagon Devices, WA, USA) measuring soil moisture, electrical conductivity and soil temperature was installed at each station, at an average depth of 5 cm. A 5TE sensor determines volumetric water content (VWC) by measuring the dielectric constant of the media using capacitance/frequency domain technology. The sensor uses a 70 MHz

frequency, which minimizes salinity and textural effects, making the 5TE accurate in almost any soil (Decagon Devices, WA, USA). Note that, because the aim of the SM measurements was to estimate the water stress level through a relative SM index from the time series of the measurements, the sensors were not needed to be calibrated for local circumstances before installation; the factory calibration was used. The measurements were recorded with the Em50 data logger (Decagon Devices, WA, USA), which was set to store data every 30 minutes, averaging measurements taken at one-minute intervals.

Before installing the PASSRHT sensors, the sensors were mounted together at the same height for a week with a recording interval of 1 min. These records were used for the inter-calibration of the sensor pairs installed at each station. The locations of the BR stations in the Konya basin are shown in Figure 3.2. These locations were chosen to account for different land cover conditions, as well as for ease of maintenance: Stations 1 and 5 are situated in agricultural plots (sugar beet and potato). BR station 2 is installed in the downstream salt marshes. The dominant plant species in the surrounding area is bulrush (Bolboschoenus maritimus), which stays green throughout the year due to the presence of shallow groundwater. Alfalfa (Medicago sativa) is grown in a controlled manner around station 3, sparse steppe vegetation is the land cover for the area represented by station 4. Stations 3 and 4 are located on sandy soils, stations 1 and 5 on calcareous clayey loams and station 2 on organic clayey soil.

### *3.2.1 Bowen ratio data*

The values of the Bowen ratio were calculated as (Ohmura, 1982):

$$BR = \frac{C_p}{\lambda}\frac{K_h}{K_w}\frac{(\theta_1 - \theta_2)}{(q_1 - q_2)} \tag{3.1}$$

where $\theta_1$ and $\theta_2$ are potential air temperatures [°C] and $q_1$ and $q_2$ are the specific humidities [kg kg$^{-1}$] at heights $z_1$ and $z_2$, respectively. For $\theta_1$ and $\theta_2$ the measured (i.e. the actual) air temperatures were used, thus ignoring the minor adiabatic effect due to the difference in measurement height. $C_p$ is the specific heat of dry air [J kg$^{-1}$ °C$^{-1}$], $\lambda$ is the latent heat of vaporization [J kg$^{-1}$], and $K_h$ and $K_w$ are the eddy diffusivities [m$^2$ s$^{-1}$] for heat and water vapour, respectively.

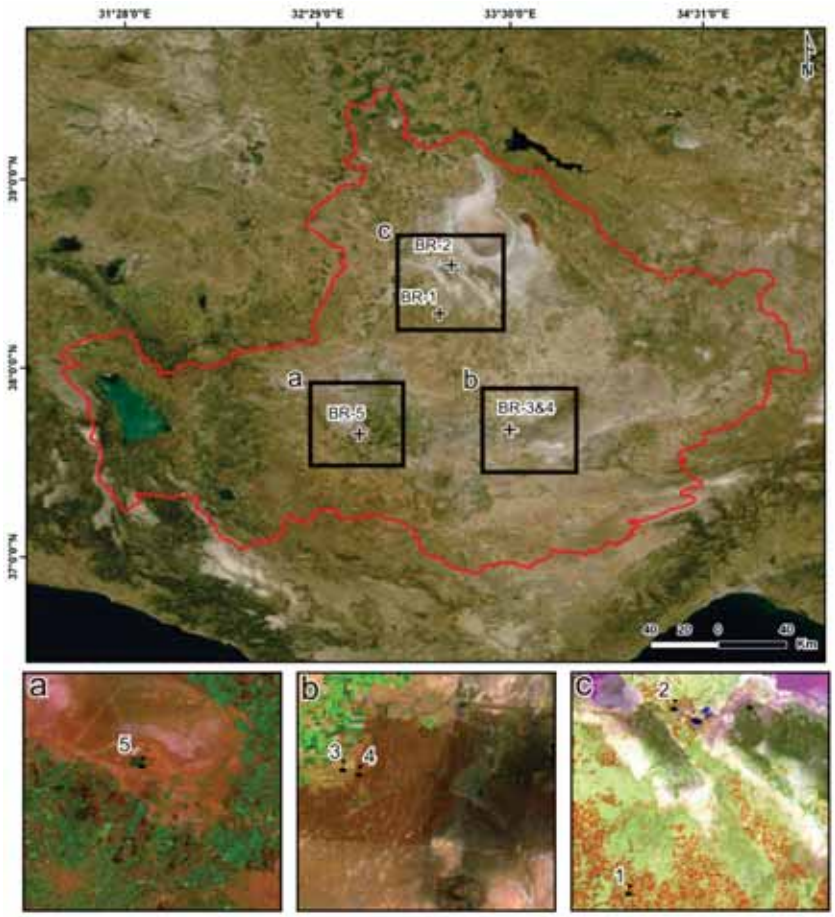


**Figure 3.2** The locations of the BR stations in the basin shown on a true-colour composite of a MODIS image, and closer views of the BR stations, superimposed on false-colour composites of Landsat images. For image a and b RGB = bands 5,4,2 and for image c RGB = bands 4,5,3.

The eddy diffusivities are assumed to be equal (Brotzge and Crawford, 2003), i.e. they cancel out. To obtain $q_1$ and $q_2$, the relative humidity measurements were first converted to actual vapour pressure values using a $6^{th}$ order polynomial (Flatau et al., 1992) after which the $q$ values were calculated using these actual vapour pressure values and air pressure measurements from nearby meteorological stations. Finally, the *BR* values were assessed for reliability, based on the detailed guidelines given by Perez et al. (1999). In particular, *BR* values corresponding to gradients of vapour pressure smaller than the sensor resolution were filtered out.

In this study, the day-time averages of half-hourly *BR* measurements were used for the period covering March to October 2010. The values of four stations were used in the analysis, since the originally planned land cover of sugar beet was changed to sunflower by the farmer in the area where *BR*-station 1 was installed. Hence, the lower sensor was not above the canopy and it did not satisfy the fetch requirements anymore. Only the days without precipitation and having a sunshine duration of at least 5 hours were used. Further filtering involved selection of those days only for which a cloud-free image of MODIS was available, to enable comparison with the results of the SEBS model. As a result, data from a total of 42 cloud-free days in 2010 were used for the analysis.

## 3.3 Methods

In this section, we first provide a short theoretical overview on the quantification of sensible heat flux. Then, we describe how the SEBS model calculates $H$, with a focus on the module to quantify aerodynamic resistance. Afterwards, we introduce our alternative approach to calculate $H$, where we integrate soil moisture values explicitly into SEBS through a modified definition of the aerodynamic resistance model.

### 3.3.1 A brief overview of sensible heat transfer theory

Surface energy balance models calculate the evapotranspiration, i.e. the latent heat flux, $\lambda E$, as the residual of the surface energy balance. Therefore, the problem of $ET$ overestimation by these models, in particular in drylands, is in fact mainly caused by an underestimation of sensible heat flux for such areas. This is obvious from the energy balance:

$$\lambda E = A - H \tag{3.2}$$

where $A$ is the available energy, which is equal to $R_n - G_0$, with $R_n$ the net radiation and $G_0$ the soil heat flux; $H$ is the sensible heat flux; and $\lambda E$ is the latent heat flux. All fluxes are in W $m^{-2}$.

Sensible heat ($H$) is calculated from the ratio of the difference between surface and air temperatures ($T_0 - T_a$) and the aerodynamic resistance ($r_{ah}$) by the bulk transfer equation:

$$H = \rho C_p \frac{T_0 - T_a}{r_{ah}} \tag{3.3}$$

where $\rho$ is the density of air [kg $m^{-3}$] and $C_p$ is the specific heat of dry air [J $kg^{-1}$ $K^{-1}$].

Despite the apparent simplicity of Eq. (3.3), (Troufleau et al., 1997) and (Verhoef et al., 1997a) indicate that problems arise especially for sparsely vegetated areas due to the definition of the "surface temperature" and quantification of the aerodynamic resistance. The notion of the "surface temperature" is different for vegetation, due to its vertical extension, compared with open water or bare soil. Furthermore, Eq. (3.3) is inferred from aerodynamic transfer equations, which means that $T_0$ is theoretically an air temperature at the theoretical "surface" level, *a priori* different from the physical temperature of the surface (Troufleau et al., 1997). As a result, the methods validated for dense crops can give contradictory results over the sparse vegetation, as validated by the FIFE field experiment (Hall et al., 1992).

To overcome the problem of defining the "surface temperature" for different land covers and canopies, Monteith (1965) introduced a theoretical level where the canopy exchanges sensible and latent heat with the atmosphere. This level is given by the sum of the zero-plane displacement height ($d$) and roughness length for momentum transfer ($z_{0m}$). Owen and Thomson (1963) and Thom (1972) showed that the transfer of heat encounters greater aerodynamic resistance than the transfer of momentum. Therefore, the effective source of sensible heat must be located at a lower level than the sink of momentum (Garratt and Hicks, 1973; Stewart and Thom, 1973), implying that the roughness length for heat transfer ($z_{0h}$) is lower than that for momentum transfer ($z_{0m}$) (Figure 3.3) (Troufleau et al., 1997). The dimensionless $kB^{-1}$ parameter was formulated (Owen and Thomson, 1963) to account for this excess resistance against heat transfer, which relates the roughness lengths of heat and momentum transfer as follows;

$$e^{kB^{-1}} = z_{0m} / z_{0h} \tag{3.4}$$

Theoretically, $d + z_{0h}$ defines the level of the effective source of sensible heat (Thom, 1972) and hence $z_{0h}$ constitutes one of the most crucial parameters for accurate calculation of sensible heat flux (Su et al., 2001; Verhoef et al., 1997a). However, a high level of uncertainty is related to the determination of the values of $z_{0h}$ since it cannot be measured directly.


**Figure 3.3** An illustration showing the source height of heat ($d+z_{0h}$) and the sink height of momentum ($d+z_{0m}$) and their relation to displacement height ($d$) and the roughness lengths of heat ($z_{0h}$) and momentum transfer ($z_{0h}$).

Estimation of the values of $kB^{-1}$ and the question which variables it depends on has been subject of numerous studies (Beljaars and Holtslag, 1991; Blumel, 1999; Blyth and Dolman, 1995; Brutsaert, 1982; Massman and Weil, 1999; Troufleau et al., 1997; Verhoef et al., 1997a). While reviewing various formulations of $kB^{-1}$ for sparse vegetation, Verhoef et al. (1997a) highlighted that it is usually more difficult to obtain suitable roughness parameters ($z_{0m}$, $d$ and $kB^{-1}$) for sparse vegetation than for dense vegetation such as agricultural crops (see also Verhoef et al., 1997b).

A wide range of values has been found for $kB^{-1}$, particularly in sparse vegetation, by different studies. Kustas et al. (1989) reported that $kB^{-1}$ values observed over several natural sparse vegetation types in California ranged from 1 to 10, and that it was a function of ($T_0 - T_a$), and wind speed. Troufleau et al. (1997) used field data over fallow savannah and millet to analyse the behaviour of $kB^{-1}$ and the results indicated a large range, varying typically from zero to about 30 with even some negative values. Verhoef et al. (1997a) found negative values for bare soil up to values of about 15 for a fallow savannah in the Sahel.

Troufleau et al. (1997) conclude that both analytical and experimental studies agree on the fact that the $kB^{-1}$ value depends on too many parameters and variables, including structural parameters (e.g. vegetation roughness parameters), environmental conditions (e.g. wind speed, surface

temperature), and also the level of water stress, to allow for prediction of $kB^{-1}$ in an operational way (e.g. for weather forecasting purposes). However, none of the $kB^{-1}$ models or equations presented in the literature so far incorporated any information on the level of water stress, which may play an important role especially for sparsely vegetated conditions, as will be detailed in Section 3.3.3.

### *3.3.2 SEBS model and data*

The Surface Energy Balance System (SEBS) was developed by Su (2002) for the estimation of atmospheric turbulent fluxes and the daily evapotranspiration using satellite earth observation data. SEBS consists of a set of equations for the estimation of the land surface physical parameters and variables, such as albedo, emissivity, vegetation coverage, land surface temperature etc., from spectral reflectance and radiance data (Su et al., 1999). It also includes an extended model for the determination of the roughness length for heat transfer (Su et al., 2001).

The evaporative fraction is estimated on the basis of the energy balance at limiting cases. Here we will only focus on the roughness length for heat transfer model and the calculation of sensible heat flux by SEBS. The details of the original SEBS formulation can be found in Su et al. (2001) and Su (2002).

In Su (2002), $H$ is obtained iteratively by solving a set of non-linear equations (Eqs. 3.5-11) and is constrained to the range determined by the sensible heat flux at the wet limit $H_{\mathrm{wet}}$, and the sensible heat flux at the dry limit $H_{\mathrm{dry}}$. In order to derive $H$, Monin-Obukhov similarity (MOS) theory is used. The roughness height for heat is calculated based on the roughness height for momentum through $kB^{-1}$. SEBS uses a physically-based model for calculating $kB^{-1}$ (Su et al., 2001) (Eq. 3.8), which mainly follows the approach of Massman and Weil (1999), but differs from it by applying a weighted average between the limiting cases of full canopy in Eq. 3.10 (Choudhury and Monteith, 1988), bare soil conditions in Eq. 3.9 (Brutsaert, 1982) and mixed vegetation in Eq. 3.11, through the implementation of a fractional coverage term.

$$H = \rho_a C_p \frac{(\theta_o - \theta_a)}{r_{ah}} \tag{3.5}$$

$$r_{ah} = \frac{\ln(h/z_{0h}) - C_w}{k u_*} \tag{3.6}$$

$$z_{0h} = z_{0m} \Big/ \exp(kB_{SEBS}^{-1}) \tag{3.7}$$

$$kB_{SEBS}^{-1} = kB_c^{-1} f_c^2 + kB_m^{-1} f_s \; f_c \; + f_s^2 kB_s^{-1} \tag{3.8}$$

$$kB_s^{-1} = 2.46(\mathrm{Re}_*)^{1/4} - \ln(7.4) \tag{3.9}$$

$$kB_c^{-1} = \frac{kC_d}{4C_t \beta \left(1 - e^{-n/2}\right)} \tag{3.10}$$

$$kB_m^{-1} = \frac{k\beta z_{0m}}{C_t^* h} \tag{3.11}$$

In the above equations, $\rho_a$ is the density of air [kg m$^{-3}$], $C_p$ is the specific heat of dry air [J kg$^{-1}$ K$^{-1}$], $r_{ah}$ is the aerodynamic resistance [s m$^{-1}$], $\theta_0$ and $\theta_a$ are the potential temperatures of the land surface and air [K], $k$ is the von Karman constant, $u_*$ is the friction velocity [m s$^{-1}$], $h$ is the height of the vegetation [m], $z_{0h}$ is the roughness height for heat [m], $C_w$ is the MOS atmospheric stability correction term, $z_{0m}$ is the roughness height for momentum [m], $f_c$ is fractional canopy coverage, $f_s$ is the fractional soil coverage ($f_s$ = 1 - $f_c$), $Re_*$ is the roughness Reynolds number, $C_d$ is the drag coefficient of the leaves, $C_t$ is the heat transfer coefficient of the leaves, $\beta$ is the ratio between the friction velocity and the wind speed at canopy height, $n$ is the cumulative leaf drag area, and $C_t^*$ is the heat transfer coefficient of the soil.

SEBS requires three sets of input data: (1) products derived from remote sensing data: albedo, emissivity, land surface temperature, Normalized Difference Vegetation Index (*NDVI*) and/or Leaf Area Index (*LAI*); (2) meteorological variables collected at a reference height (air pressure, temperature, relative humidity, wind speed, sunshine hours); and (3) atmospheric radiation fluxes (downward shortwave radiation, downward longwave radiation).

### a. EO and meteorological data used in the case study

In this study, MODIS level 1B data (visible and near infrared bands 1 to 7 with 250-500 m spatial resolution, thermal emissive bands 31 and 32 with 1 km spatial resolution) and the MODIS LAI product (MOD15A2) were used to retrieve the necessary EO-based parameters for the SEBS model, corresponding to the satellite overpass for 42 cloud-free days between March and October 2010. The Konya basin is located in MODIS window h20v05.

To provide the land surface temperature input ($T_0$) for SEBS, we used a split window technique to calculate $T_0$ based on the equation of (Sobrino and Raissouni, 2000), which uses the derived emissivities and the band brightness temperature to calculate $T_0$. The MODIS level 1B data (visible and near infrared bands) were atmospherically corrected using the SMAC algorithm (Rahman and Dedieu, 1994), for the calculation of albedo (Liang, 2001) and emissivity (Sobrino et al., 2003). Additionally, the down-welling short-wave radiation flux ($R_{swd}$) was obtained from the LSA_SAF facility by EUMETSAT, which provides half-hourly radiation products from the MSG/SEVIRI instrument.

The meteorological driving data were obtained from the Turkish Meteorological Service for the 18 stations located in and around the basin. All data were spatially interpolated before serving as input to the SEBS model. As the air temperature at the time of satellite overpass is one of the most sensitive inputs in the calculation of sensible heat, the hourly temperature data were analysed in terms of local lapse rate to account for elevation changes in the mountainous region. For the other meteorological data, a trend surface analysis that minimizes the residual error with the observations was used for the spatial interpolation.

For the case of the Konya basin, the SEBS model was implemented with the freeware ILWIS software, which can be downloaded from the web portal of 52°North Initiative for Geospatial Open Source Software GmbH (http://52north.org/). All the modules of SEBS model are available in ILWIS, which allows extracting and processing the necessary RS data, solving and providing the outputs of energy balance terms and daily *ET*.

**b. Soil moisture data used in the case study**

Both field and remotely sensed data of soil moisture were used in this study. The field observations of soil moisture were obtained from the sensors installed at 5 cm depth at each Bowen ratio station. The daily average values of half hourly *SM* measurements were used in the analyses. For mapping the spatial distribution of soil moisture, the daily 0.25 degree surface soil moisture data product from AMSR-E observations (Owe et al., 2008) was used in this study. The *SM* product is derived according to the Land Surface Parameter Model (LPRM) (Owe et al., 2008), which uses a dual polarized channel (either 6.925 or 10.65GHz). The data set has global spatial coverage

and is provided twice a day (ascending retrieval during day time, descending retrieval during night time). Owe et al. (2008) also present the validation of the product with ground observations and discuss consistency with the other global retrieval products. Although they report that the satellite and ground data agree quite well, they also mention the limitations of such validation exercises, especially due to differences in spatial and vertical resolutions and differences in acquisition times. For this study, we used the descending retrievals, which had an overpass time around 11 p.m. (GMT time). To be able to calculate yearly minimum and maximum *SM* distributions in the Konya basin, a total of 88 days of *SM* retrievals (with 2 to 5 daily intervals) were used from March to November 2010. For the integration of *SM* into the mapping of daily *ET*, a relative *SM* ($SM_{rel}$ in Eq. 3.14) map was created based on the minimum and maximum *SM* distributions in 2010, and volumetric *SM* retrieval on 8th August, 2010. The data were obtained from the ADAGUC web portal hosted by VU University, Amsterdam (http://geoservices.falw.vu.nl/adaguc/ )

### *3.3.3 Soil moisture integrated SEBS: a new approach in the calculation of sensible heat*

Our field measurements of near surface soil moisture and evaporative fraction (i.e. the ratio of latent heat to available energy) confirmed a strong relationship between the near-surface soil moisture content and the partitioning of available energy (Figure 3.4).

There have been recent efforts such as the study by Miralles et al. (2011) towards integrating soil moisture stress in estimating the global land-surface evapotranspiration through modifying the Priestley and Taylor (1972) equation, a semi-physical method to calculate potential *ET*, with an empirical stress factor parameterized from soil moisture characteristics. However, current physically-based surface energy balance models, including SEBS, do not explicitly incorporate soil moisture data, but assume that its information is implicitly incorporated in the land surface temperature state variable used in the calculation of sensible heat flux. Here, we propose an explicit integration of *SM* information as a water stress index through a modified definition of $kB^{-1}$, since the vertical distribution of the sources of sensible heat change considerably under increasing levels of water stress, as explained below.

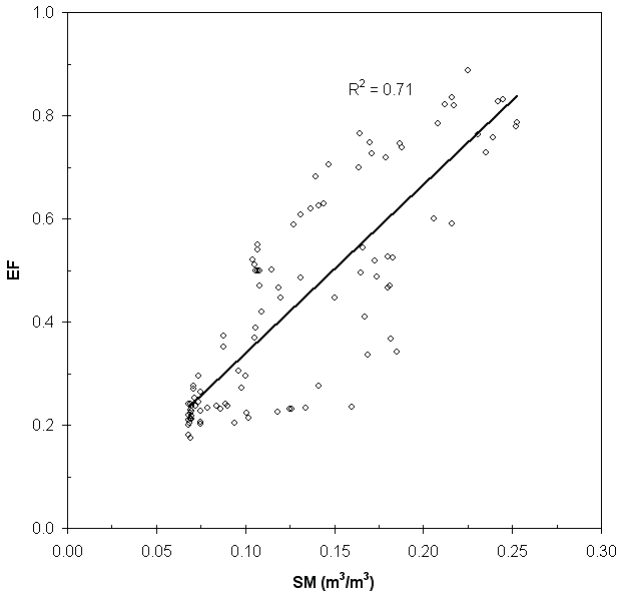


**Figure 3.4** Relationship between near-surface soil moisture content and evaporative fraction for the Konya Basin, Turkey. *SM* is soil moisture daily average values of half hourly measurements at 5cm depth; *EF* is evaporative fraction calculated from day-time averages of half hourly Bowen ratio measurements at BR3 and BR4 stations for sandy soils and clear sky days in 2010.

When using the remainder of the energy balance ($R_n$ - $H$ - $G_0$) to estimate $ET$ by e.g. using the set of formulations given in Eqs. 3.5-11, we face the problem that the equation for $H$ does not contain a variable that is a direct estimator of plant water stress, such as surface resistance, $r_s$, in the Penman-Monteith equation or in the bulk transfer equation for evapotranspiration. In these equations, plant water stress causes a decrease in stomatal conductance, leading to increased values of $r_s$.

We therefore propose to include information on the water stress level in the $kB^{-1}$ model used by SEBS, which already incorporates vegetation-related structural parameters and environmental conditions (wind speed and friction velocity). In addition to these, we take explicitly into account that water stress will increase $z_{0h}$, i.e. the source of heat, thereby reducing $kB^{-1}$, assuming $z_{0m}$ stays the same.

The reason for this can be explained as follows. Stomatal control is more efficient for the top layers in a canopy where the aerodynamic resistance is at

a minimum. Top leaves have more vigor and have higher stomatal conductance values, $g_s$, under non-water stressed conditions, i.e. when $T_0 \sim T_a$. The leaves higher in the canopy with greater conductance are also subject to greater evaporative demands. In these leaves, the potential water loss rate is disproportionately greater than in the lower canopy (e.g., Hinckley et al., 1994), indicating that stomata may exert increasingly greater control over water use with increasing irradiance in the canopy, i.e. when we move from the bottom to the top of the canopy (Niinemets et al., 1999).

Under water-stressed conditions stomata of leaves nearer to the top of the canopy will close progressively, and $T_0$ will increase much more in the top layers than in lower layers since the available energy is higher near the top. It is expected that lower canopy layers have less fluctuations in $T_0$-$T_a$, which means that as plant water stress intensifies the source of heat will increasingly move towards the top of the canopy, thereby increasing $z_{0h}$ and thus reducing $kB^{-1}$.

There is, indeed, experimental evidence in the literature showing that leaf exposition to different levels of irradiance within the canopy may alter foliage responses to water stress through structural and physiological responses. An example is the work by (Niinemets et al., 1999) who found that stomatal conductances reached in conditions of severe water stress were relatively lower in the upper than in the lower canopy in two natural mixed deciduous tree stands composed of shade-intolerant *Populus tremula* L. and shade-tolerant *Tilia cordata* Mill. Similar findings have been reported for crops.

Furthermore, if water stress becomes so severe that temporary wilting occurs, this will in addition cause $z_{0m}$ to go down as the effective $LAI$ and plant breadth decrease when leaves start to droop. These structural parameters play an important role in determining $z_{0m}$ and $d$ (see Raupach, 1994; Verhoef et al., 1997b). This effect will contribute to a decrease in $kB^{-1}$ under water-stressed conditions, although the increased light levels for the deeper canopy layers may partly counteract this, unless these leaf layers have also reached the temporary wilting stage.

Note that the drying out of the soil due to evaporation, before plants start to experience water stress and hence reduce their transpiration, will cause the soil surface to become a more prominent source of heat through an increase

in $T_0$, especially for sparse canopies. This would bring $z_{0h}$ down and hence increase $kB^{-1}$ with diminishing soil moisture levels. However, this effect is only important until the near-surface soil layer has dried out to such an extent that a hydraulic discontinuity develops, thereby avoiding further drying. Thereafter, the soil will not act as an important source of heat, rather its influence will stay constant, and the effect of the canopy water stress will take over.

Taking these considerations into account, the SEBS $kB^{-1}$ value is modified using a scaling factor, $SF$, represented by a sigmoid function;

$$kB^{-1} = SF \times kB^{-1}_{SEBS} \tag{3.12}$$

where

$$SF = a + \frac{1}{1 + \exp(b - c \times SM_{rel})} \tag{3.13}$$

$a$, $b$, $c$ are the coefficients of the sigmoid function, which e.g. can be determined from an optimization by reducing the error between observed and modelled sensible heat flux values from BR stations and SEBS. We used root mean square error (RMSE) and normalized RMSE for quantifying the errors and determining the optimum coefficient values. The water stress level is determined using a relative soil moisture value, $SM_{rel}$;

$$SM_{rel} = \frac{SM - SM_{min}}{SM_{max} - SM_{min}} \tag{3.14}$$

Here, $SM_{rel}$ is the relative soil moisture, $SM$ the actual soil moisture in [$m^3$ $m^{-3}$], $SM_{min}$ and $SM_{max}$ are minimum and maximum soil moisture in [$m^3$ $m^{-3}$]. The $SM_{min}$ and $SM_{max}$ values can be obtained using a time series analysis of the soil moisture data on annual or long-term basis. In the Konya basin case, annual minimum and maximum values of $SM$ were considered. Also, RS data of soil moisture with high temporal resolution will help to determine the $SM_{min}$ and $SM_{max}$ values of soil moisture explicitly for each pixel. This means that relative soil moisture values can be determined for different soil types, and represent the specific water stress conditions of each pixel.

A sigmoid function for $SF$ (Figure 3.5) was selected because it considerably lowers the $kB^{-1}$ value for relatively dry conditions ($SM_{rel}$ is approaching 0), while soil moisture influence on the value of $kB^{-1}$ is not significant for wet

conditions ($SM_{rel}$ approaching 1). Hence, it both fits to the conceptual framework for water-limited evapotranspiration regime better (Figure 3.1) and also allows the contrasting behaviour of the irrigated fields and the extremely dry landscape surrounding them to be distinguished.

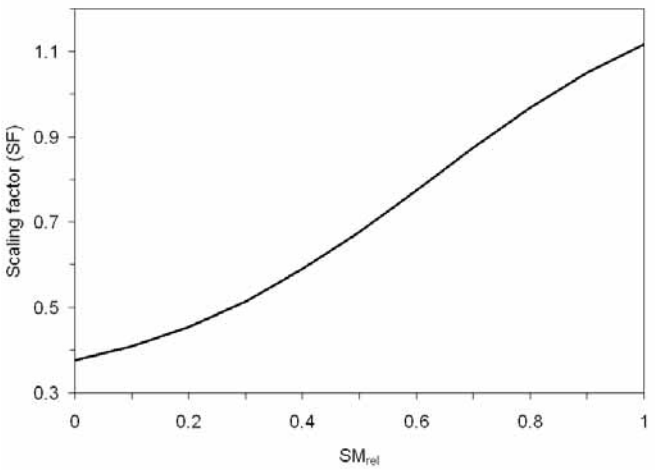


**Figure 3.5** The scaling effect of soil moisture to the $kB^{-1}$ parameter in SEBS under different levels of relative soil moisture content.

The minimum and maximum scaling boundaries of the sigmoid function were adjusted through changing the values of the coefficients (*a*, *b* and *c*) and minimizing the error between observations and model outputs (RMSE and rRMSE). All of the four BR station data, representing different land cover conditions, were combined to obtain optimum coefficients for the sigmoid function so that it can be applied over the entire region. Hence, Figure 3.5 represents an average sigmoid function. Figure 3.5 shows that the upper boundary can even be slightly above 1. This makes sense when taking into account the plant physiological discussion (Niinemets et al., 1999), and the initial effect of soil evaporation before water stress, slightly lowering rather than increasing $z_{0h}$, presented above.

## 3.4 Results and discussion

### 3.4.1 Comparison of BR observations with original and soil moisture integrated SEBS

To be able to analyse if integrating soil moisture into SEBS via $kB^{-1}$ improves the sensible heat estimates in this semi-arid region, *H* measurements from

the BR stations were compared with the $H$ calculated by the original SEBS (Figure 3.6a) and the soil moisture integrated SEBS (Figure 3.6b) for the land covers of sparse steppe, agricultural crops (potato and alfalfa) and wetland. Figure 3.6a indicates a clear underestimation of $H$ by the original SEBS ($H_{SEBS}$), especially for the high ranges of $H$, compared to field results from BR ($H_{BR}$). The grey-shaded area represents the largest underestimations of sensible heat, which implies that underestimation occurs especially for sparse steppe land cover and also partly for agricultural crops. The calculated $H_{SEBS}$ match best with the $H$ measurements for the wetland land cover, where sensible heat flux is generally low and water stress will be negligible.

By fitting the sigmoid function for an optimum $kB^{-1}$ definition, the parameters $a$, $b$, $c$ were obtained as 0.3, 2.5 and 4, respectively. As a result, much better agreement was obtained between $H_{BR}$ and $H_{SEBS\text{-}SM}$ (Figure 3.6b). There is still some scatter around the 1:1 line but the SM-integrated SEBS (SEBS-SM) captures the high values of $H_{BR}$ for sparse steppe much better, while it works well also for the lower $H_{BR}$ ranges as observed for wetland and crops. Yet, despite the clear overall improvement in the $H$ calculation, some largely underestimated values of $H$ are still visible in the grey shaded area of the plot, for sparse steppe and agricultural crops.

To further analyse why there are still large differences for sparse vegetation cover between $H_{SEBS\text{-}SM}$ and $H_{BR}$ values for these points, the sensible heat fluxes were plotted against the time series of soil moisture field measurements (Figure 3.7a), and temperature gradient $T_0$-$T_a$ (Figure 3.7b). Figures 3.7a and 3.7b show that the difference between $H_{BR}$ and $H_{SEBS\text{-}SM}$ is the largest either for the periods immediately after some intensive rain events (grey-shaded area in Figure 3.7a) and/or when the $T_0$-$T_a$ gradient is relatively small (grey-shaded area in Figure 3.7b).

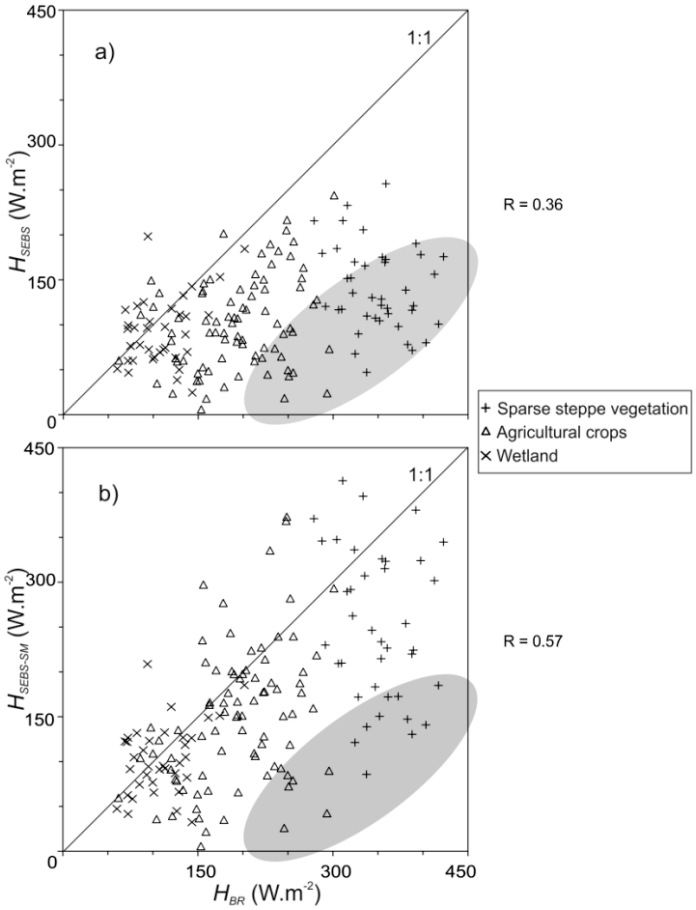


**Figure 3.6** Comparison of observed $H$ from BR stations with (a) the original SEBS and (b) the SM-integrated SEBS. R indicates the correlation coefficient.

As explained in Section 3.3.3, near surface soil moisture becomes an important source of evaporation after rain events, in particular under sparse vegetation conditions. Furthermore, increased SM values also lead to higher stomatal conductance and transpiration, which would fit with the relatively lower sensible heat flux values predicted by SEBS-SM. Therefore, for the periods after rainfall events when the water availability is high for latent heat flux i.e., evapotranspiration, the lower $H_{SEBS-SM}$ estimates are likely to be closer to reality than very high $H_{BR}$ values measured by the Bowen ratio station (grey-shaded area in Figure 3.7a).

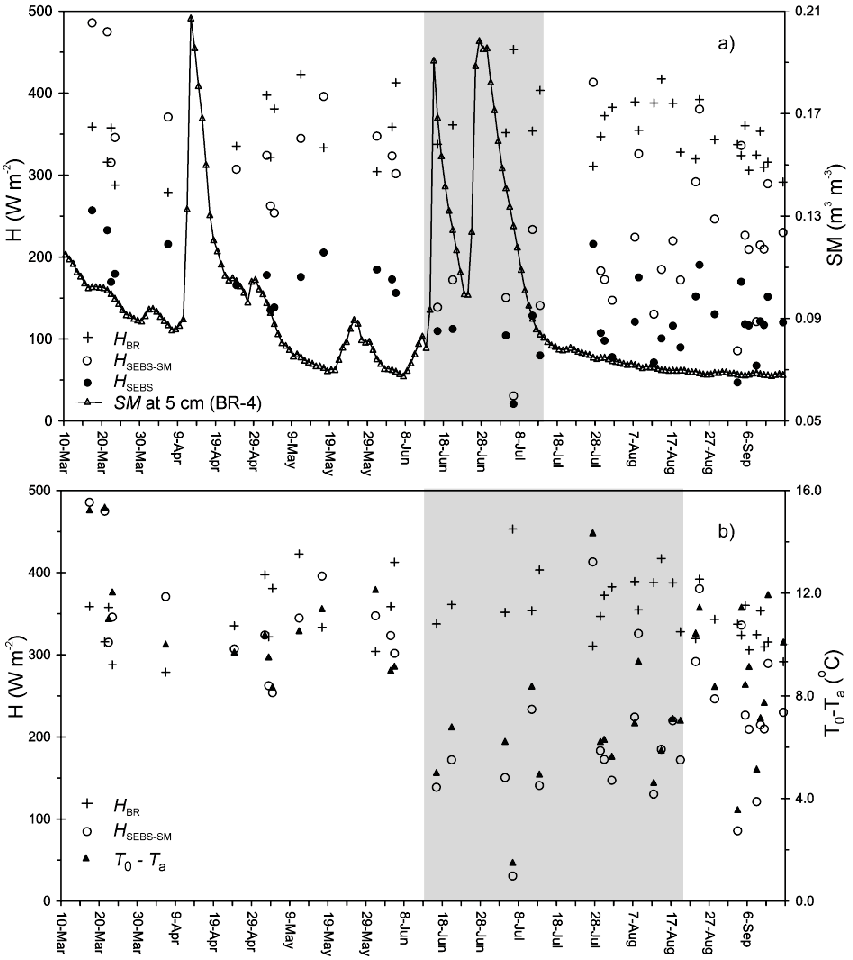


**Figure 3.7** Time-series of measured day-time average $H_{BR}$ (plus) and estimated $H_{SEBS}$ (filled circle) and $H_{SEBS\text{-}SM}$ (circle) compared with (a) the near-surface soil moisture measurements (triangle) and (b) the temperature gradient ($T_0$-$T_a$) for sparse steppe (BR-4).

However, some important differences are also observed during the long dry period after mid-July for the sparse steppe vegetation (Figure 3.7a & b). These days correspond to lower $T_0$-$T_a$ values ranging from 1.5 (6$^{th}$ July) to 6.3 K (30$^{th}$ July). As shown in Eq. 3.3, $T_0$-$T_a$ is the driving force for the sensible heat transfer and especially for low $T_0$-$T_a$ values, $H$ becomes less sensitive to the magnitude of aerodynamic resistance ($r_{ah}$) presented in the denominator in Eq. 3.3. Hence, the $T_0$-$T_a$ gradient has a more dominant role in the magnitude of $H$. In such cases, the integration of *SM* into SEBS in the calculation of $H$,

through modifying the $r_{ah}$, becomes less effective due to low $T_0$-$T_a$ values provided to SEBS. As a result, SEBS-SM still calculates relatively low $H_{SEBS\text{-}SM}$ values similar to the original $H_{SEBS}$ (e.g. some of the points shown between end of July and mid-August in Figure 3.7a) even though the BR station measurements (for sparse steppe vegetation) indicate very high $H_{BR}$ values, which makes sense for these extended dry periods. This finding implies that the land surface temperature ($T_0$) signal from RS and the resultant ($T_0$-$T_a$) input value to SEBS for the pixel does not reflect the local conditions around the BR station for these particular days and $T_0$ measured by RS for the pixel is possibly affected by some other sources.

In fact, the time series of soil moisture and sensible heat fluxes $H_{SEBS\text{-}SM}$ and $H_{BR}$ in the adjacent alfalfa field (BR-3 in Figure 3.2) in Figure 3.8 clearly indicate that supplementary irrigation took place at the end of July, which can cause considerable advection between the neighbouring irrigated fields and the dry sparsely vegetated steppe area. This, in turn, can greatly affect the land surface temperature signal measured by MODIS satellite for these two adjacent pixels depending on the viewing angles of the sensor and can explain the persistently large error for certain days. Geometric corrections (e.g. registration and resampling of pixels) employed by the MODIS team can contribute some additional error, especially for adjacent pixels.

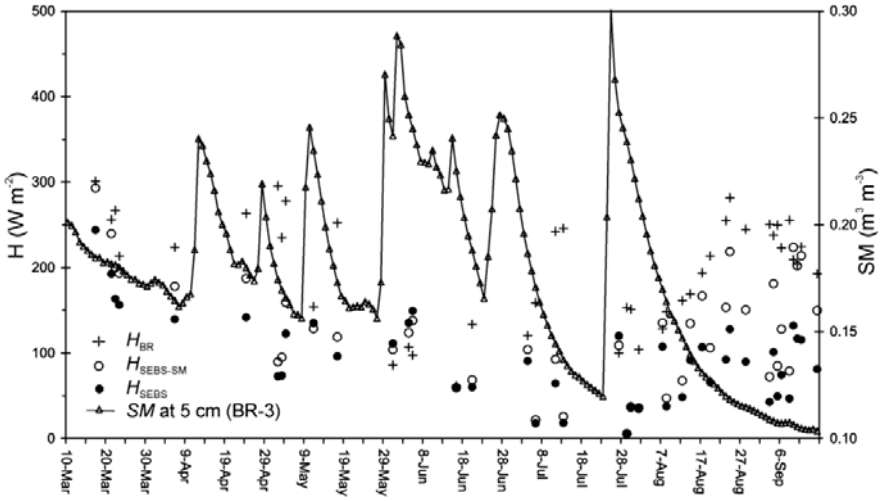


**Figure 3.8** Time-series of measured day-time average $H_{BR}$ (plus symbol) and estimated $H_{SEBS}$ (filled circle symbol) and $H_{SEBS\text{-}SM}$ (circle symbol) compared with the near-surface soil moisture measurements for alfalfa field (BR-3) during the study period.

In addition to these specific factors (especially for the case of sparse vegetation), there are also more generic factors that can cause uncertainties in comparing point-based BR observations with the pixel-based SEBS outputs. The possible error sources and uncertainties are further analysed in Section 3.4.2.

### *3.4.2 Error evaluation*

Based on the *H* measurements from the BR stations, RMSE (Eq. 3.15) and rRMSE (Eq. 3.16) values for original SEBS and SEBS-SM were compared, to assess the effect of including soil moisture in the *H* calculation (Table 3.1).

$$RMSE = \sqrt{\frac{\sum_{i=1}^{n}(X_i - \bar{X}_i)^2}{n}} \tag{3.15}$$

$$rRMSE = \left(\frac{RMSE}{\bar{X}_{\max} - \bar{X}_{\min}}\right) * 100 \tag{3.16}$$

Here, $X_i$ is the model estimation, $\bar{X}_i$ is the observation from the BR stations, $n$ is the number of the samples, $\bar{X}_{\max}$ and $\bar{X}_{\min}$ are the maximum and minimum observations, respectively.

The results indicate not only a clear improvement for sparse vegetation with a large reduction in RMSE (and 40% reduction in rRMSE); there is also a slight improvement for the agricultural crops while keeping the good results (low RMSE values) for the wetland. As a result, there is an overall improvement of 40 W m$^{-2}$ (and 10% in terms of rRMSE) when soil moisture is incorporated explicitly in the calculation of sensible heat by SEBS.

***Table 3.1*** Absolute and relative root mean square error of *H* (RMSE and rRMSE) comparison between the original SEBS ($RMSE_{SEBS}$) and the *SM*-integrated SEBS ($RMSE_{SEBS\_SM}$). *H* estimates from the original SEBS and the SEBS-SM were compared with the *H* observations from the BR stations. *n* is the number of samples.

| Land cover | *n* | $RMSE_{SEBS}$ [W m$^{-2}$] | $rRMSE_{SEBS}$ | $RMSE_{SEBS\_SM}$ [W m$^{-2}$] | $rRMSE_{SEBS\_SM}$ |
|---|---|---|---|---|---|
| ***Sparse steppe*** | 42 | 226.1 | 129.7 | 153.8 | **88.2** |
| ***Crops*** | 83 | 113.0 | 47.2 | 90.7 | **37.9** |
| ***Wetland*** | 36 | 44.1 | 31.1 | 42.1 | **29.7** |
| ***Overall*** | **161** | **142.7** | **36.3** | **103.9** | **26.4** |

However, except for the wetland which has less than 50 W $m^{-2}$ RMSE, the overall RMSE of 100 W $m^{-2}$ is relatively high, mainly due to high RMSE values for sparse vegetation even when soil moisture is integrated to SEBS. This is partly caused by the fact that very high values of $H_{BR}$ are observed for bare land or sparse vegetation in semi-arid regions (up to 450 W $m^{-2}$ in the Konya basin during the day-light hours), which also causes larger errors in absolute terms. In fact, in terms of relative RMSE, which could be a better indicator for operational implementation, SM-integrated SEBS has an acceptable overall rRMSE value of about 25 % with an improvement of 10 % compared to the original SEBS.

Comparison of RMSE values allows comparing the performance of SEBS with and without integration of soil moisture to the BR measurements. The $H_{BR}$ measurements are assumed to be correct values in the analyses, upon which all the error quantification is based. Possible errors due to deficiencies in the BR system setup, differences in spatial representativeness of BR and SEBS, the inaccuracies in the input variables of SEBS (which can propagate into the model results), are not explicitly accounted for in the comparison. The major possible error sources are elaborated in further detail below.

Firstly, the spatial representativeness of the BR measurements and the SEBS calculations are different. If we consider the fetch guidelines by Brutsaert (1982) and Shuttleworth (1992), a BR station has a source area up to approximately 100 times the upper sensor's height, which makes 200 m the upper limit for our experimental set-up (top sensor was at 2 m height). We also carried out a foot print analysis for the BR stations 3 (alfalfa field) and 4 (sparse steppe vegetation) based on an approximate analytical model by Hsieh et al. (2000) and the results indicated that 80% of the total flux measured by both BR-3 and 4 originated from a source area ranging between 80 to 220 m in the wind direction during the study period. Because we respected the fetch requirements of homogeneous land cover for a distance more than 200 m while establishing the stations, we can assume that the BR flux measurements were representative of the homogeneous land cover they were installed in. On the other hand, due to the use of MODIS thermal band data in quantifying land surface temperature, SEBS had a fixed output pixel size of 1 $km^2$, which is much larger than the source area of a BR station. Due to this large grid size, SEBS outputs represent a different source area in terms of spatial dimensions which will contain more heterogeneity in land cover

compared to the BR stations. Therefore, there is a certain amount of error due to the difference in terms of spatial coverage of the two methods and the heterogeneity in the large grid output provided by SEBS.

Secondly, BR measurements and therefore also the $H$ measurements, are based on temperature and humidity measurements from the sensors at two heights in each station. However, in the SEBS calculations, the land surface temperature from MODIS thermal bands and air temperature data from 18 meteorological stations in the study area were used as the input in the calculation of $H$. Although they should not necessarily match perfectly in terms of temperature gradient, the air temperature measurements from the weather stations (used in SEBS) and the temperature measurements at the upper sensor of each BR station are assumed to be in a similar range, since both were measured at around 2 m reference height. Spatial interpolation errors in air temperature from the meteorological stations and measurement errors of temperature sensors at BR stations occasionally cause contradicting temperature gradients and $H$ results. This explains some of the mismatches observed in Figures 3.6 and 3.7.

Thirdly, for the calculation of $H_{BR}$, BR values from half hourly measurements were averaged over the day-light hours. Assuming that the evaporative fraction stays constant during cloud-free day-light hours with a concave-up during sunrise and sunset due to lower available energy (Crago, 1996; Gentine et al., 2007), which is also confirmed by our half hourly BR measurements (Figure 3.9), $H_{BR}$ was calculated by multiplying the daytime average $EF_{BR}$ with the daytime average net radiation. The net radiation is assumed to be the same as calculated with SEBS, since there was no measurement of net radiation at the BR stations. Therefore, rather than a direct flux measurement, $H_{BR}$ is calculated from the average evaporative fraction values obtained through BR measurements. In contrast, SEBS solves the surface energy balance instantaneously at the time of satellite overpass, while it upscales the instantaneous solution to daily $ET$ by assuming a constant evaporative fraction during the day. Therefore, the sensible heat flux calculation by SEBS represents the temperature gradient at the time of satellite overpass. As a result, some error can be attributed to the difference in the calculation of $H$ by SEBS and BR methods, although this error will be limited since this study was only conducted for cloud-free days, when the evaporative fraction is indeed relatively constant.

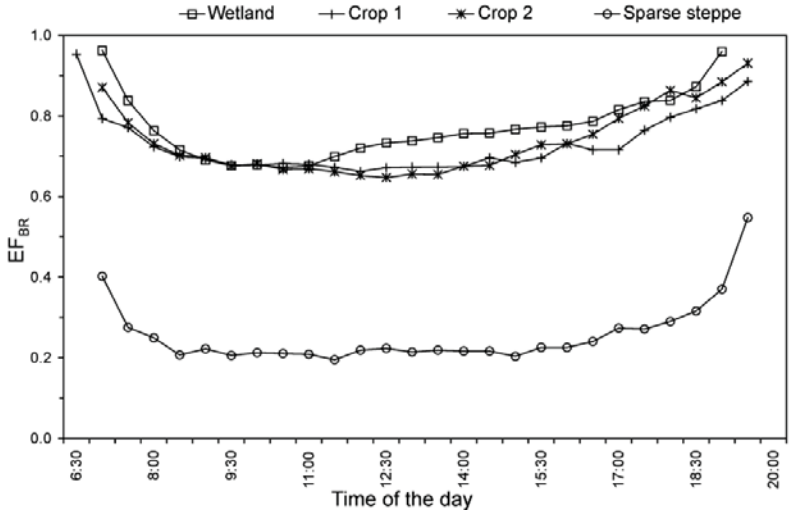


**Figure 3.9** Diurnal change of evaporative fraction over different land covers. Shown here is the average of clear sky days in July 2010 based on half hourly BR measurements.

Finally, if we look at the accuracy of the temperature measurements as one of the most sensitive variables for both SEBS and BR, the accuracy of the temperature/humidity sensor used in the BR stations is reported to be 0.5 °C for the measurement range between 5-40 °C, and up to 1 °C for the rest, while ±2% for the relative humidity (Decagon Devices, WA, USA). As explained in the field setup section, the sensors used in the BR stations were inter-calibrated before installation to avoid a possible bias, since the focus of the BR method is on the gradient and the relative accuracy rather than the absolute accuracy of the measurements. However, we can still consider a possible total error of 1 °C in the temperature gradient measured by the BR station based on the reported sensor accuracies for the average conditions during the study period excluding the winter season. By comparison, an observation precision uncertainty of less than 2 K is generally reported for atmospherically corrected surface temperature obtained from remote sensing (French et al., 2005; Timmermans et al., 2007), which is the most sensitive input parameter for SEBS. Indeed, Su (2002) indicates the sensitivity of $H$ to be $\Delta H = 10\ \Delta(T_0\text{-}T_a)$ on average (value of 10 can change depending on the aerodynamic resistance), which would mean an error of up to 30 W $m^{-2}$ considering a maximum error of 3 K in the temperature gradient assuming an extra error of 1 K from air temperature measurements. Also, adding the hypothetical total error of 1 K from BR measurements, a total error of

40 W $m^{-2}$ could potentially result from temperature-related error sources in the calculation of *H*.

### *3.4.3 Daily ET mapping by SM-integrated SEBS*

The main aim of this study was to improve the regional *ET* mapping by SEBS for semi-arid regions through operational integration of soil moisture in the calculation of sensible heat flux by the model. Figures 3.10a and 3.10b show the daily *ET* maps generated by SEBS without and with integration of soil moisture information, respectively, on a dry summer day in August 8$^{th}$, 2010. As Figure 3.10a indicates, the original SEBS produced a daily *ET* map output with minimum values generally above 3.0 mm $d^{-1}$ (with an overall average of 5.6 mm $d^{-1}$ and std. deviation of 1.9 mm $d^{-1}$), which is in the range given by previous studies (Lubczynski and Gurwin, 2005; Timmermans and Meijerink, 1999; Van der Kwast et al., 2009). Considering this daily *ET* map belongs to a dry summer season and the precipitation is spatially ranging from 250 to 800 mm $year^{-1}$ in the region, a yearly *ET* map produced by the original SEBS would represent an overestimation for the non-irrigated and dry parts of the region. Furthermore, the large temperature gradient, reaching around 20 ℃ (Figure 3.10c), and bare to very sparsely vegetated conditions observed in a large part of the region (*LAI* map in Figure 3.10d) confirm very dry and water-limited conditions implying very low values of actual *ET* for this particular day.

In contrast, when soil moisture information from microwave remote sensing is integrated into SEBS, the model not only produced daily *ET* values lower than 2.0 mm $d^{-1}$ but also had a much higher spatial variability compared to original SEBS (with an overall average of 4.3 mm $d^{-1}$ and std. deviation of 2.4 mm $d^{-1}$) (Figure 3.10b). While the daily *ET* values are largely reduced for the drier and bare to sparsely vegetated parts in Figure 3.10b, the high *ET* values for densely vegetated parts or water surfaces are kept in the same range given by the original SEBS (Figs. 3.10a and b). In this regard, the daily *ET* map generated by the SM-integrated SEBS in Figure 3.10b reflects the overall contrast generally observed in semi-arid regions between the irrigated fields and the extremely dry surrounding landscape better (Gowda et al., 2007).

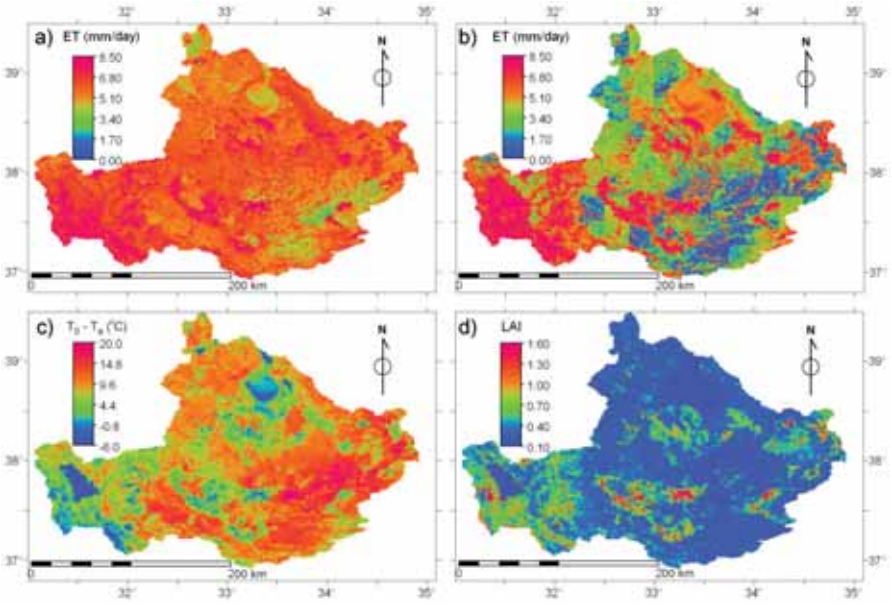


**Figure 3.10a)** Daily *ET* map obtained with the original SEBS, b) daily *ET* map from the SM-integrated SEBS, c) the temperature gradient and d) *LAI* distribution in August 8th, 2010, in the Konya basin

While field measurements of soil moisture were used in testing and validating the proposed method for integrating SM into the *H* calculation by SEBS, passive microwave measurements of SM were used in the final mapping of daily *ET* to achieve operational application. To be able to calculate the $kB^{-1}$ map that integrates the passive microwave *SM* data, first the relative *SM* (Eq. 3.14) was calculated based on the volumetric *SM* map of August 8th, 2010 and the $SM_{min}$, $SM_{max}$ maps that were obtained from the daily time series of passive microwave *SM* in 2010 from AMSRE satellite data. Next, the $kB^{-1}$ map was calculated using the relative *SM* map obtained from the passive microwave data and the scaling factor (*SF*) obtained from Eq. 3.13. The passive microwave *SM* data has a coarser spatial resolution (~ 25 km) compared to the MODIS thermal bands with 1 km resolution. Still, the integration of such coarse resolution *SM* data into the MODIS-based medium resolution input did not result in a considerable deterioration in the spatial resolution of the regional *ET* output map from SEBS-SM (Figure 3.10b). This is mainly due to the fact that *H* is obtained solving a set of non-linear equations (Eqs. 3.5-3.11) in SEBS using a number of input data including *SM* (section 3.3.2). In addition, the integration of *SM* in the $kB^{-1}$ calculation (Eqs.

3.12-3.14) was also implemented in a non-linear manner using a sigmoid function (Figure 3.5). Therefore, while the explicit integration of soil moisture data into SEBS affects greatly the daily *ET* output map, its influence on the daily ET output is not linear.

## *3.5 Conclusions*

Remote sensing models that obtain evapotranspiration, *ET*, from the energy balance do not take below-ground processes explicitly into account. The effects of soil evaporation, soil moisture redistribution, stomatal regulation and related transpiration, and interception storage are all implicitly incorporated in the resulting land surface temperature. This simplification is usually adequate where available energy is the limiting factor for *ET*, but problems appear when water availability becomes limiting for *ET*, which will often be the case in semi-arid regions. In this regard, although SEBS and other physically-based SEB models are found to work well for different kinds of crops and dense land covers, the daily evapotranspiration calculated by RS-based SEB models is often overestimated for sparse vegetation experiencing temporary water stress in (semi-)arid regions, as well as in sub humid regions (Figure 3.6).

This study integrated soil moisture data explicitly in the calculation of sensible heat flux by introducing a soil moisture dependent scaling factor in the parameter $kB^{-1}$ that plays a role in the aerodynamic resistance. The rationale behind this approach is based on plant physiology that plant water stress will have a relatively larger effect on the leaf layers near the top of the canopy. This will cause surface temperatures higher in the canopy to increase disproportionally under conditions of water stress. Hence the overall source level of heat transfer is located at a higher level, which reduces $kB^{-1}$.

The new approach was tested by comparing it with observations from BR stations. The results indicated not only a clear improvement for the case of sparse non-irrigated vegetation, with a large reduction in RMSE (and 40% reduction in rRMSE), but also a slight improvement for agricultural crops, while keeping the good results (low RMSE values) for the wetland areas. As a result, an overall accuracy improvement of 40 W $m^{-2}$ (and 10% in terms of rRMSE) was obtained when soil moisture is integrated explicitly in the calculation of sensible heat flux by SEBS.

Finally, to test if the new approach provides an important operational improvement for regional *ET* mapping, microwave soil moisture data were integrated into SEBS for mapping daily *ET* in a semi-arid region. The daily *ET* map generated by SM-integrated SEBS captured the low *ET* values observed in drylands better, and also reflected the overall contrast generally observed in semi-arid regions between the irrigated fields and the neighbouring dry areas better (Gowda et al., 2007). Additionally, despite the relatively coarse scale of passive microwave measurements compared to the thermal bands of MODIS, there was no important deterioration in the continuity of *ET* distribution (Figure 3.10b).

Further validation of the method will be carried out in Chapter 4 through quantifying the yearly water fluxes and analysing the closure of the water balance in the region.

The proposed integration of soil moisture into SEBS may require further tuning of the parameters of the sigmoid function through which the level of water stress is incorporated in the sensible heat calculation. Nevertheless, the new approach can also be applied in other regions or for regional, continental or global mapping of *ET*. Such an improved mapping of regional *ET* by SM-integrated SEBS has a large potential in providing a more accurate estimation of energy and water fluxes in continuously or seasonally water-stressed regions. This will contribute to a better understanding of the water cycle, water use and interrelations between hydrological fluxes and ecosystem functioning, especially in (semi-)arid regions.

# Chapter 4

## Assessing groundwater storage changes using RS-based evapotranspiration and precipitation

**Abstract**: We present a method which uses remote sensing based evapotranspiration and precipitation estimates with improved accuracies under semi-arid conditions to quantify a spatially distributed water balance, for analyzing groundwater storage changes due to supplementary water uses. The method is tested for the semi-arid Konya basin (Turkey), one of the largest endorheic basins in the world. The storage change estimated as the residual of the spatially distributed water balance was validated by the volume change calculated from groundwater table observations.

This chapter is based on:

Gokmen, M., Vekerdy, Z., Lubczynski, M. W., Timmermans, J., Batelaan, O., and Verhoef, W.: Assessing groundwater storage changes using RS-based evapotranspiration and precipitation at a large semi-arid basin scale, Journal of Hydrometeorology, 2013, doi:10.1175/JHM-D-12-0156.1.

## 4.1 Introduction

In arid and semi-arid regions, characterized by low precipitation (*P*) and high potential evapotranspiration (*PET*), the accurate knowledge of *P*, of actual evapotranspiration (*ET*) and the balance between the two (*P-ET*) as well as their spatio-temporal distribution are essential for sustainable management of the scarce water resources. In such dry, water-limited regions, groundwater (*GW*) is often the only reliable water resource.

Since the 1950's, groundwater resources of many arid and semi-arid areas have been affected by a number of non-climatic forcings, such as heavy groundwater abstraction for irrigation purpose. These often resulted in lowering of the groundwater table, reflecting a loss of aquifer storage (Green et al., 2011). If groundwater abstraction exceeds the net groundwater recharge over prolonged periods, persistent groundwater depletion occurs (Gleeson et al., 2010). For such cases, Wada et al. (2012) explicitly use the term non-renewable groundwater abstraction. The semi-arid Konya basin in central Anatolia (Turkey), which is one of the biggest endorheic basins in the world, is a typical example of groundwater resources under strong anthropogenic pressure. Over the last few decades, the basin experienced huge groundwater abstraction for irrigation, which caused approximately 1 m $year^{-1}$ head decline (Bayari et al., 2009).

Assessing the spatial and temporal distribution of hydrological fluxes using RS methods has been the focus of many recent research efforts (McCabe et al., 2008), because of their potential to provide spatially continuous and temporally recurrent estimates over regional to global scales (Alsdorf and Lettenmaier, 2003). Precipitation is regularly retrieved from multi-sensor microwave and infrared data using a variety of techniques (e.g., Joyce et al., 2004). One of the recent datasets is the Tropical Rainfall Measuring Mission (TRMM) Multi-satellite Precipitation Analysis (TMPA), which is designed to combine precipitation estimates from various satellite systems, as well as land surface precipitation gauge analyses where possible (Huffman et al., 2007). Furthermore, evapotranspiration can be determined from RS-based solutions of the surface energy balance (Su et al., 2005). Such global ET products from the RS retrievals are becoming increasingly available (Ghilain et al., 2011; Su et al., 2010; Vinukollu et al., 2011).

However, the capabilities of RS to "look below the ground surface" and to detect the groundwater conditions directly are limited (Green et al., 2011). One of the major exceptions to this is the satellite-based observations of earth's gravity field: changes in total surface and subsurface storage can be derived using gravity anomaly measurements with the GRACE satellites (Swenson and Wahr, 2002). However, with a spatial resolution of a few hundred kilometers this technique can provide changes of groundwater storage over regions of about 150,000 $km^2$ or larger at 10 daily to monthly temporal scale (Wahr et al., 2006). Therefore, in smaller regions or at a basin scale, where most of the water resources, meteorological, agricultural, and natural hazard investigations are carried out, satellite gravimetry is often not applicable. An alternative is to infer changes in the water storage (ΔS) by estimating the difference between *P*, *ET* and runoff (*R*) (Brunner et al., 2004), integrating remote sensing retrievals and ground measurements. Tang et al. (2010) followed such a methodology to assess the temporal variations of terrestrial *ΔS* from surface *P* observations, satellite-based *ET* estimation, and gauge *R* measurements for two major river basins, and found that human influences have extensively altered the natural hydrological processes and seasonal *ΔS* in the study area. Differently, exploring the feasibility of entirely RS-based water budget for a ground-data constrained basin, Armanios and Fisher (2012) concluded that such a purely RS-based methodology is more appropriate for long-term water resources assessment (e.g. annual scale) than an "instantaneous" or short-term one.

Estimates based on models or reanalysis (combinations of models and observations) make use of other methods to estimate the terrestrial water storage or the changes in water storage (*ΔS*). However, Tang et al. (2010) note that the main limitation in using the modelled terrestrial water storage is at the river basin scale, where water management (e.g. man-made reservoirs and irrigation water withdrawals) substantially affects the land surface hydrological dynamics, as these effects are not represented in most land surface models.

In this study, we propose a relatively simple method that integrates RS-based seasonal and yearly *P* and *ET* estimates with minimum ground data for assessing water balance and storage changes in a spatially distributed manner. The methodology is tested and applied for the large semi-arid Konya basin (approximately 54,000 $km^2$) where i) both human activities (agriculture) and

natural ecosystems are highly groundwater dependent and ii) the limited surface runoff is managed through man-made reservoirs for supplying irrigation. More specifically this study aims at:

1) Quantifying by remote sensing the spatiotemporal *P* and *ET* fluxes with improved accuracy under semi-arid conditions at the large basin scale, combining them with field data where needed and available.
2) Analysing the spatiotemporal water balance to assess water availability (surface runoff), consumptive water use (irrigation), *GW* storage changes and GW discharge using the spatially distributed, yearly *P*, *ET* fluxes.
3) Assessing the consistency and errors of RS-based water balance and storage change estimates with groundwater observations.

## 4.2 Materials and methods

### 4.2.1 Spatiotemporal distribution of precipitation

To quantify precipitation we estimated rainfall and snow water equivalent (*SWE*) separately, combining RS-based approaches and gauge measurements. The flowchart (Figure 4.1) explains the determination of the rainfall, the *SWE* and the total precipitation. The yearly precipitation was calculated per hydrological year (from 1 October to 30 September next year), and per season (the wet season covers 6 months between 1 October and 31 March, and the dry season covers 6 months between 1 April and 30 September).

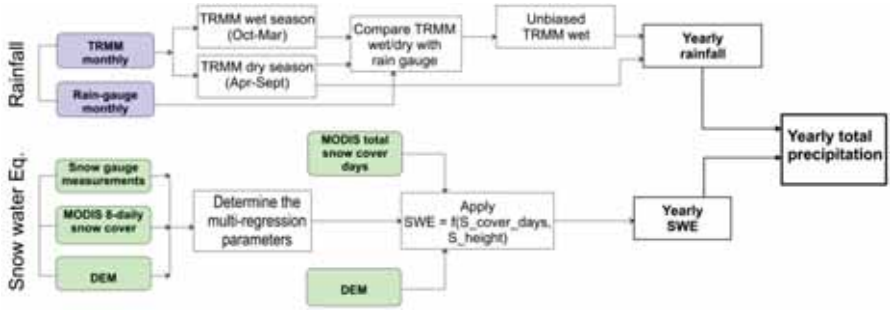


**Figure 4.1** Flowchart for determining the yearly rainfall, the snow water equivalent (*SWE*), and the total precipitation. All fluxes are in mm $y^{-1}$.

To estimate the rainfall distribution, we used the monthly product of the Tropical Rainfall Measuring Mission (TRMM-3B43) combined with local rain gauge measurements. The TRMM algorithm combines 4 independent sources: 1) monthly average TMI (TRMM Microwave Imager) estimate, 2) monthly

average SSM/I (Special Sensor Microwave/Imager) estimate, 3) the merged-infrared (IR) estimate, and 4) the monthly accumulated CAMS (Climate Assessment and Monitoring System) and GPCC (Global Precipitation Climatology Centre) rain gauge analysis. The TRMM 25 * 25 km gridded estimates extend from 50 degrees south to 50 degrees north (http://mirador.gsfc.nasa.gov/collections/TRMM_3B43__006.shtml) and have a temporal resolution corresponding to a calendar month.

Pan et al. (2008) indicated that TRMM products have large differences with ground observations at short time intervals (3-hourly) but the discrepancies become smaller as the aggregation time increases. They also reported a positive bias of the TRMM product. To ensure improved spatiotemporal rainfall estimation for the Konya basin, we first aggregated the monthly TRMM data to wet and dry season rainfalls, compared them with the gauge observations and where necessary, carried out a linear rescaling for correcting the bias. Also, we resampled the originally 25 km spatial resolution to 1 km resolution using bi-cubic interpolation in order to match it with the resolution of *ET* flux for the spatially distributed water balance analysis.

It should be highlighted that both, the TRMM rainfall product and the rain gauge observations (as they are not located at higher altitudes), do not sufficiently capture the snow-fall contribution to the total precipitation. In the TRMM-3B43 product document it is stated that the snowfall regions are identified through the use of AMSU-A measurements and falling snow is assigned a rate of 0.1 mm $hr^{-1}$ (Huffman and Bolvin, 2012). Due to the coarse resolution of AMSU-A (50 km at nadir, Prigent et al., 2005) and the mountainous topography of the study area, the TRMM-3B43 product was considered to be insufficient to detect the snowfall contribution in the Konya basin.

Direct, in-situ measurements and RS estimates of *SWE* (Serreze et al., 1999) are extremely limited (Tang et al., 2010). To date, most robust global data records for *SWE* are derived by satellite-based microwave sensor systems such as the Scanning Multi-Channel Microwave Radiometer (SMMR), the Special Sensor Microwave/Imager (SSM/I) and the Advanced Microwave Scanning Radiometer for the NASA Earth Observation System (AMSR-E) (Muskett, 2012). However, satellite-based SWE data and applications usually cover high latitudes (65°N and higher) and relatively flat terrains (e.g.

Biancamaria et al., 2008; Chang et al., 2005; Derksen et al., 2010), so those are not easily applicable to the Konya basin. Therefore, to estimate the spatiotemporal *SWE* in the Konya basin, we applied a multivariate linear regression approach. As dependent variables we used the available ground measurements from snow gauges within the basin (Figure 4.2). As independent variables we considered the total number of snow cover days from the 8-daily snow cover product of MODIS (MOD10A2) as well as the elevation of the location of snow measurements obtained from the digital elevation model. After determining the multivariate regression parameters for each year separately, we applied them using the inputs of total snow cover days from MODIS and the DEM of the basin to estimate the yearly total *SWE* distribution for each year during the study period (2005 - 2009).


**Figure 4.2** The locations and altitudes in m a.s.l. of the ground snow measurements around the Konya basin. The background image shows the total amount of snow cover days from MOD10A2 product in 2005-2006 (between October and April).

The data of in-situ snow measurements were obtained from the State Hydraulic Works (DSI) of Turkey (unpublished data). The snow measurements were conducted on a monthly basis (Figure 4.2) by DSI between October and May, recording the average snow depth, snow water equivalent and snow density values. In the multivariate regression analysis, we used the maximum snow depth and corresponding *SWE* values (usually occur in April/May) as the yearly *SWE* values, assuming the major snow melting occurs in spring and snow mainly stays in the solid state throughout the winter seasons. Finally, the total yearly precipitation was estimated by summing the bias-corrected yearly rainfall and the yearly *SWE*.

### *4.2.2 Spatiotemporal distribution of evapotranspiration*

#### a. Actual evapotranspiration

RS-based surface energy balance models are increasingly used to determine the distribution of evapotranspiration from field to global scales. The physically based and single source SEBS (Surface Energy Balance System) model (Su, 2002) is one of the widely used surface energy balance models, which has been applied in many regional to global studies (Jia et al., 2003; Jin et al., 2009; Ma et al., 2012; Ma et al., 2007; Oku et al., 2007; Pan et al., 2012; Pan et al., 2008; Vinukollu et al., 2011). The SEBS model estimates actual evapotranspiration (*ET*) using RS retrievals and in-situ measurements to define incoming surface radiation, surface skin temperature, surface meteorology, and surface and vegetation properties (Su et al., 2005). Latent heat flux, or equivalently evapotranspiration, is estimated considering the surface energy balance and the evaporative fraction.

Comparing three process-based models (i.e. SEBS, Penman-Monteith, Priestley-Taylor) to *ET* at the global scale, (Vinukollu et al., 2011) concluded that all of them appear to underrepresent the sensitivity to soil moisture over water limited regions, and because of that overestimate *ET*. To handle this problem, in this study we used besides SEBS a modified version of SEBS called SEBS-SM (Chapter 3) too, which additionally integrates soil moisture data in SEBS through incorporating a water stress index in a modified definition of the aerodynamic resistance. The details of the SEBS-SM are provided in Chapter 3, while the original SEBS is described in Su et al. (2001) and Su (2002).

Figure 4.3 provides a flowchart explaining the acquisition of daily, monthly and yearly *ET* by SEBS-SM. The SEBS-SM model was run on a daily interval using MODIS input data with 1 km spatial resolution on the thermal bands. The model output had some missing days, either due to cloud coverage or unreliable data, masked out by the quality control of the MODIS team, in the input variables such as emissivity or land surface temperature ($T_0$). For filling the *ET* data gaps, we implemented a monthly average compositing by dividing the sum of the available daily *ET* estimates by the number of days with available *ET* estimates for each pixel. In the next step, the monthly total *ET* values were calculated by multiplying the average daily *ET* (for the month) by 30 days except for the 3 winter months from December to February, when

the monthly total *ET* were estimated by multiplying the average daily ET by 15 considering the following: 1) The maximum available cloud-free data were rarely above 15 unlike the other months, 2) occasions of day long cloud-casting or inversions that minimize evaporation were more common in winter months due to dominance of frontal weather systems and continental climate.

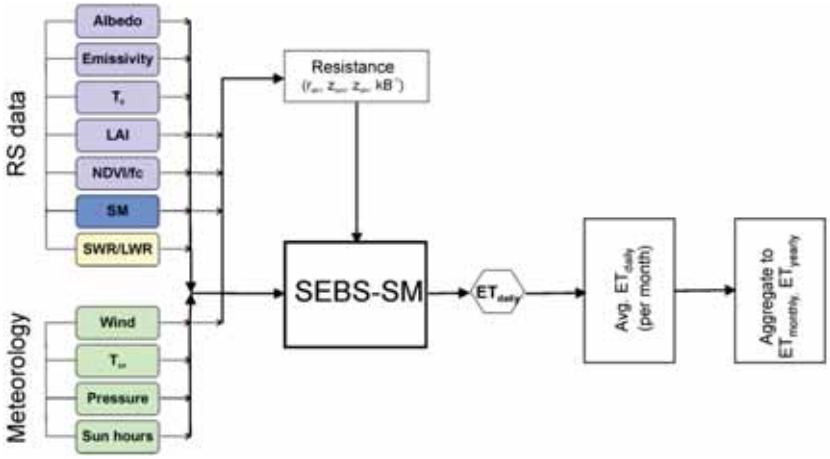


**Figure 4.3** Input data for SEBS-SM and flowchart of aggregating ET.

To obtain the necessary input parameters for the SEBS-SM model, we used MODIS land products (the variables in purple colour in Figure 4.3) (https://lpdaac.usgs.gov/products/modis_products_table) and AMSR-E soil moisture products (Owe et al., 2008) as listed in Table 4.1. The study covered the period between 2005 and 2009.

In addition to the RS data, the necessary meteorological forcing data (Figure 4.3) were obtained from the Turkish Meteorological Service for the 18 stations located in and around the basin (Figure 2.1). The point measurements of the stations were spatially interpolated using the natural neighbour interpolation, a method that is based on Voronoi tessellation. With respect to instantaneous and daily air temperature, additionally, the local lapse rates were calculated for the mountainous areas and integrated (based on a DEM) in the interpolation of air temperature data.

Finally, the down-welling short-wave and long-wave radiation flux ($R_{swd}$ and $R_{lwd}$), boundary layer height and dew point temperature at 2 m height were retrieved from the high-resolution gridded ECMWF (The European Centre for Medium-Range Weather Forecasts) interim reanalysis dataset (http://data-portal.ecmwf.int/ ).

**Table 4.1** The details of the RS data used in the study.

| Name of Sensor | Product code | Product name | Spatial resolution | Temporal resolution | Temporal coverage |
|---|---|---|---|---|---|
| **MODIS** | MCD43A3 | Albedo | 500 m | 16-daily | **2000 -** |
| **MODIS** | MOD11A1 | Emissivity & land surface temperature | 1,000 m | Daily | **2000 -** |
| **MODIS** | MCD15A2 | Leaf Area Index | 1,000 m | 8-daily | **2002 -** |
| **MODIS** | MOD13A2 | NDVI | 1,000 m | 16-daily | **2000 -** |
| **AMSR-E** | | Surface soil moisture | ~25 km | 2-3 daily | **2002 - 2011** |

### b. Potential evapotranspiration

In addition to actual *ET*, we also used the data of potential evapotranspiration (*PET*), which is a representation of the atmospheric demand for evapotranspiration. When a natural surface, uniformly covered with active vegetation is amply supplied with moisture, the actual *ET* taking place from it said to equal *PET* (Kahler, and Brutsaert, 2006). In this study, *PET* data was used in determining the distribution of water limitation in the region based on the criterion for the water-limited environments. According to the definition by Parsons and Abrahams (1994), a region is considered water limited when the ratio of annual precipitation (*P*) to annual *PET* (*P*/*PET*) ranges from about 0.03 to 0.75. The spatiotemporal *PET* distribution of the Konya basin was obtained using the class-A pan evaporation data from the 18 meteorological stations (Figure 2.1) and the simplified formula by Snyder et al. (2005).

### *4.2.3 Spatially-distributed water balance*

The water balance equation for a basin with coinciding surface and groundwater divides can be written in a simple form as Eq. (4.1) (Pagano and Sorooshian, 2006; Penck, 1896):

$$P - ET - R \pm \Delta S = 0 \tag{4.1}$$

where $P$ is precipitation, $ET$ is actual evapotranspiration, $R$ is total runoff and $\Delta S$ is the change in storage. Figure 4.4 shows this general water balance for a basin. Note that Figure 4.4 does not represent changes in storage caused by anthropogenic activities such as groundwater pumping, artificial recharge, and other modifications.

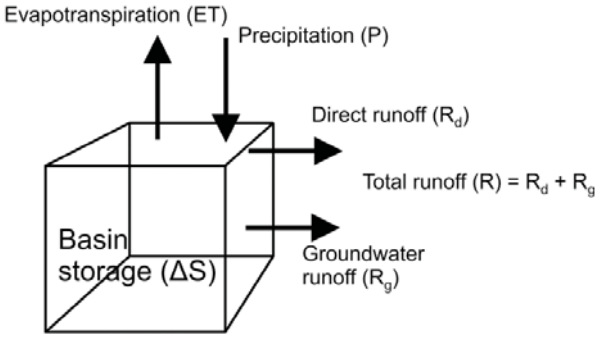


**Figure 4.4** Simplified water balance in a basin. Modified after Oki (1999).

Figures 4.5a & b present the conceptual model of the hydrological fluxes in the Konya basin. The Taurus Mountains in the south and southwest are the main water source areas, where high rainfall and snowmelt feed the ephemeral rivers and recharge the aquifer. Due to a well-developed karst geology, the (semi-)arid climate and the huge plain areas in the mid- and downstream parts, the Konya basin has no well-established drainage network. The water from the ephemeral rivers is either stored in reservoirs to facilitate irrigation, or it feeds the groundwater along the foot-slopes of the mountains. The basin is hydrologically closed, meaning that the horizontal fluxes of surface and groundwater are retained in the basin terminating at the Tuz Lake in the north (Bayari et al., 2009). The evapotranspiration constitutes the only out-flux from the basin and controls salinization of the surface water bodies such as the hyper-saline Tuz Lake (Bayari et al., 2009). Considering that the Konya basin is closed, its water balance equation can be simplified as:

$$\Delta S = P - ET \tag{4.2}$$

However, the objective of this study is to develop a spatially distributed water balance. For applying the water balance equations (Eqs. 4.1 and 4.2) in a distributed manner, we considered the basin as two major units with different hydrological regimes: 1) the mountainous parts of the basin produce

runoff that is transferred to the 2) central plains and used for irrigation in extensive croplands (surrounded by non-irrigated croplands and natural steppe vegetation). Although the abstracted *GW* is the main source of water supply for irrigation (Bayari et al., 2009) in the plains, the *SW* contributes with ~15 - 30% to the irrigation demand in the plain area (unpublished data from DSI) through *SW* transfer from the mountainous area (Figure 4.5b). This water is first stored in reservoirs at the mountain foot-slopes, and later transferred to irrigated croplands in the plain area through a system of canals with monitored discharge. Figure 4.5b illustrates schematically the flux exchange between these two sub-regions and their simplified water balance equations.

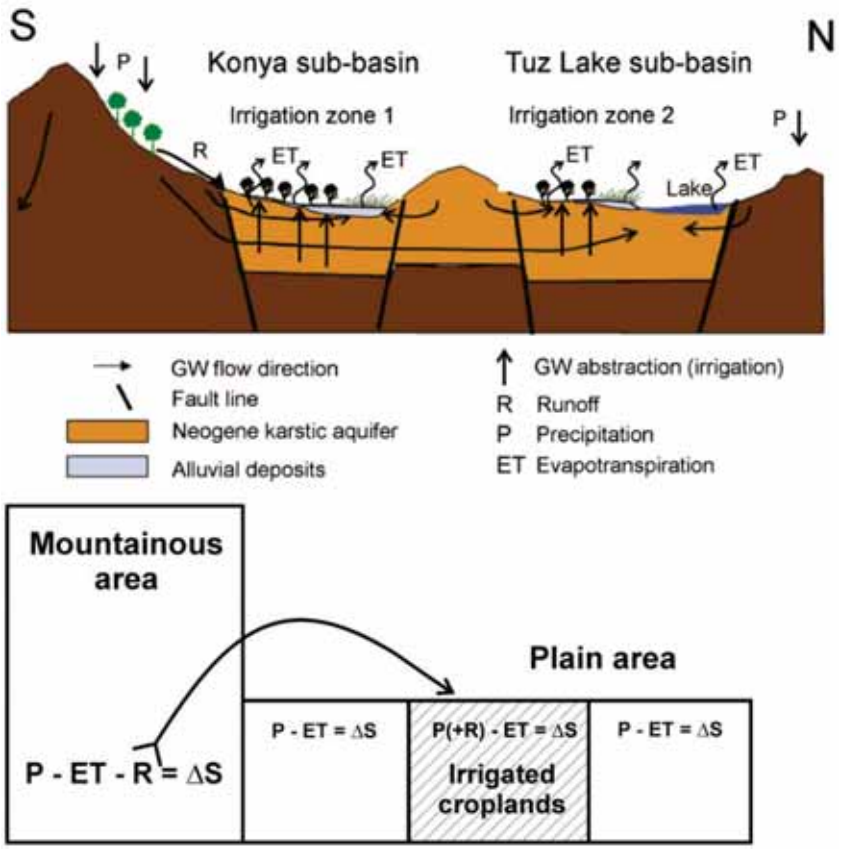


**Figure 4.5a** Conceptual model of the Konya basin (modified after Bayari et al., 2009; Naing, 2011), **5b.** Water balance equations for the mountainous area (left block) and plain area (right block).

Based on the conceptual model and the related water balance equations in Figure 4.5b, the following steps describe the procedure of transferring the surface runoff ($R$) generated in the wet season (in the mountainous part) as surface water irrigation to the irrigated croplands in the plain part in the dry season and then determining the overall spatially distributed yearly water balance (also shown in the flowchart in Figure 4.6). For obtaining the spatially distributed water balance, the wet (from 1st Oct. to 31st Mar.) and dry (1st Apr. to 30th Sept.) periods $P$ ($P_{wet}$ and $P_{dry}$) and $ET$ ($ET_{wet}$ and $ET_{dry}$) fluxes were used as input (Figure 4.6). Note that $P_{wet}$ integrated the separate estimations of rain (unbiased TRMM product) and snowfall contributions, while $P_{dry}$ was solely based on TRMM rainfall, assuming that all the accumulated snow melts down by the end of wet period (section 4.2.1).

i. Define the surface water source (in the mountainous part) and sink (i.e. irrigated croplands) areas
   - Sources areas ($A_S$) were determined by applying the criteria [elevation > 1,800 m and $(P - ET)_{wet} > 0$],
   - Irrigated areas ($A_I$) were determined using CORINE land cover map,
ii. Define the fraction of surface water generation ($f_{SW}$) out of the total water excess in the wet period $(P - ET)_{wet}$
   - The data of 2 sub-basins, which had additionally surface outflow data ($R_{out}$), in the upstream mountainous part were used,
   - $f_{SW} = R_{out} / (P - ET)_{wet}$
   - It is assumed that $f_{SW}$ factor (average of the two sub-basins during the study period) is the same spatially in the source areas.
iii. Determine the total volume of the surface water ($R_V$) in the specific year that is going to be transferred from the source areas (on a pixel basis) to irrigated lands
   - $R_V = f_{SW} \times (P - ET)_{wet} \times A_S$,
iv. Finally, the spatially distributed water balance on a pixel basis is calculated based on the conceptual model in Figure 4.5b.
   - The source areas in the mountainous part: $\Delta S = (P - ET)_{year} - R_V/A_S$,
   - Irrigated croplands: $\Delta S = (P - ET)_{year} + R_V/A_I$,
   - Rest of the areas: $\Delta S = (P - ET)_{year}$,

Afterwards, to assess the budget closure at the locations (pixels) of *GW* observation wells, the storage change estimated from RS ($\Delta S_{RS}$, based on the description under item iv. above) were compared with the $\Delta S_{GW}$ calculated based on groundwater level observations. However, to enable this

comparison, it was necessary to bring both to the same terms. For instance, the RS-based water balance ($\Delta S_{RS} = P \pm R - ET$) for a particular pixel (over land surface) corresponds to the total subsurface change in water storage, both in the unsaturated zone ($\Delta S_{SM}$), and groundwater ($\Delta S_{GW}$), since $\Delta S_{RS} = \Delta S_{SM} + \Delta S_{GW}$. Therefore, to minimize the effect of changes in the soil moisture on the total storage change, the spatially-distributed $P$, $ET$ fluxes and the water balance were calculated for an extended period of 5 years between 2005 and 2009, i.e. assuming that $\Delta S_{SM} \approx 0$ and $\Delta S_{RS} \approx \Delta S_{GW}$. On the other hand, we calculated $\Delta S_{GW}$ values (effective groundwater loss from aquifer) based on the $GW$ level observations and the estimated specific yield of the aquifer. Due to karstic formation of the aquifers and equipment limitation, it was not possible to parameterize the specific yield experimentally. Hence, we assumed a conservative range of 0.05-0.20 based on literature overview (Bolster et al., 2001; Johnson, 1967).

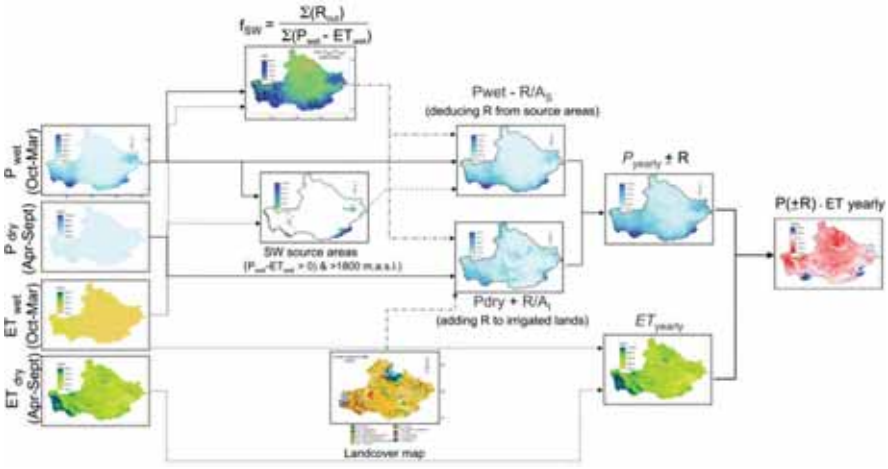


**Figure 4.6** Flowchart for determining the yearly water balance in the Konya basin.

## 4.3 Results

### 4.3.1 Spatial distribution of precipitation

Figures 4.7a and 4.7b show the comparison of the 6-monthly sums of the TRMM rainfall product and the ground-based rain-gauge measurements in dry (April-September) and wet (October-March) seasons, in the Konya basin. In both seasons, a significant linear relationship ($p < 0.001$) is confirmed, and a consistent positive bias of around 80 mm by TRMM is observed for the wet

seasons (2005 - 2009). Furthermore, the correlation for the wet season ($R^2 = 0.58$) was higher compared to the dry season ($R^2 = 0.39$). Figure 4.7c shows the yearly average rainfall distribution after removing the bias in the wet season (2005 - 2009). The rainfall in the mountainous area (outside the polygon in Figure 4.7c) is of the order of 1,000 mm $y^{-1}$ or more towards the higher parts of the mountains, while in the plain (inside the polygon in Figure 4.7c), the rainfall is quite uniform, ranging from 250 to 300 mm $y^{-1}$.

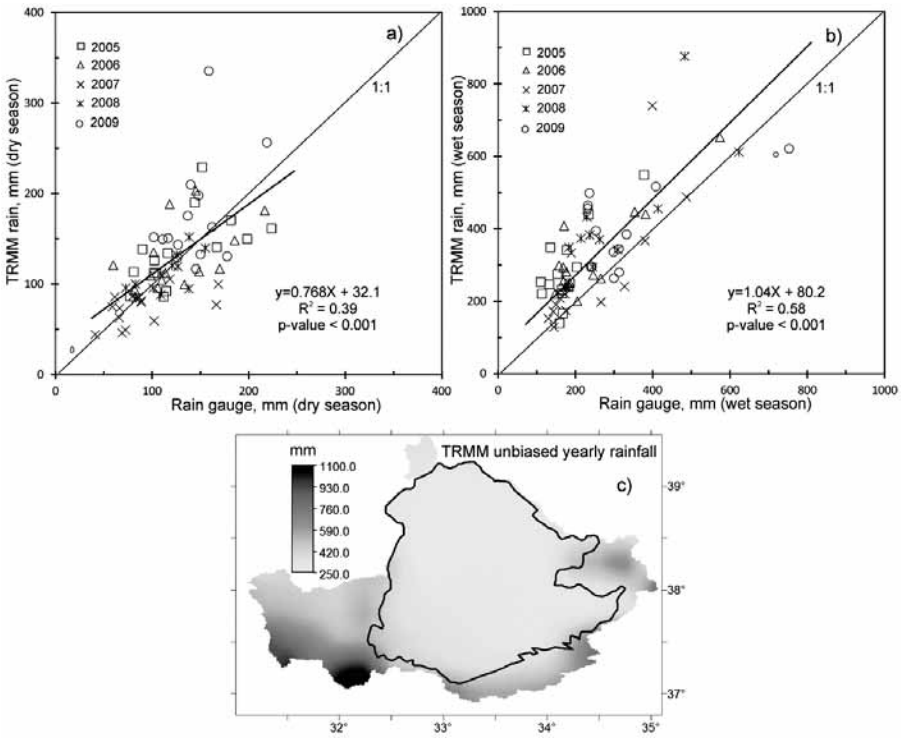


**Figure 4.7a-b)** Comparison of TRMM seasonal rainfall with ground-based rain-gauge measurements in the dry season (Apr-Sept), in the wet season (Oct-Mar), respectively, and **c)** the distribution of average unbiased yearly TRMM rainfall in the Konya basin (2005-2009). The polygon delineates the plain areas from mountainous areas.

Figure 4.8 shows the results of the multiple regression analysis and the yearly *SWE* for the year 2008 as an example, because the analysis was carried out separately for each year during the study period. Figures 4.8a and 4.8b show the relationship between *SWE* and elevation and total snow cover days, respectively. Although the coefficients of determination ($R^2$) were in a similar range for both linear relationships, the one with total snow cover days had

higher $R^2$ value ($R^2$=0.65). On the other hand, a multi-regression model combining the two variables explained the variation of *SWE* slightly better than the individual linear models: $R^2$ increased to 0.68. As a result, Figure 4.8c shows the distribution of the yearly *SWE* in the Konya basin, obtained from the multiple regression model and indicates values of about 300 mm in the mountainous upstream parts of the basin (> 2,000 m a.s.l.). Finally, Figure 4.8d shows the distribution of the yearly total precipitation in the Konya basin, which was obtained by summing the yearly rainfall and *SWE*.

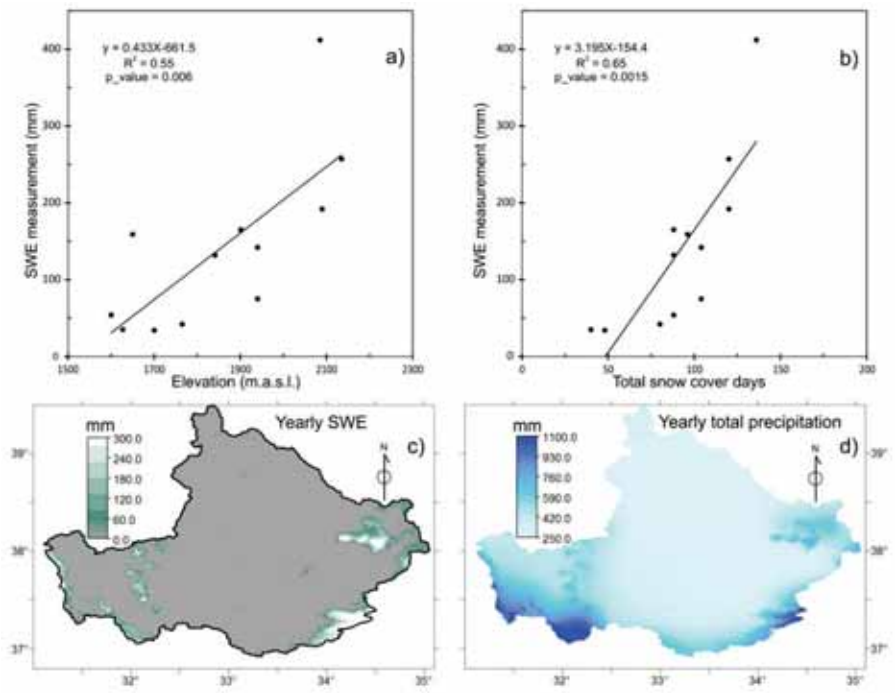


**Figure 4.8a-b)** Dependence of yearly SWE measurements on elevation and, total snow cover days (source: MOD10A2 product), respectively, **c)** the yearly SWE map, and **d)** the yearly total precipitation map. Data of the year 2008 were used in all the figures.

### *4.3.2 Spatial distribution of evapotranspiration*

Figure 4.9 shows the comparison of the average yearly *ET* estimated by the original SEBS and the modified SEBS-SM models for the Konya-basin. The two models give similar results in the "wet" areas such as the mountainous upstream areas in the southwest and east (outside the polygon in Figs. 4.9), in the irrigated croplands in the plain areas (see the land cover map in Figure 4.12c), and in the water bodies and wetlands, where water limitation on *ET* is

not relevant. However, the two models are quite different in the "dry" areas (non-irrigated parts inside the polygon), where water limitation on *ET* is more important.

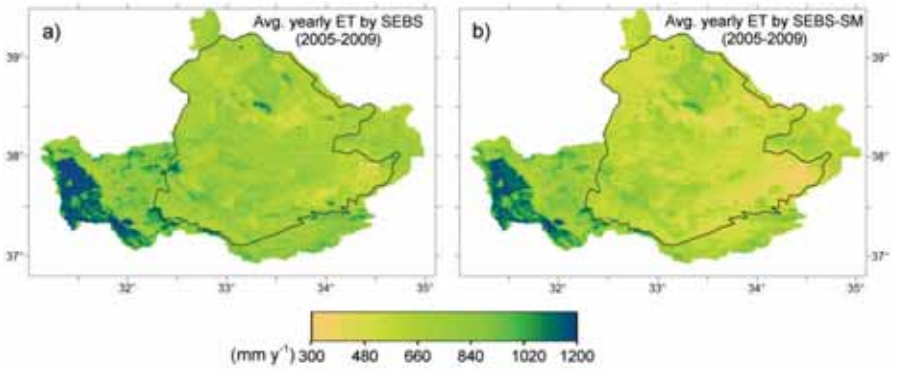


**Figure 4.9** Average yearly *ET* during the study period (2005-2009) by: a) the original SEBS (Su, 2002), b) the modified SEBS-SM (Chapter 3).

Table 4.2 summarizes the comparison of the yearly *ET* estimates by SEBS and SEBS-SM for different land cover types in the basin. According to Table 4.2, the yearly *ET* estimated by SEBS-SM was lower for all the land covers in the basin. The difference varied among the land covers: 50-60 mm lower in shrub, forest and water body land covers, 90-100 mm lower in wetland and irrigated croplands, and 150-160 mm lower in non-irrigated croplands, sparse vegetation, pasture and grassland land covers on average.

**Table 4.2** Comparison of the average yearly *ET* (2005-2009) estimated by SEBS and SEBS-SM in the Konya basin. Note that the aerial land cover percentages do not sum up to 100% since only the major land cover units were considered.

| *Unit* | *Flux* | *Area* (%) | *Avg.* yearly ET (mm) | *Std. dev.* (mm) |
|---|---|---|---|---|
| Konya basin | SEBS | 100 | 772 | 155.2 |
| | SEBS-SM | | 647.2 | 176.9 |
| Irrigated croplands | SEBS | 16.2 | 736.2 | 111.9 |
| | SEBS-SM | | 632.2 | 118.2 |
| Non-irrigated croplands | SEBS | 21.5 | 709.7 | 93.7 |
| | SEBS-SM | | 558.2 | 92.2 |
| Mixed-croplands | SEBS | 7.0 | 648.3 | 162.1 |
| | SEBS-SM | | 767.5 | 142.7 |
| Wetland | SEBS | 1.2 | 798.5 | 197.3 |
| | SEBS-SM | | 708.9 | 219.2 |
| Sparse steppe veg. | SEBS | 12.9 | 802.8 | 162 |
| | SEBS-SM | | 644.2 | 185.7 |
| Pasture+ Grassland | SEBS | 15.0 | 731.1 | 125.4 |
| | SEBS-SM | | 578.9 | 130.5 |
| Shrub | SEBS | 4.7 | 964.5 | 152.1 |
| | SEBS-SM | | 900.3 | 167.6 |
| Forest | SEBS | 1.1 | 1,046 | 151.9 |
| | SEBS-SM | | 998.4 | 156.9 |
| Water body | SEBS | 2.9 | 983.5 | 202.3 |
| | SEBS-SM | | 922.2 | 206.3 |

### *4.3.3 Surface runoff generation and its redistribution*

Figure 4.10 shows the distribution of the average wet season excess $P_{wet}$-$ET_{wet}$ during the study period (2005-2009) in the Konya basin. Based on the measured outflows ($R$) (source: DSI) from the Beysehir and Yesildere sub-basins (Figure 4.10) and applying Eq. 4.3, we found an average factor surface water fraction ($f_{SW}$) of 0.4, ranging between 0.25 and 0.55 depending on the year of assessment (Figure 4.11a). According to Figure 4.11b, the surface water generation ranged from 100 to 400 mm $y^{-1}$ in the mountainous source areas (2005-2009). Finally, Figures 4.11c and 4.11d show the distributions of the modified $P_{wet}$ and $P_{dry}$, respectively, when the $SW$ sources in Figure 4.11b were subtracted from $P_{wet}$ and then redistributed evenly over the irrigated pixels in $P_{dry}$ (inside the irrigated croplands polygons in Figure 4.11d based on land cover map). As a result, a range between 29 mm (2007) and 92 mm (2009)

of *SW* irrigation was added per irrigated pixel for the study period (2005-2009).

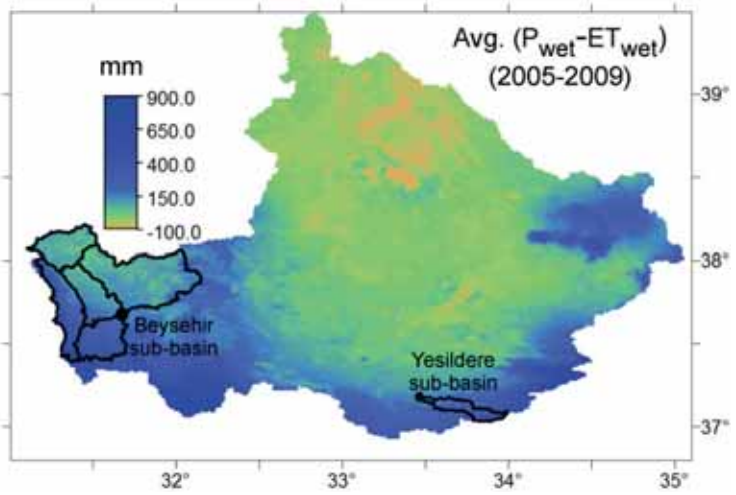


**Figure 4.10** The distribution of the average $P_{wet}$-$ET_{wet}$ during the study period (2005-2009) including the locations of Lake Beysehir and Yesildere sub-basins.

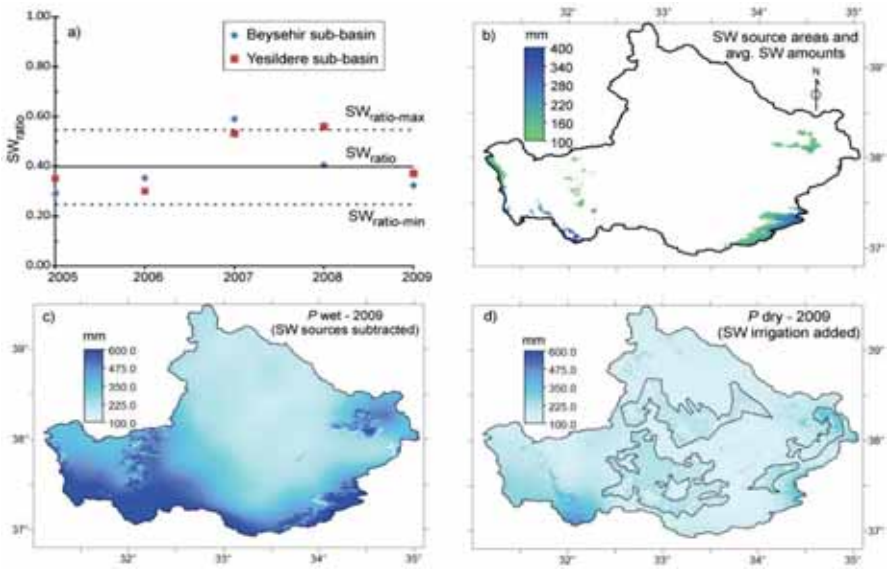


**Figure 4.11** Assessment of *SW* irrigation: **a)** average, yearly changes and std. devs. of the $f_{SW}$ in Beysehir and Yesildere sub-basins; **b)** distribution of the *SW* source areas and quantities identified from ($P_{wet}$-$ET_{wet}$), **c)** $P_{wet}$ after transferring (subtracting) the generated *SW*, and **d)** $P_{dry}$ after transferring in the *SW* as irrigation within the delineated polygons. Figure 4.11b represents the average of the period 2005 - 2009, Figs. 4.11c and d represent the year 2009.

### *4.3.4 Spatially distributed water balance*

#### a. Distribution of water limitation and P-ET anomaly

We firstly analysed the degree of water limitation in the Konya basin by estimating the aridity ratio of precipitation to potential evapotranspiration ($P/PET$), as shown in Figure 4.12a. Based on the criterion for water-limited environments ($P/PET < 0.75$) defined by Parsons and Abrahams (1994), we can say that except for the upstream mountainous parts in the southwest, south and east, the whole Konya plain (indicated by the polygon line in Figs. 4.12a&b) can be classified as highly water-limited environment with a $P/PET$ ratio of about 0.3.

The next step was to quantify the spatial distribution of $P - ET$, where positive values ($P > ET$) indicate potential for surface runoff and/or for $GW$ recharge, while negative values ($P < ET$) indicate actual consumption of supplementary water resources. In Figure 4.12b, the large $P - ET$ deficits (negative values) mainly correspond to the irrigated croplands where irrigation water is used from groundwater and/or surface water sources. The irrigation water use (the gross consumption from surface and groundwater) for 2005 - 2009, within the water-limited Konya plain (inside the polygon in Figure 4.12a), ranged up to -500 mm $y^{-1}$ with a mean of -308 mm $y^{-1}$. Additionally, large $P - ET$ deficit values occurred in lakes and wetlands, indicating significant groundwater and/or surface water inflow. In particular, the mean yearly $P - ET$ deficit over the water bodies was -495 mm for lakes (~ -600 mm in the freshwater Lake Beysehir in the southwest, -475 mm in the hyper-saline Tuz Lake in the north) and -422 mm for the wetlands.

The $P - ET$ surplus (positive values in Figure 4.12b) was of the order of 300 mm $y^{-1}$ and occurred mainly in the mountainous upstream areas in the southwest and southeast where considerable surface runoff generation and/or $GW$ recharge took place. According to the histogram of $P - ET$ for the whole basin (Figure 4.12d), the majority of pixels have a negative balance with a mean $P - ET$ of -238 mm $y^{-1}$.

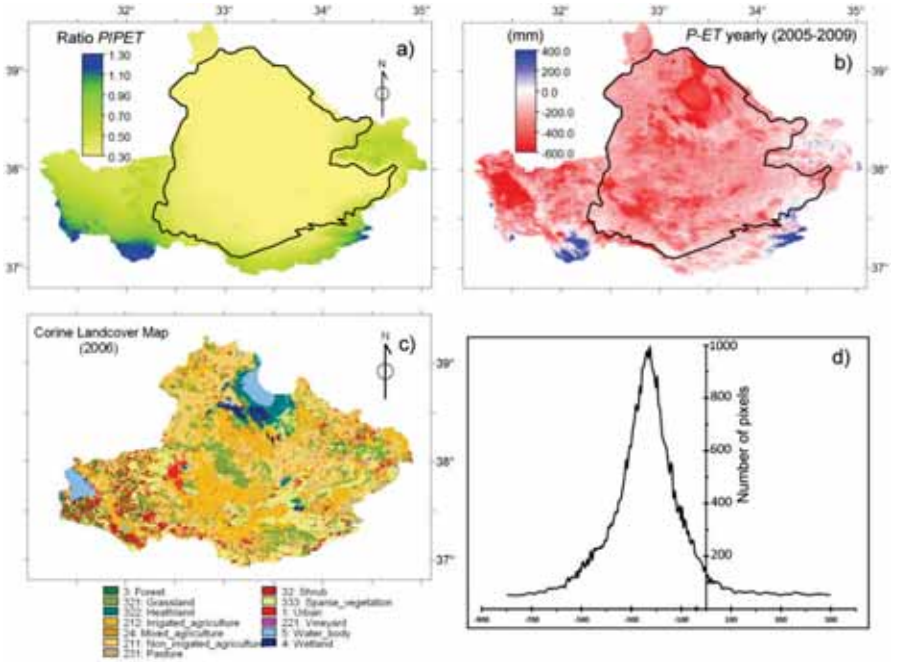


**Figure 4.12 a)** Water limitation as defined by the *P*/*PET* ratio; **b)** *P-ET* in the Konya basin; **c)** CORINE Land cover map, source: Ministry of Environment of Turkey; **d)** histogram of *P* - *ET*.

Table 4.3 provides a summary of the yearly *P*, *ET*, and (*P* - *ET*) fluxes in the water-limited Konya plain. The average yearly total storage change (*P* - *ET*) for the whole Konya plain is ~-8,500 MCM (-270 mm $y^{-1}$). In the case of croplands, the mean *P* - *ET* deficits are -308 mm $y^{-1}$ and -230 mm $y^{-1}$ for irrigated and non-irrigated croplands respectively, with a total volume of around -4,700 MCM per year together. Although the mean *P* - *ET* deficit for non-irrigated crops is considerably lower than for irrigated crops, -230 mm $y^{-1}$ still indicates considerable *ET* excess in non-irrigated agricultural lands. The smallest yearly *P* - *ET* deficit occurred in the sparse steppe vegetation (avg. -209 mm $y^{-1}$), which is still around 70% in excess of the total *P* influx.

**Table 4.3** Summary of the average yearly *ET* and *P* fluxes (2005-2009) in the Konya plain - note that the aerial percentages of the land covers, do not sum up to 100% since only the major land cover units are considered.

| ***Unit*** | ***Flux*** | ***Area*** (%) | ***Avg.*** (mm) | ***Std. dev.*** (mm) | ***Total vol.*** (MCM) |
|---|---|---|---|---|---|
| Konya plain | P | 100 | 306 | 59 | 9,711 |
| | ET | | 576 | 115 | 18,296 |
| | P - ET | | -270 | 189 | -8,585 |
| Irrigated crops | P | 23.2 | 313 | 49 | 2,312 |
| | ET | | 622 | 112 | 4,586 |
| | P – ET | | -308 | 132 | -2,274 |
| Non-irrigated crops | P | 34.1 | 313 | 68 | 3,393 |
| | ET | | 544 | 82 | 5,894 |
| | P – ET | | -231 | 91 | -2,499 |
| Wetland | P | 1.7 | 262 | 19 | 140 |
| | ET | | 683 | 206 | 365 |
| | P – ET | | -422 | 209 | -225 |
| Sparse steppe veg. | P | 9.0 | 299 | 46 | 853 |
| | ET | | 508 | 99 | 1,451 |
| | P – ET | | -210 | 92 | -598 |
| Pasture+Grass | P | 16.8 | 306 | 56 | 1,627 |
| | ET | | 534 | 88 | 2,840 |
| | P - ET | | -228 | 92 | -1,213 |
| Shrub | P | 0.4 | 395 | 119 | 55 |
| | ET | | 756 | 147 | 105 |
| | P - ET | | -361 | 119 | -50 |
| Water body | P | 2.7 | 266 | 22 | 224 |
| | ET | | 761 | 75 | 642 |
| | P - ET | | -495 | 76 | -418 |

**b. Distribution and closure of water balance**

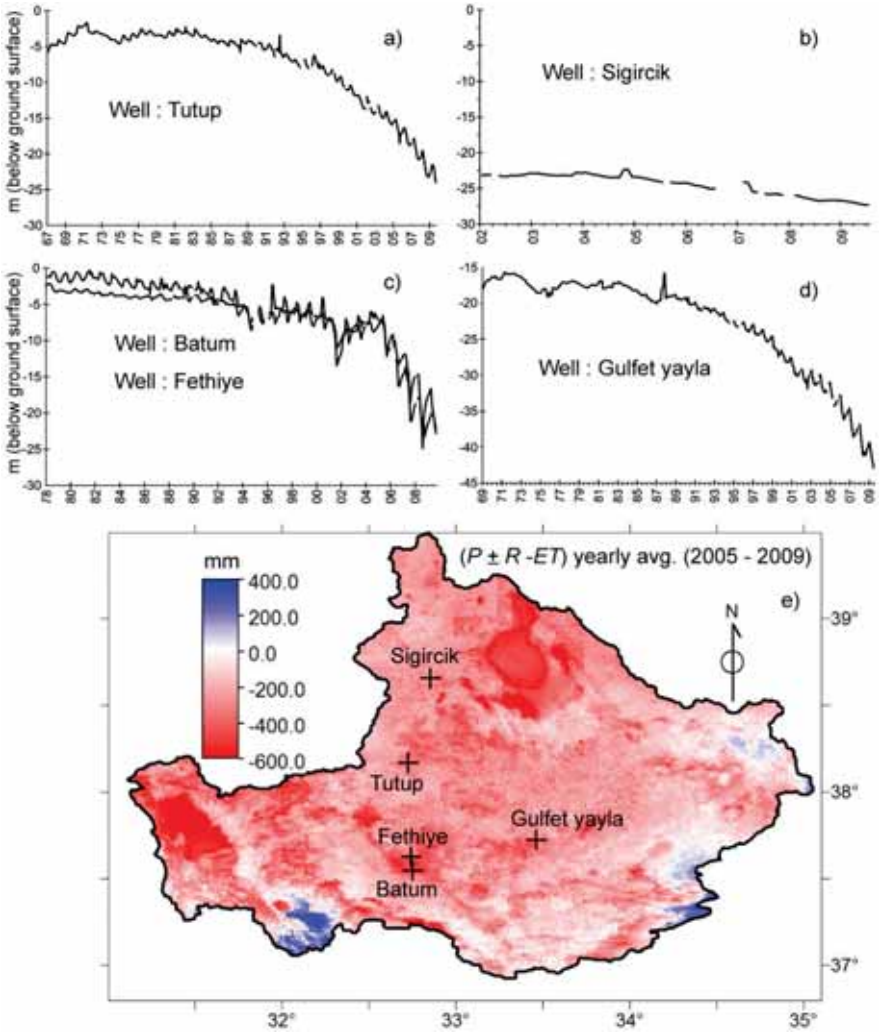


**Figure 4.13** Trends in groundwater observation wells and the net spatially distributed water balance map ($P + R - ET$).

Figure 4.13 shows both the records of five *GW* observation wells (Figs. 4.13a-d) and the yearly water balance ($P \pm R - ET$) (Figure 4.13e), which includes redistribution of the surface water ($R$) originating from wet season precipitation in the mountainous areas, over the irrigated areas of the Konya plain in the dry season (Figure 4.13e) as schematically presented in Figure 4.5b. The groundwater observation wells Fethiye and Batum are

located in the oldest irrigation region of the Konya basin. These wells show a decreasing trend of 0.3 m $y^{-1}$ between 1978 and 2004 (Figure 4.13c) according to linear least squares fitting, while after 2004 an even steeper trend of > 2 m $y^{-1}$ is observed. According to the hydrogeological report by DSI, most of the aquifers in the Konya plain are confined, due to a thick layer of Pliocene sandy clay deposits (Figure 4.5a), but the degree of confinement is variable. The two other wells in irrigated fields (Tutup and Gulfet yayla, Figure 4.13a and Figure 4.13d) also indicate a significantly decreasing trend of around 1 m $y^{-1}$ after the mid 90's.

In Figure 4.13, both the RS-based water balance estimation and the records of *GW* observation wells indicate a widespread and varying decrease in storage. To be able to check if the water budget can be closed at the locations (pixels) of the *GW* observation wells, we compared the average yearly $\Delta S_{RS}$ estimates from the RS-based water balance ($P \pm R - ET$) with the average $\Delta S_{GW}$ ranges for the five monitored wells between 2005 and 2009 (Table 4.4 and Figure 4.14).

**Table 4.4** Comparison between the effective *GW* loss observations from the field data and the average yearly water balance ($P + R - ET$) estimated by RS-based methods for several locations in the Konya basin during the study period (2005-2009).

| Name of GW well | Field data | | | RS estimation |
|---|---|---|---|---|
| | Sy (specific yield) | Avg. GW level change ($mm \cdot y^{-1}$) | Effective GW change, $\Delta S_{GW}$ ($mm \cdot y^{-1}$) | $(P+R-ET)$ $\Delta S_{RS}$ ($mm \cdot y^{-1}$) |
| | | 2005-2009 | 2005-2009 | 2005-2009 |
| Sigircik | 0.05 - 0.2 | -750 | -37.5 to -150 | (255.4+0.0-482.4) -227.0 |
| Tutup | | -1,560 | -78 to -312 | (294.5+62.5-650.3) -293.3 |
| Batum | | -2,870 | -143.5 to -574 | (364.4+62.5-836.2) -409.3 |
| Fethiye | | -2,170 | -108.5 to -434 | (349.3+62.5-746.4) -334.6 |
| Gulfet yayla | | -1,890 | -94.5 to -378 | (284.4+62.5-585.3) -238.4 |

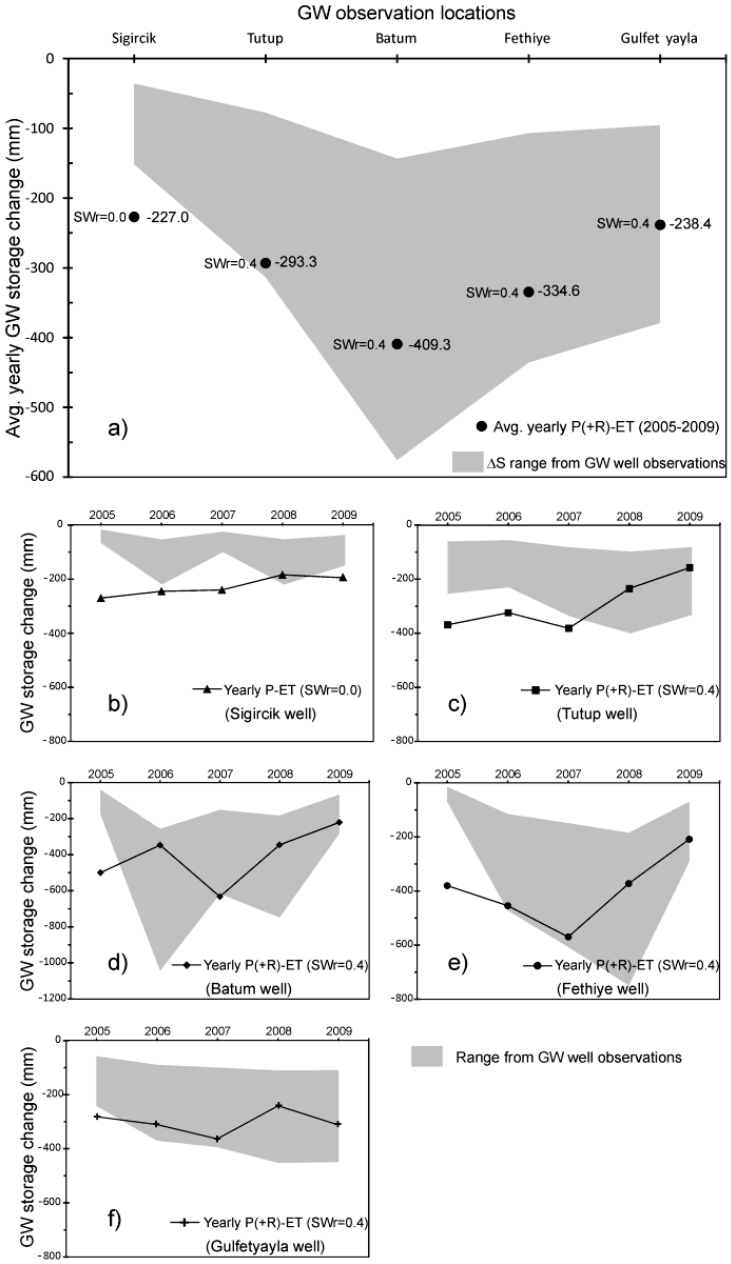


**Figure 4.14** Comparison between the RS-based change of storage ($\Delta S_{RS} = P + R - ET$) and the change of *GW* storage ($\Delta S_{GW}$) based on the observation wells: a) as the yearly average of 2005-2009, **b-f)** yearly changes for each monitoring well (Note that *SW* irrigation (*R*) was estimated separately for each year).

According to the Table 4.4 and Figure 4.14a, the average yearly storage change ($\Delta S_{RS}$) estimated from the RS-based water balance falls within the range of $\Delta S_{GW}$ constrained by a karst $S_y$ range of 0.05 - 0.20, with the exception of the Sigircik well. Figure 4.14a and Table 4.4 also show that the relative magnitudes match well: the highest storage changes (both $\Delta S_{RS}$ and $\Delta S_{GW}$) are observed for the Batum and Fethiye wells ($\Delta S_{RS}$ = -409 and -335 mm $y^{-1}$, respectively), while the lowest storage changes are observed for the Sigircik and Gulfet yayla wells ($\Delta S_{RS}$ = -227 and -238 mm $y^{-1}$, respectively). Figures 4.14b-f show the yearly comparison between the $\Delta S_{RS}$ and the $\Delta S_{GW}$ at each monitoring well during the study period.

## 4.4 Discussion

There is an increasing trend of using RS data and RS-based models in hydrological research, but they still have their drawbacks, among others, regarding accuracy, difficulties in validation, scale issues, spatial and temporal resolution limitations. Studies of Gao et al.(2010), Sahoo et al. (2011), and Sheffield et al. (2009) evaluated the water budget closure in major river basins using RS data and they all concluded that achieving budget closure from remote sensing is not possible yet. They indicated that the largest uncertainties were found in satellite precipitation products. On the other hand, a global scale *ET* study by Vinukollu et al. (2011) concluded that the three RS-based *ET* models they tested (including SEBS) underrepresent the sensitivity to soil moisture over water limited regions.

Our study is similar to those studies in utilizing RS-based estimates of *P*, *ET* to obtain a distributed water balance. However, the current study differs firstly in that instead of a purely RS-based approach (e.g. Sheffield et al., 2009; Sahoo et al., 2011; Armanios and Fisher, 2012) we followed an integrated approach combining RS and ground-based methods. Secondly, we evaluated the budget closure of a spatially distributed water balance again in a spatially distributed manner by comparing the storage change inferred as the residual of the water balance with the distributed GW level observations, not in a lumped way (.e.g. Armanios and Fisher, 2012). Furthermore, as it was applied in a semi-arid closed-basin where limited water resources (both surface and groundwater) are strongly affected by human interaction, our study focused on the ways of improving *P* and *ET* estimations under semi-arid conditions through integrating different data/methods (i.e. RS and ground), and introducing most up to date models.

### *4.4.1 Improvement of P, ET fluxes*

With respect to improving the estimate of the distribution of *P*, two steps were taken: bias removal of RS rainfall products, and integration of *SWE* contribution to the total precipitation. Firstly, we assessed the monthly product TRMM (3B43). Similar to Pan et al. (2008), who found a positive bias in the TRMM monthly rainfall product, we have also detected a positive bias of around 80 mm in the TRMM monthly product in the Konya basin. Furthermore, a separate analysis of the wet and dry periods showed that the bias was consistent in the wet season (Oct-Mar), but not in the dry season (Apr-Sept). We argue that such a seasonal difference can be attributed to the higher intensity of the rainfall and also to the dominance of a frontal type of rains during the wet season, compared to the spatio-temporally scattered convective rains in the dry season.

Secondly, neither the TRMM product nor the rain gauge observations represent snowfall contribution to the total precipitation in the mountainous areas because the rain gauges are located at relatively low altitudes. Furthermore, the number of in-situ snowpack measurement sites is very low (Serreze et al., 1999). Possibilities of *SWE* measurement from RS are limited (Tang et al., 2010) and anyway, the available RS-products from microwave sensors are known to be less accurate in regions of complex terrain due to topography effects and limitations in the instantaneous field of view of the sensors, which can cause underestimations on mountains of complex geometry (Muskett, 2012). Therefore, alternatively we applied a multiple regression approach using the snow-gauge measurements, DEM and RS-based snow cover data to obtain the distribution of the yearly *SWE* in the Konya basin. While snow cover data is an indispensable variable to identify snow-covered areas, it has long been known that topography plays important physical roles in influencing the magnitude of precipitation (Muskett, 2012). Our results indicate that snowfall may contribute up to 25 - 30% (~300 mm SWE) to total yearly precipitation in the higher upstream areas (> 2,000 m.a.s.l. in the Konya basin), which is neglected by the TRMM precipitation estimates. Therefore, we suggest including the *SWE* of the snowpack in the precipitation distribution to avoid serious underestimation of *P* in high altitude terrains, where major surface water generation and groundwater recharge are occurring.

With respect to improving the distribution of *ET* under semi-arid conditions, our study applied a modified version of the SEBS model (SEBS-SM), which explicitly incorporates soil moisture information in the calculation. With that model we have overcome the problems of non-sensitivity of previous RS-based *ET* models to soil moisture over water-limited regions as indicated by the studies of Vinukollu et al. (2011), Van der Kwast et al. (2009), Lubczynski and Gurwin (2005). Principally, as it was put forward by the conceptual model of Seneviratne et al. (2010), lowering of soil moisture has a decreasing effect on the evaporative fraction (the portion of available energy spent for evapotranspiration) due to greater stomatal control on the water use by plants and increasing soil resistance to evaporation under water-stress conditions (Chapter 3). Along these lines, this study showed quantitatively that the integration of soil moisture in SEBS-SM had a lowering effect in the estimation of yearly *ET* compared to SEBS in the water limited Konya basin. That magnitude of lowering was proportional to the aridity of the area (mean: ~-120 mm, min: ~0 mm, max: ~-400 mm), being the largest in the regions under the strongest water stress areas (Figure 4.9), i.e. in the plain areas with low *P* values (~250-400 mm, Figure 4.8d) and no supplementary water input (i.e. irrigation or groundwater discharge).

### 4.4.2 Distribution of P - ET anomaly, water balance and budget closure

After obtaining improved distributions of the yearly *P* and *ET* in the Konya basin, we assessed *P* - *ET* anomalies, the storage change as the residual of the water budget equation ($P \pm R - ET$ or, $\Delta S$), and finally the budget closure at the locations of groundwater level observations. According to Contreras et al. (2011), areas with excess of *P* over *ET* generate surface runoff or *GW* recharge to the aquifers, while excess of *ET* over *P* results in the consumption of supplementary water resources (i.e. direct use of phreatic groundwater, groundwater discharge to a wetland, natural surface water contributions and water withdrawal for irrigation). In the Konya basin, the distribution of *P* - *ET* and the water balance ($P \pm R - ET$ or, $\Delta S$) indicate a widespread negative water balance (i.e. negative storage change) of varying magnitude during the study period of 2005 - 2009. These negative water balance values can be mainly related to the enhancement of *ET* by the extensive and intensive agricultural activities stimulated by supplementary groundwater use for irrigation purposes. The largest negative *P* - *ET* values were found over water bodies and wetlands, suggesting that these ecosystems are highly dependent

on groundwater (and/or surface water) inputs to sustain the excess *ET* (Table 4.3).

Afterwards, to assess the budget closure at the locations (pixels) of *GW* observation wells, $\Delta S_{RS}$ estimated from *RS* (*P* ± *R* - *ET*) were compared with the $\Delta S_{GW}$ calculated based on the yearly groundwater decline and we found that the average yearly $\Delta S_{RS}$ values were within the ranges of $\Delta S_{GW}$ for 4 out of 5 wells estimated, assuming an $S_y$ range between 0.05 and 0.20. These findings suggest that the RS-based estimate of $\Delta S_{RS}$ was capable of estimating the magnitude and the distribution of groundwater storage depletion in the semi-arid Konya basin, which had also been reported by Bayari et al. (2009). A similar approach was also documented by Tang et al. (2010), but our study differs in that we validated the spatially distributed water balance directly with *GW* level observations, while they validated their satellite-based water balance against streamflow data for two river basins.

### *4.4.3 Evaluation of the error sources and the uncertainties*

Despite the effectiveness of the RS-based *P* ± *R* - *ET* in capturing groundwater depletion as reflected by storage change, estimation of each water balance flux component separately and the methodology of spatio-temporal water balance assessment are still prone to a variety of error sources and uncertainties. Firstly, the CORINE land cover map (Figure 4.12c) used in analysing the land cover based *ET* and *P* fluxes was rasterized from originally a polygon map and resampled to 1 km resolution. Because of the rather coarse spatial resolution (1 km), such a procedure is subject to a mixed-pixel effect, i.e. *ET* and *P* fluxes were likely to represent a mixture of different land cover types. Still, one would expect that the long term yearly averages of *P* and *ET* in the relatively flat terrain, with little surface runoff, should be in a similar range for land covers like sparse steppe vegetation. Despite that the smallest yearly *P* - *ET* difference occurred in the sparse steppe vegetation (avg. -209 mm $y^{-1}$), the yearly *ET* was still around 70% in excess of the total *P* influx. This large difference can mainly be attributed to the low value of P in the Konya plain (~300 mm $y^{-1}$), which causes a higher relative uncertainty per unit absolute error for low values of *P*. Our comparison of the TRMM rainfall product with the rain gauges showed a significant positive bias ($p < 0.001$) in the wet season and the correlation coefficient was not high ($R^2 = 0.58$), implying that the magnitude of the bias varies considerably among the stations and the years of the study period (Figure 4.7b). In response to that

we subtracted a bias of ~80 mm from the yearly *P* before the analysis. Such a bias removal had relatively more influence and gave more uncertainty in the plain, low *P* areas compared to mountainous, high *P* areas.

Despite the improvements by using SEBS-SM in representing the *ET* in water-limited environments, an overall relative error (rRMSE) of 26% for the SEBS-SM results (which was originally 36% for SEBS) was reported in Chapter 3, by comparing the model output with observations from the Bowen ratio stations installed in the Konya basin. It should be noted that even ground-based flux measurements derived from Bowen ratio and eddy covariance systems have an uncertainty of around 20 - 30% (Kalma et al., 2008 and references therein). Besides the uncertainties in estimating the daily *ET*, the process of filling the data gaps in daily *ET* values for obtaining monthly and yearly *ET* is also prone to uncertainties which have been studied by several studies (e.g. Anderson et al., 2012; Delogu et al., 2012; Ferguson et al., 2010; Gao et al., 2006). In an effort to further minimize the errors in estimating monthly and yearly *ET*, an option was to densify and extend the sampling (i.e. more frequent RS flux estimations in a longer study period). Therefore, we ran the SEBS-SM model on a daily interval taking advantage of the daily data availability from MODIS satellite and meteorology data. However, as shown in Figure 4.15, the RS data availability varied largely in the Konya basin due to weather variations and due to the data quality policy applied by the MODIS team on certain variables such as land surface temperature or emissivity variables. Comparing the data availability (Figure 4.15) with the land cover map of Figure 4.12c, we can conclude that there was a generally good data availability (averagely about 200 days per year in 2005 - 2009) for the croplands, while the availability was generally lower (50 - 100 days per year) for the natural steppe vegetation (sparse vegetation and pasture areas), mountainous upstream areas, and water bodies. This can be attributed to the higher cloud coverage in the mountainous areas, and the higher uncertainties in the calculation of emissivity, especially for the sparsely vegetated areas. In fact, in contrast to those data sparse areas, we can claim lower uncertainties in quantifying the yearly *ET* for the data intensive areas such as croplands, which is supported by the general agreement between the $\Delta S_{RS}$ estimates and the $\Delta S_{GW}$ from the groundwater level observations in Table 4.4 and Figure 4.14.

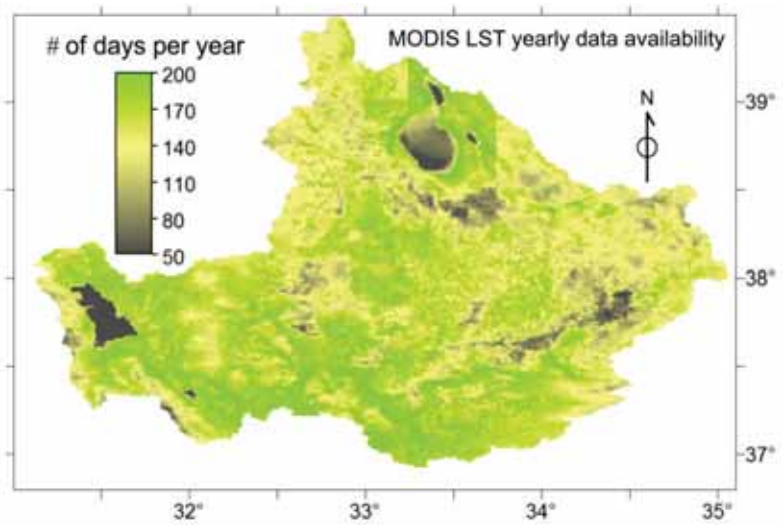


**Figure 4.15** The distribution of the average number of days that the MODIS land surface temperature (*LST*) data was available during the study period in the Konya basin.

Finally, besides the uncertainties in quantifying the individual fluxes, there are also some methodological uncertainties in comparing the $\Delta S_{RS}$ and $\Delta S_{GW}$. Firstly there is a difference in terms of representativeness. The $\Delta S_{RS}$ estimated by RS methods, represents the whole storage change beneath the surface (soil moisture in the unsaturated zone, *GW* in the saturated zone), while the measurements of the *GW* level change represent only the *GW* storage change. To minimize the effect of the variations in soil moisture in the unsaturated zone ($\Delta S_{SM}$), we used an extended study period of 5 years, which helped to balance out the variations in $\Delta S_{SM}$ and $\Delta S_{RS}$ estimation so as to primarily represent changes in the groundwater storage. Secondly, not only the uncertainty of $\Delta S_{RS}$ but also the uncertainty of the $\Delta S_{GW}$ plays a role in explaining some of the misfit between $\Delta S_{RS}$ and $\Delta S_{GW}$ (Figs. 4.14b-f). The $\Delta S_{GW}$ is dependent on the accuracy of the $S_y$ estimate, which for the karstic rocks is highly uncertain (due to the unpredictable type and the degree of karstification), so it could even be off the variability range defined in this study. In fact, it is shown in Figure 4.14 that the uncertainty of $\Delta S_{GW}$ due to the uncertainty of specific yield (grey shaded area) was considerable. In addition, assigning a spatially constant $f_{SW}$ that is estimated in a few selected sub catchments of the mountainous areas represents a simplification because the mountainous areas are heterogeneous and the $f_{SW}$ may vary with altitude, topography, soil type, vegetation, etc. However, according to our testing of

the different $f_{SW}$ range given in Figure 4.11a, the effect of varying the $f_{SW}$ on $R$ and thereby also on $\Delta S_{RS}$ (i.e. $P \pm R - ET$) was low compared to the effect of $S_y$ on $\Delta S_{GW}$ because the contribution of $R$ was only ~20% to the total water use (i.e. irrigation) in the Konya basin, which is highly groundwater dependent (Table 4.4).

## 4.5 Conclusions

In this chapter, we aimed at developing a method for improved RS-based estimations of yearly $P$, $ET$ and $R$ water fluxes for evaluation of the storage changes in the water limited Konya basin in a spatially distributed manner. For assessing the effectiveness of the methodology, we compared the results with groundwater storage changes estimated by water table decline in boreholes. The proposed methodology relies on the integrated assessment (i.e. RS and ground methods) of individual fluxes. Important aspects in the assessment of $P$ are i) the correction of the TRMM rainfall product with ground-based rainfall estimates in gauges and ii) an estimate of the snowfall contribution to precipitation from the $SWE$ of the snowpack based on RS and field measurements. The assessment of $ET$ confirmed the advantage of SEBS-SM over the standard SEBS by its better accounting for water stress conditions (i.e. soil moisture limitation on $ET$), which was reflected in estimating a lower yearly $ET$ compared to SEBS with varying magnitude. The supplementary $SW$ transfer for irrigation ($R$) from mountainous areas to lowland plain areas was defined as the product of the $f_{SW}$ representing surface water outflow characteristic of the mountainous areas and the RS-defined water surplus $P_{wet}$-$ET_{wet} > 0$. The mean $SW$ irrigation estimated during the 5 years of the study period was 63 mm $y^{-1}$ (~20% of total irrigation), which is well in agreement with the estimate by the local water authority. The remaining 80% of the irrigation was originating from groundwater. The overall irrigation (estimated as $P - ET$ deficit) from the irrigated croplands was found to reach up to -500 mm $y^{-1}$ (with a mean of -308 mm $y^{-1}$) with a total volume change of -2,270 MCM $y^{-1}$ (total -4,700 MCM $y^{-1}$ for all croplands) in the study period (2005-2009). The maximum yearly $P - ET$ differences were observed for wetlands (avg. -422 mm $y^{-1}$) and water bodies (avg. -495 mm $y^{-1}$), showing that they receive large groundwater and/or surface water inputs to sustain such excess $ET$.

In an effort to minimize the uncertainty in estimating the monthly and yearly $ET$, we employed the strategy of a frequent and long period of $ET$ flux

estimations, i.e., 5 years with a daily time step of SEBS-SM. This particularly helped to reduce the uncertainty of the yearly *ET*, especially in data intensive areas (Figure 4.14). The comparison of the RS-based change of storage ($\Delta S_{RS}$) with the change of groundwater storage ($\Delta S_{GW}$) showed that: i) there was better agreement between the $\Delta S_{RS}$ and ground based $\Delta S_{GW}$ when analysing 5 years period than while analysing yearly data because the 5 years data were less affected by yearly unsaturated storage changes; ii) the yearly changes and patterns of $\Delta S_{RS}$ and $\Delta S_{GW}$ were similar; iii) the $\Delta S_{GW}$ uncertainty due to the uncertainty of $S_y$ was significant and mainly because of the highly heterogeneous and unpredictable karst aquifer.

Our study showed that RS-based *P* and *ET* estimates are capable of estimating the spatially distributed water balance and storage changes with good accuracy in a large semi-arid basin. The proposed method can also be applied in other large basins, especially in semi-arid and arid regions, where there are higher potentials for obtaining long time series of frequent optical remote sensing data. The yearly *ET* estimations can still be improved in RS data scarce areas (e.g. due high cloud coverage areas) by using radar/microwave RS in *ET* estimation (no limitation of clouds). Furthermore, more advanced RS-based precipitation products will help further to reduce the uncertainties in quantifying the spatially distributed water balance. The RS-based spatiotemporally distributed water balance products, as presented in this study, can be very useful for water managers as well as in agricultural, climate and ecohydrological studies, among others, and provide assessments of a type that would not be feasible using only point-based ground measurements.

# Chapter 5

## Spatiotemporal trends in the ecohydrology of a semi-arid region

**Abstract**: We present a regional framework for an integrated and spatiotemporally distributed assessment of human-induced trends in the hydrology and the associated ecological health of a semi-arid basin, where both human activities (i.e. agriculture) and natural ecosystems are highly groundwater dependent. To achieve this, we analysed the recent trends (from year 2000 to 2010) in precipitation, evapotranspiration (actual and potential) and vegetation greenness (i.e. *NDVI*) using a combination of satellite and ground-based observations. The trend assessment was applied for the semi-arid Konya basin (Turkey), one of the largest endorheic basins in the world.

This chapter is based on:

Gokmen, M., Vekerdy, Z., Verhoef, W. and Batelaan, O.: Satellite based analysis of recent trends in the ecohydrology of a semi-arid region, Hydrol. Earth Syst. Sci., 17, 3779-3794, 2013.

## 5.1 Introduction

In recent years, the response of water cycle components and vegetation to the changing climate and to anthropogenic effects has been discussed and studied widely at global and regional scales (e.g. Douville et al., 2012; Fensholt et al., 2012; Jung et al., 2010; Liu et al., 2013; Milliman et al., 2008; Zhang et al., 2009). Satellite observations have been increasingly used in such studies, exploiting their potential of providing spatially continuous and temporally recurrent estimates over regional to global scales (Alsdorf and Lettenmaier, 2003).

New et al. (2001) used gauge and satellite merged precipitation data to analyse trends over global land areas in the 20$^{th}$ century and found a century-long trend of 9 mm (a trend of 0.89 mm/decade), which was considered quite small compared to multi-decadal (and also inter-annual) variability of precipitation. Also, Zhang et al. (2007a) used monthly precipitation observations over global land areas to analyse precipitation trends in two 20$^{th}$ century periods (1925–1999 and 1950–1999), and showed that anthropogenic forcing has had a detectable influence on observed changes in average precipitation within latitudinal bands, and that these changes cannot be explained by internal climate variability or natural forcing. Apart from global-scale studies, others (e.g. Du et al., 2011; Fensholt and Rasmussen, 2011; Hatzianastassiou et al., 2008; Lebel and Ali, 2009; Zhang et al., 2005) assessed the regional/continental precipitation trends and showed their influences on stream flow, water level, soil moisture and vegetation changes.

Jung et al. (2010) assessed the trends in global land evapotranspiration (*ET*) and its spatial distribution over the past 27 years. They compared the *ET* trends and their distribution with the trends in global potential evapotranspiration (*PET*) and soil moisture distributions, and showed that increasing soil-moisture limitations on evapotranspiration largely explain the recent declining trend of global land-evapotranspiration. On the other hand, Zhang et al. (2012) assessed the decadal trends in global evaporation using satellite and gridded meteorological data, and found that evaporation estimated from water balances of 110 “wet” and 87 “dry” catchments do not match with the estimates from three alternative *ET* models. Along these lines, Teuling et al. (2009) put forward a regional perspective on the trends in evaporation, identifying that the trends in evapotranspiration (and hence

runoff) can only be understood regionally (and temporally) by considering regional (and temporal) variations in the main drivers of evapotranspiration, because the factors controlling *ET* (i.e. energy demand and moisture supply) vary from region to region. Accordingly, several studies (Morrow et al., 2011; Ryu et al., 2008; Zhang et al., 2009; Zhang et al., 2001; Zhang et al., 2007b) conducted regional or catchment-scale analysis of trends in *ET* based on satellite observations, meteorological data, water balance and energy balance approaches.

With respect to vegetation trends, satellite-based vegetation indexes such as Normalized Difference Vegetation Index (*NDVI*) are widely used to examine the dynamics of vegetation health, density, land cover and phenological stage. However, it remains a challenge to produce a long-term, consistent, vegetation index time series across the sequence of multiple sensor systems, not only due to their different spectral responses, spatial resolutions, swath width and orbiting geometry, but also to cope with sensor degradations and drift in satellite overpass times. Therefore, several studies (Alcaraz-Segura et al., 2010; Beck et al., 2011; Fensholt and Proud, 2012; Fensholt and Rasmussen, 2011, among others) focused on intercomparisons between different sensor datasets. Other studies (e.g. Evans and Geerken, 2004; Fensholt et al., 2012; Fensholt and Rasmussen, 2011; Heumann et al., 2007; Julien et al., 2006) used *NDVI* time series to assess the trends and the responses of vegetation greenness to the changes in the climatic (e.g. rainfall and air temperature) or anthropogenic drivers.

Apart from analysing the trends, some studies (Douville et al., 2012; Evans and Geerken, 2004; Milliman et al., 2008; Sharma et al., 2000; Zhang et al., 2007a) particularly focused on coupling these trends either to changes in climatic variables (e.g. incoming radiation and temperature changes) or to anthropogenic effects (e.g. changes in land use or land cover). Others also looked at the associated changes in the water budget and resources (Famiglietti et al., 2011; Konikow and Kendy, 2005; Morrow et al., 2011; Rodell et al., 2007; Rodell et al., 2009; Tiwari et al., 2009; Wada et al., 2012; Yang et al., 2007; Zhang et al., 2009) and showed an increase of non-renewable groundwater depletion and an increase/decrease of river discharges in different regions.

Detection of trends and their significance generally requires consistent and long term records of variables. However, some human-induced trends such as land-use changes are likely to have an important role regionally (Jung et al., 2010) and, if severe, their impacts can be detected in relatively short periods. For example, assessing the satellite based estimates of groundwater depletion in India during six years, Rodell et al. (2009) stated that despite the relatively short period of evaluation, other evidences supported their conclusion that severe groundwater depletion is occurring as a result of human consumption rather than natural variability. As revealed by many other studies (Famiglietti et al., 2011; Karami and Hayati, 2005; Konikow and Kendy, 2005; McGuire, 2009; Rodell et al., 2009; Scanlon et al., 2010; Tiwari et al., 2009), persistent groundwater depletion has been occurring in different regions, leading to falling groundwater levels (Gleeson et al., 2010). The results of a global scale study by Wada et al. (2012) show that non-renewable groundwater abstraction (to sustain irrigation) globally contributes nearly 20% to the gross irrigation (for the year 2000) and has more than tripled since 1960. Groundwater is not only essential to global food security providing an irrigation buffer against climate extremes but also affects terrestrial ecosystems by sustaining river base-flow and root-zone soil water in the absence of rain (Fan et al., 2013). Therefore, the value of groundwater is expected to increase in the coming decades, as the temporal variability in precipitation, soil moisture and surface water is projected to increase under more frequent and intense weather extremes associated with climate change (Taylor et al., 2012), and also along with the rising population and their food demands, particularly in emerging countries such as India, Pakistan, China, Iran, Mexico and Turkey, among others. The semi-arid Konya basin in central Anatolia (Turkey), which is one of the biggest endorheic basins in the world, is a characteristic example of groundwater resources under strong anthropogenic pressure. Over the last few decades, the basin experienced a huge non-renewable groundwater abstraction for irrigation, which caused approximately 1 m $year^{-1}$ head decline (Bayari et al., 2009).

In this study, we analyse the recent trends (from 2000 to 2010) in precipitation, evapotranspiration (actual and potential) and vegetation greenness (i.e. *NDVI*) using satellite-based observations. On this basis, we assess the distribution of the human-induced changes in the hydrology and the associated ecological health of the semi-arid Konya basin, where both

human activities (agriculture) and natural ecosystems are highly groundwater dependent. More specifically, this study aims at:

1) Providing a framework for a RS-based and integrated assessment of eco-hydrological trends and their causes at regional scale.
2) Detecting trends and their significance in consistently established time series of actual and potential evapotranspiration, precipitation, vegetation greenness (i.e. *NDVI*) in a spatially distributed manner.
3) Inter-comparison of the observed trends and analysing the correlations in order to identify consistencies between them and to attribute the trends to the climate and/or human-induced changes.
4) Analysing inter-relations between the trends in the hydrological variables and ecological health in the region.

## *5.2 Materials and methods*

A systematic framework is essential for detecting trends (Burn and Elnur, 2002). In this regard, we first established a consistent and spatiotemporally continuous time series of the variables, and then applied widely used statistical tests such as Mann Kendall's trend and Pearson's correlation tests, and linear models to detect the significance, direction and magnitude of the trends and correlations. Figure 5.1 presents a flowchart of the analysis. The methods and the datasets are described below.

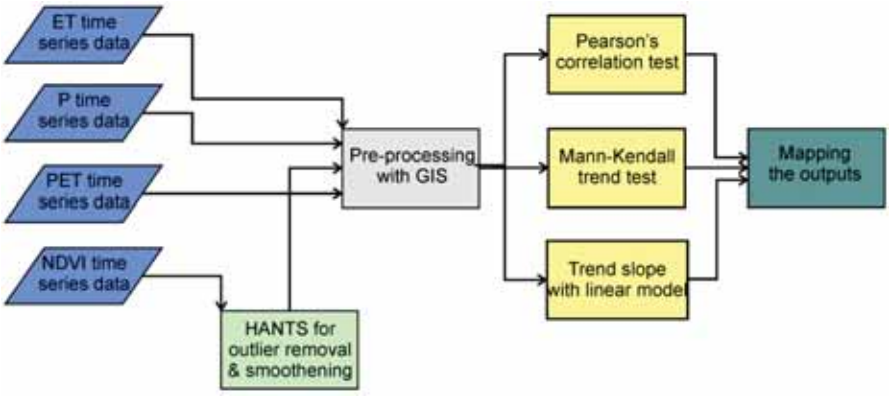


**Figure 5.1** Flowchart of trend analysis using satellite-based datasets

### 5.2.1 Harmonic analysis of time series

A Harmonic ANalysis of Time Series (HANTS) algorithm was developed by Verhoef et al. (1996), which uses an iterative curve fitting starting with all data points and sequentially removing the most pronounced negative outliers. Clouds always have a negative influence on the *NDVI* and therefore taking the maximum value of the *NDVI* over a limited period (i.e. maximum value compositing, MVC) tends to remove most cloud-contaminated observations. The HANTS algorithm also removes the effect of clouds on the *NDVI* value, in this case by using an iterative curve fitting procedure, i.e. a least squares curve is estimated based on all current data points, and the observations that have the greatest negative deviation from the curve are removed first. Next, a new curve is computed based on the remaining points and the process is repeated (Julien et al., 2006) until either the fit is sufficiently good, or the number of remaining points becomes too small. Eventually the iteration leads to a smooth curve that approaches the upper envelope over the data points. As a result, more reliable estimates of yearly *NDVI* averages and first harmonic amplitudes and phases are achieved. The amplitude of the first harmonic indicates the variability of vegetation greenness over the year. The phase of the first harmonic indicates the earliness of vegetation green-up.

### 5.2.2 Trend and correlation analyses

The time series of all the hydrologic variables and vegetation greenness (*NDVI*) were analysed using the Mann-Kendall non-parametric test for trend. Mann (1945) originally designed this test and Kendall (1975) subsequently derived the test's statistic distribution. The Mann-Kendall test has two parameters that are of importance for trend detection: the significance level that indicates the trend's strength (*p* value), and the slope magnitude (Kendall's Tau) estimate that indicates the direction as well as the magnitude of the trend. After detecting the significance, direction and magnitude of trends by the Mann-Kendall test, the quantities (slopes) of trends are determined using linear models. In order to apply the trend analysis in a spatially distributed manner, the Mann-Kendall test was applied using the R software and the Kendall package for R (http://cran.r-project.org/web/packages/Kendall/Kendall.pdf).

Pearson's correlation test was applied to assess the correlations between the time series of different variables. The test has two key properties of magnitude and direction indicated by Pearson's *r* value ranging between -1

and 1. Pearson's correlation test was applied using the R software and rcorr function of the Hmisc package for R (http://cran.r-project.org/web/packages/Hmisc/Hmisc.pdf).

### *5.2.3 Data*

Table 1 provides a summary of the input data that were used to obtain the hydrological and vegetation variables for time series analysis. Our study covered the period between 2000 and 2010, which was mainly limited by the start of MODIS satellite observations. MODIS data are highly suitable for regional scale studies due to its moderate spatial resolution (1 km) and its high temporal frequency (daily), and formed the core datasets for ET and the vegetation variables in this study. Further details of data and models that were used to obtain the time series of variables are described in the following sub-sections.

**Table 5.1** The summary of the data used in the study

| Variable | Input data | Source | Spatial resolution | Temporal resolution | Temporal coverage |
|---|---|---|---|---|---|
| Evapotranspiration | *Albedo* | MODIS | 500 m | 16-daily | 2000 - 2010 |
| | *Emissivity* | MODIS | 1,000 m | Daily | 2000 - 2010 |
| | *Land surface temperature* | MODIS | 1,000 m | Daily | 2000 - 2010 |
| | *Leaf area index* | MODIS | 1,000 m | 8-daily | 2002 - 2010 |
| | *NDVI* | MODIS | 500 m | 16-daily | 2000 - 2010 |
| | *Surface soil moisture* | TRMM-TMI | ~25 km | 2-3 daily | 2000 - 2002 |
| | | AMSR-E | ~25 km | 2-3 daily | 2002 - 2010 |
| | *Short & long wave radiation* | ECMWF | ~75 km | Daily | 2000 - 2010 |
| | *Wind* | Meteo.station | Point data | Daily | 2000 - 2010 |
| | *Air Temperature* | Meteo.station | Point data | Hourly | 2000 - 2010 |
| | *Pressure* | Meteo.station | Point data | Daily | 2000 - 2010 |
| | *Sunhours* | Meteo.station | Point data | Daily | 2000 - 2010 |
| Precipitation | *TRMM-precipitation* | TRMM | ~25 km | Monthly | 2000 - 2010 |
| | *Gauge-precipitation* | Rain gauges | Point data | Monthly | 2000 - 2010 |
| Vegetation greenness | *NDVI* | MODIS | 500 m | 16-daily | 2000 - 2010 |
| Potential ET | Pan evaporation | Meteo.station | Point data | Daily | 2000 - 2010 |

### a. *ET* data

Nowadays RS-based surface energy balance models are increasingly used to estimate the distribution of evapotranspiration from field to global scales. The physically based and single source SEBS model (Su, 2002) is one of the surface energy balance models widely used by the scientific community. SEBS estimates actual evapotranspiration (*ET*) using RS retrievals and meteorology data, and it has been applied in many regional to global studies (Jia et al.,

2003; Jin et al., 2009; Ma et al., 2012; Ma et al., 2007; Oku et al., 2007; Pan et al., 2012; Pan et al., 2008; Vinukollu et al., 2011). The details of the SEBS algorithm are provided in Su (2002) and Su et al. (2001).

In this study, we used a modified version of SEBS called SEBS-SM (Chapter 3) for the estimation of the spatiotemporal distribution of actual evapotranspiration. The SEBS-SM integrates soil moisture through incorporating a water stress index into the model to better account for a moisture-limited evapotranspiration regime (Chapter 3), which is typical for semi-arid regions. The performance of SEBS-SM was tested in Chapter 3 through comparing it with ground data by Bowen ratio stations, and also through establishing a yearly water budget (Chapter 4), and proved to be an overall improvement to the original model under water-stressed conditions.

Figure 5.2 provides a flowchart of obtaining the daily, monthly and yearly *ET* by SEBS-SM. The SEBS-SM was run on a daily interval for the study period (2000-2010). For filling the data gaps and obtaining monthly/yearly *ET*, we followed the methodology described in Chapter 4.

To collect the necessary input parameters for the model, we used MODIS land products (https://lpdaac.usgs.gov/products/modis_products_table) and AMSR-E and TRMM-TMI soil moisture products (Owe et al., 2008). As shown in Table 1, the Leaf Area Index (*LAI*) product of MODIS was available only after July 2002. For the missing *LAI* input data during 2000-2002, we used alternatively the formula by Wang et al. (2005) to estimate the *LAI* from *NDVI*. Furthermore, for soil moisture input data, we used the AMSR-E and the TRMM-TMI soil moisture products in combination, because the AMSR-E product was available starting from June 2002. The use of two different data sets did not necessitate any inter-calibration procedure because, as described in Chapter 3 in detail, SEBS-SM utilizes the time series of soil moisture information as relative soil moisture (wetness) values that represent the water stress conditions, and it is insensitive to the absolute values of soil moisture.

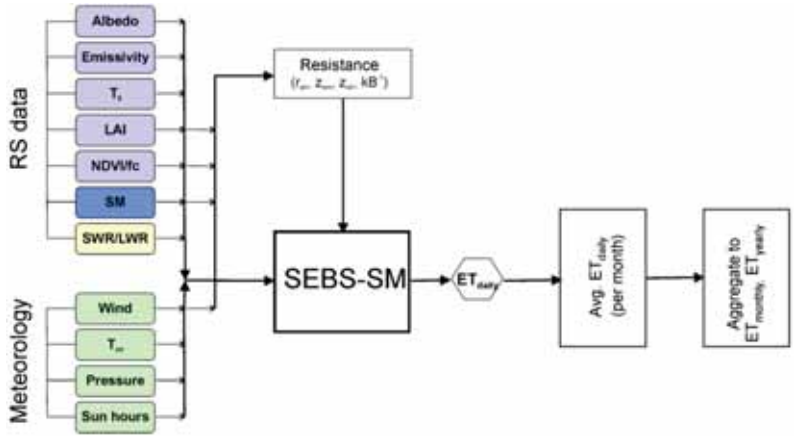


**Figure 5.2** Input data for SEBS-SM and flowchart for obtaining yearly *ET* (Adapted from Gokmen et al., 2013). In the figure, $T_0$ = surface temp., $T_{air}$ = air temp. at reference height, *LAI* = Leaf Area Index, *NDVI* / *fc* = normalized difference vegetation index/fraction of vegetation cover, *SM* = soil moisture, *SWR*/*LWR* = shortwave & longwave incoming radiation, $r_{ah}$ = aerodynamic resistance, $z_{0h}$ = roughness height for heat, $z_{0m}$ = roughness height for momentum, $kB^{-1}$ = dimensionless excess resistance parameter.

In addition to the RS data, the necessary meteorological forcing data were obtained from the Turkish Meteorological Service for the 18 stations located in and around the basin (Figure 2.1). The point measurements of the stations were spatially interpolated using the natural neighbour interpolation method. With respect to instantaneous and daily air temperature, additionally, the local lapse rates were calculated for the mountainous areas and integrated (based on a DEM) in the interpolation of air temperature data. Finally, the downwelling shortwave and longwave radiation fluxes ($R_{swd}$ and $R_{lwd}$), the boundary layer height and dew point temperature at 2 m height were retrieved from the high-resolution gridded ECMWF (The European Centre for Medium-Range Weather Forecasts) interim reanalysis dataset (http://data-portal.ecmwf.int/ ).

In addition to actual *ET* time series, we also used the time series of potential evapotranspiration (*PET*), which is a representation of the atmospheric demand for evapotranspiration. *PET* can be considered as an indicator of climate-related changes as its magnitude depends on variables including incoming radiation, vapour-pressure deficit (often associated with temperature). The spatiotemporal *PET* distribution of the Konya basin was

obtained using the class-A pan evaporation data from the 18 meteorological stations (Figure 2.1) and the simplified formula by (Snyder et al., 2005).

### b. *NDVI* data

We used the MODIS *NDVI* product MOD13A1, which is designed to provide consistent spatial and temporal comparison of vegetation conditions. Global MOD13A1 gridded data are provided every 16 days (as 16-daily composite) at 500 m spatial resolution. This product is computed from atmospherically corrected bi-directional surface reflectances that have been masked for water, clouds, heavy aerosols, and cloud shadows. The accuracy of these MODIS Vegetation Indices has been assessed over a widely distributed set of locations and time periods via several ground-truth and validation efforts (https://lpdaac.usgs.gov/products/modis_products_table/mod13a1).

Although the 16-daily composite *NDVI* product removes most of the cloudy pixels by selecting the highest value of *NDVI* during each 16-day period for each pixel, there may still be some remaining cloud or haze contaminated pixels, especially in regions experiencing a long winter/wet season with continuous cloud casting. Therefore, we applied the HANTS algorithm for removing the remaining effects of clouds and haze on the *NDVI* value. Finally, we resampled the originally 0.5 km spatial resolution of MODIS *NDVI* product to 1 km resolution using bicubic interpolation in order to match it with the resolution of other variables.

### c. Precipitation data

To establish the time series of the precipitation distribution, we used the monthly product of the Tropical Rainfall Measuring Mission (TRMM-3B43), combined with local rain gauge measurements. Please see section 4.2.1 for the details of the TRMM data.

Pan et al. (2008) indicated that TRMM products have large differences compared to ground observations at short time intervals (3-hourly) but the discrepancies become smaller as the aggregation time increases. They also report a positive bias of the TRMM product. Similarly, in Chapter 4 we compared the wet and dry season 6-monthly TRMM rainfall data with the gauge observations, and found a positive bias of around 80 mm by TRMM for the wet seasons in the Konya basin. Therefore, we used a bias-removed time series of TRMM rainfall data based on the comparison in Chapter 4. Although

the TRMM data is available starting from 1998, we used a dataset between the year 2000 and 2010 to be consistent with the other times series.

## 5.3 Results

### 5.3.1 ET trends

Figure 5.3a shows the distribution and the direction of significant trends in the yearly *ET* in the Konya basin. According to Figure 5.3a, the areas with significant ($p < 0.1$) increasing yearly *ET* are much larger than the areas with decreasing trend, although the increasing trend is not basin-wide but spatially clustered in certain areas, especially in the Konya plain part (inside the polygon). When we look at the rate of change (Figure 5.3b), the highest increasing rates are observed in the Konya plain part and reach up to 30 mm $y^{-1}$, which would mean more than 300 mm increase in the yearly *ET* during the study period (2000 - 2010). With respect to the distribution of these increasing *ET* areas over different land covers, Figure 5.3c clearly shows that this trend mostly occurred in irrigated croplands, followed by non-irrigated croplands, pasture and grassland. In terms of decreasing trend of *ET*, Figures 5.3a, 5.3b and 5.3d show that the decreasing trend of yearly *ET* occurred only in certain distinctive places (e.g. around Lake Beyşehir and the wetlands in the Konya plain indicated by smaller polygons), while the rate of decreasing trend was especially higher in the wetlands reaching around -30 mm $y^{-1}$ (Figure 5.3b).

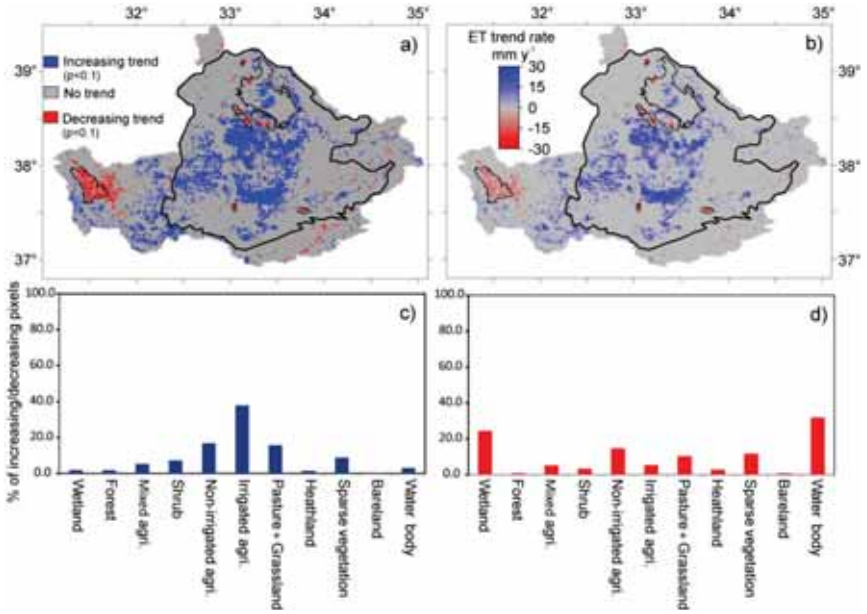


**Figure 5.3** The distributions of **a)** significant trends, and **b)** the magnitudes of the trends of yearly ET in the Konya basin, and the histograms of the areas with **c)** increasing trend, **d)** decreasing trend for different land covers.

Results of the seasonal *ET* trend analysis are shown in Figures 5.4a-d and Figures 5.5a-d. The distribution and direction of the trend (Fig 5.4a-d), except for winter, shows generally a similar pattern as the yearly trend with a dominantly increasing trend especially in the plain part. The distribution was more spatially concentrated in the summer compared to a more dispersed distribution in spring and autumn. Comparing the seasons, the decreasing trend was largest in winter, especially in the mountainous part (outside the polygon). On the other hand, from the distribution of the rate of trends for each season (Figs. 5.5a-d) it is clear that the highest rate of change (both increasing and decreasing) among all seasons occurred in the summer, as can be expected, since this season has the highest atmospheric demand for evapotranspiration. On the opposite, the change of seasonal *ET* was lowest in winter (Figure 5.5d), since the contribution of the winter *ET* to the overall yearly *ET* trend is the least among the seasons.

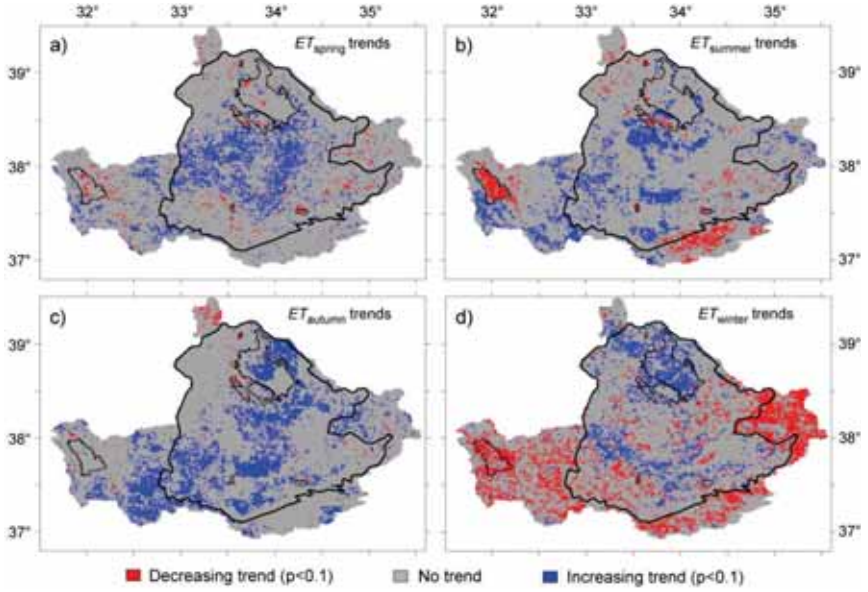


**Figure 5.4** Distributions of trends in the seasonal ET in the Konya basin for **a)** spring, **b)** summer, **c)** autumn, **d)** winter between 2000 and 2010.

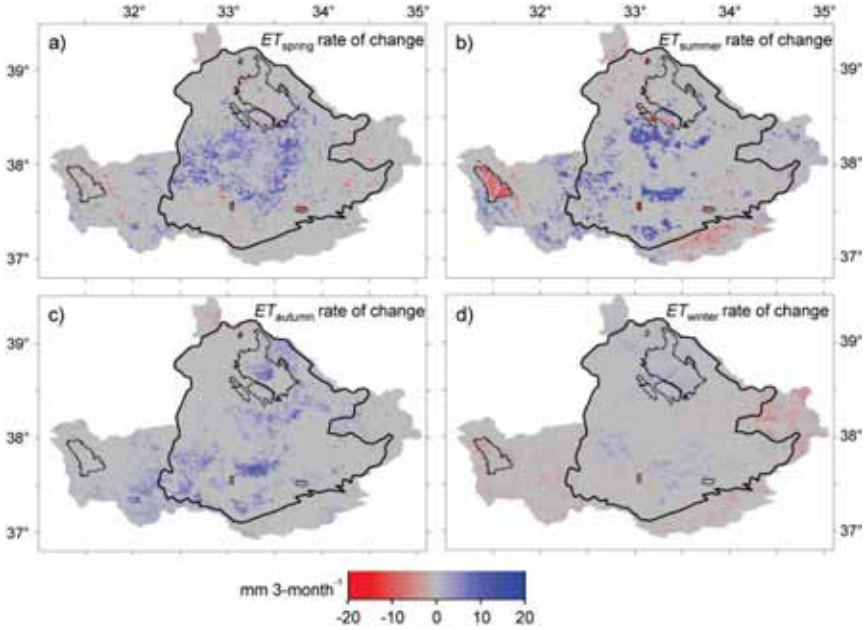


**Figure 5.5** The distributions of the magnitudes of the trends in the seasonal *ET* in the Konya basin for **a)** spring, **b)** summer, **c)** autumn, **d)** winter.

### *5.3.2 Trends in vegetation greenness*

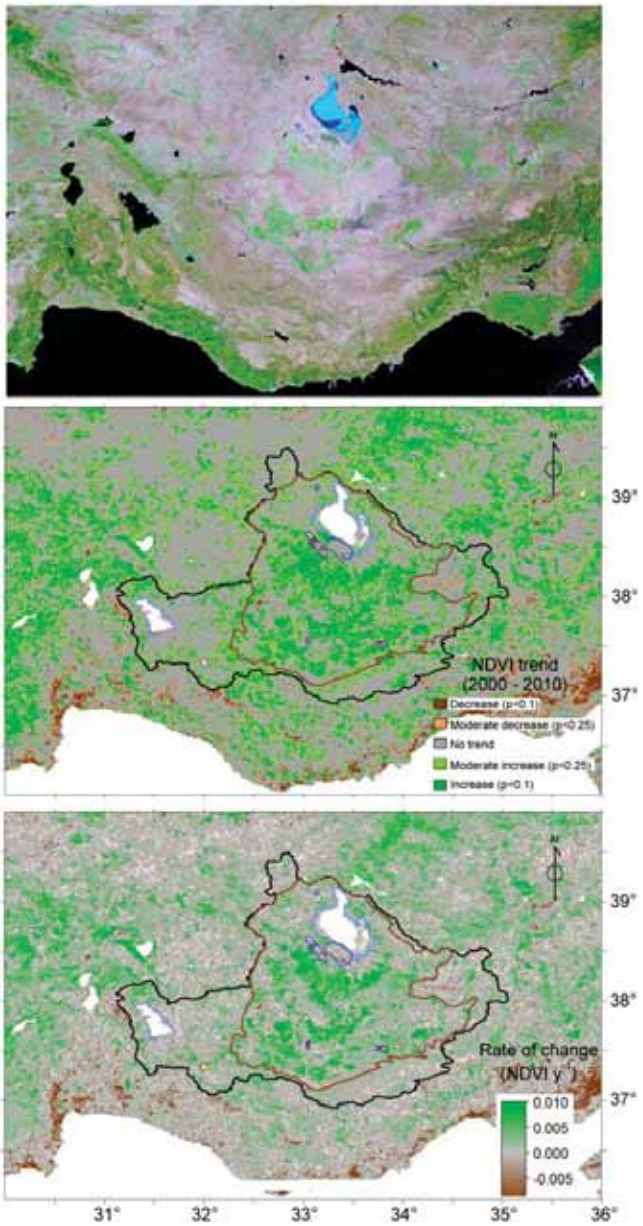


**Figure 5.6a** False-colour composite of MODIS image (RGB= bands 7, 2, and 1), **b)** distribution of *NDVI* trends and, **c)** magnitudes of the trends in the yearly average *NDVI*.

Figure 5.6a shows a false colour composite image (of mid-July, 2012) and Figures 5.6b and 5.6c the distribution and the magnitudes of trends in the average yearly NDVI in and around the Konya basin during the study period (2000 – 2010). Figure 5.6b reveals two different regional trends: a generally decreasing trend in the mountainous range along the Mediterranean coast in the south, while in the inner parts where continental climate prevails, increasing trend areas are generally observed including the Konya basin, as indicated by the polygon. In addition, Figure 5.6c indicates that the areas with the highest rates of increasing trend are observed in the Konya basin (inside the polygon) with rates reaching around 0.01 *NDVI* $yr^{-1}$.

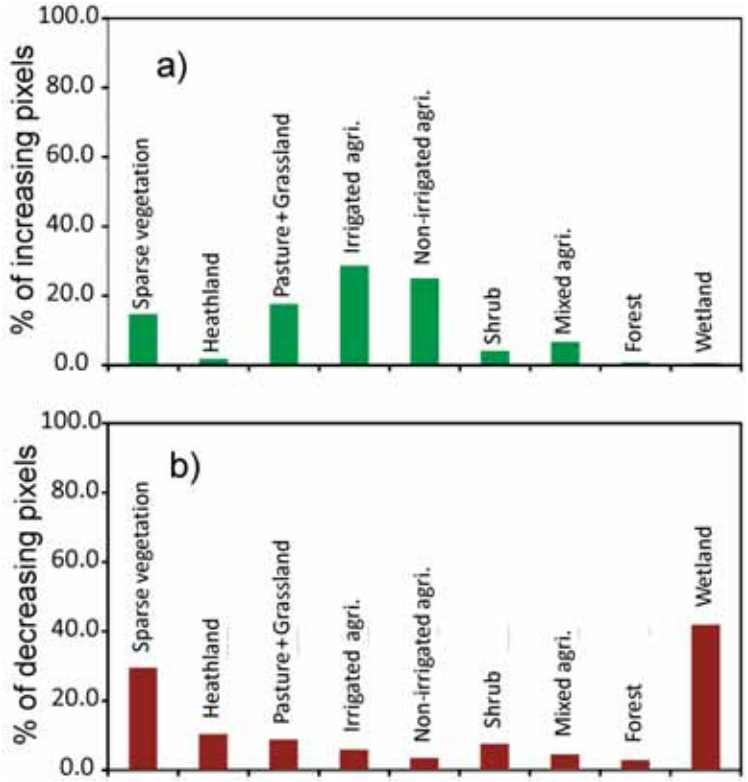


**Figure 5.7** The distribution of areas with **a)** increasing trend, **b)** decreasing trend in yearly average NDVI for different land covers in the Konya basin.

When we focus on the distribution of the average *NDVI* trends inside the Konya basin (black-coloured polygon in Figure 5.6b), we observe that the increasing trend is mainly in the plain areas (inside the brown-coloured

polygon) rather than in the mountainous parts (between black and brown-coloured polygons). Furthermore, crossing the mean *NDVI* trends (Figure 5.6b) with the land cover map (Figure 2.2a), we found that the increasing trend of mean *NDVI* was mostly observed in irrigated and non-irrigated croplands, followed by the pasture and grassland (Figure 5.7a). On the other hand, Figure 5.7b shows that the decreasing *NDVI* areas are mainly wetlands (small polygons) and sparse vegetation.

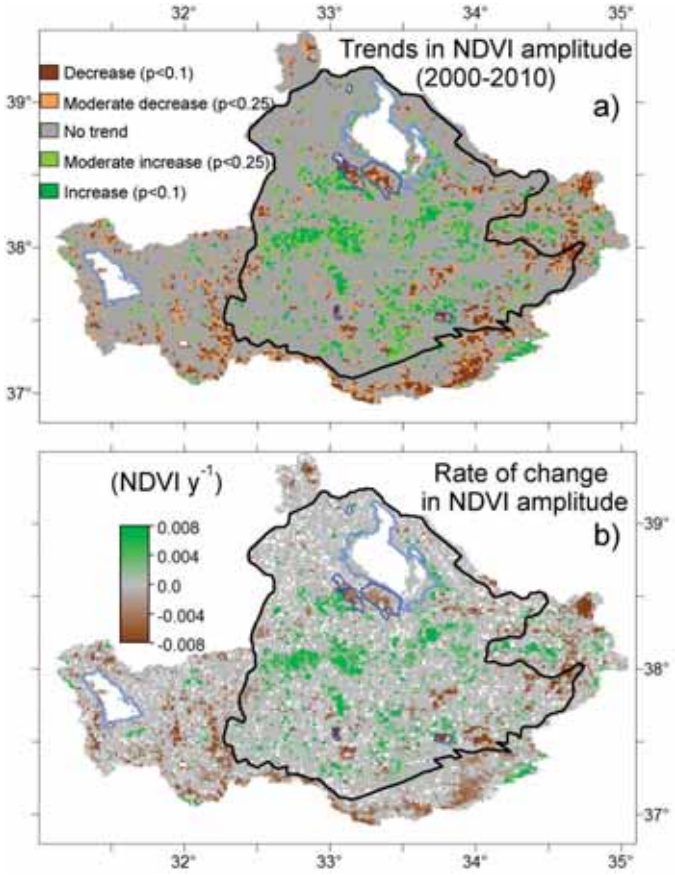


**Figure 5.8a** Distribution, and **b)** magnitude of trends in the yearly amplitude of *NDVI* in the Konya basin. Note that white coloured parts are either water bodies (inside light blue polygons) or no result pixels.

Lastly, Figures 5.8a and 5.8b show the distribution of the trend and the rate of change in the amplitude of *NDVI*. Amplitude indicates the level of temporal variation in *NDVI* and high amplitude means a wide range due to seasonal

variation. Compared to the large areas with an increasing trend for the mean *NDVI* (Figure 5.7b), the areas with increasing trend of *NDVI* amplitude are smaller in the Konya plain (inside the black coloured polygon). These areas are mainly related to the increase in the maximum *NDVI* values due to intensification of irrigation and land cover changes. With respect to the decreasing trend in the *NDVI* amplitudes, those are observed in the wetlands (dark-blue coloured polygons) and also in the mountainous parts (outside the black polygon – mostly shrub and forest land covers), which can be related to the either decreasing *NDVI* maximum values or increasing *NDVI* minimum values. With respect to the rate of change in *NDVI* amplitude, Figure 5.8b shows that highest rate of increasing or decreasing amplitudes were localized in some parts of the basin instead of a general homogeneous spread.

### *5.3.3 Partitioning of the anthropogenic effects from the climate-driven changes in ET trends*

In order to attribute the causes of *ET* trends and their distribution, it is first needed to reveal the distribution of the controlling factors of *ET* (i.e. energy demand and moisture supply) (Teuling et al., 2009). Figure 5.9a shows the distribution of the water limitation given by the criterion of Parsons and Abrahams, (1994) who defined the water-limited environments as the areas having a *P*/*PET* ratio less than 0.75. We can conclude that except for the upstream mountainous parts in the southwest, south and east, the whole Konya plain (indicated by the polygon in Figure 5.9a) can be classified as a highly water-limited environment with a *P*/*PET* ratio of about 0.3. Additionally, we assessed the correlation between precipitation and actual evapotranspiration using Pearson's correlation test: Figure 5.9b not only confirms the pattern provided by *P*/*PET* map (Figure 5.9a) about the division of moisture supply/energy demand control of *ET* between Konya plain and mountainous parts, respectively, but also indicates some patches of energy-limited areas in the Konya plain despite the low precipitation input ('no correlation' areas in Figure 5.9b). This can be partly related to additional groundwater discharge to the wetlands (smaller polygons indicated by purple colour) and water bodies (e.g. hyper-saline Tuz Lake in the north), which show that these ecosystems are more groundwater- than precipitation-dependent to sustain high evapotranspiration rates. Apart from these naturally groundwater-fed areas, the other energy-limited areas in the Konya plain mostly correspond to irrigated croplands where additional water supply

(mainly from groundwater) is provided to sustain the crop water requirements.

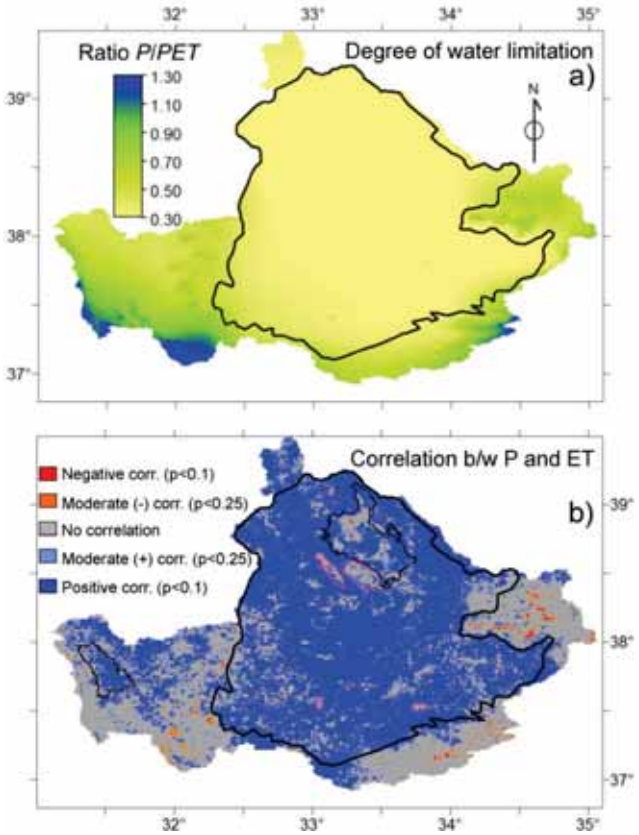


**Figure 5.9** The distribution of **a)** water limitation **b)** the correlation between *P* and *ET*

To reveal further the causes of *ET* trends in the Konya basin, Figures 5.10a-d show the distributions of the significance and rate of trends in the climate-related variables of potential evapotranspiration (*PET*) and precipitation (*P*). According to Figure 5.10a, *PET* has an increasing trend in the southwest of the basin, which includes the mountainous upstream part and the southwest corner of the Konya plain (green areas inside the black polygon). In terms of rate of *PET* trend (Figure 5.10c), the increasing trend reaches to 15 mm $y^{-1}$ in the mountainous part and gradually decreasing towards the inner plain part. Note that the *PET* map is an interpolation result of point data (see sub-section 5.2.3.a), so the level of spatial detail is coarser than the satellite image based maps, i.e. *P* and *ET*. With respect to precipitation (Figure 5.10b), there was only some small patches of areas which had moderate ($p<0.25$)

decreasing and increasing trends in the west (in and around lake Beysehir) and east of the basin, respectively. In these patches, the rates of decreasing and increasing trends were around 10-15 mm $y^{-1}$.

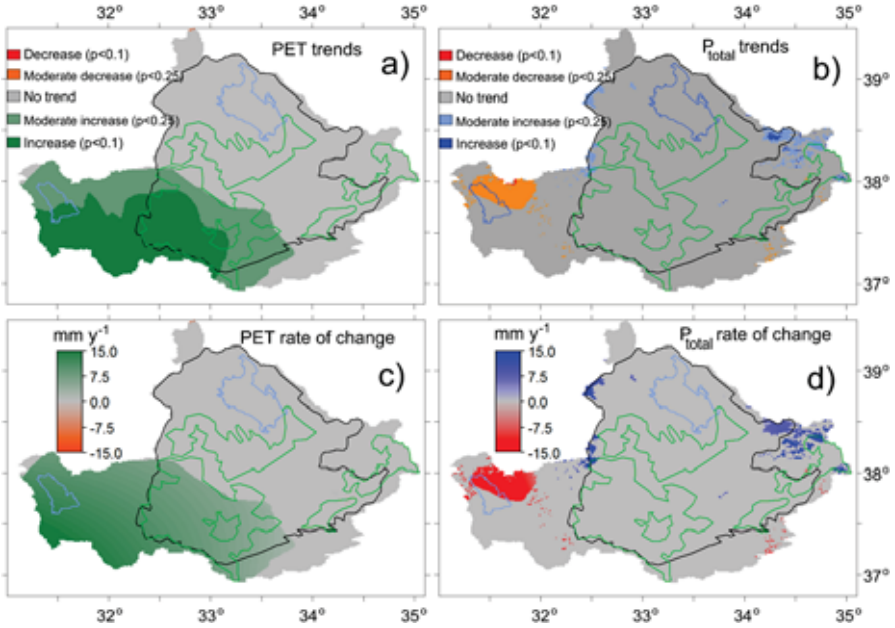


**Figure 5.10a** The distribution and direction of PET trends, **b)** the distribution and direction of P trends **c)** the magnitude of PET trends, **d)** the magnitude of P trends. The black polygon shows the water-limited part, the green polygons indicate the irrigated croplands and the blue polygons the lakes.

Finally to be able to partition quantitatively the causes of *ET* trends between anthropogenic (e.g. irrigation) and climate drivers (i.e. *P* and *PET*), Figures 5.11a-b firstly show the cross maps of *ET* versus *PET* and *P* trends, respectively. Overlaying the trend distributions of *ET* and *PET* we can observe that most of the areas with significant *ET* increase and decrease (dark blue and red colours, respectively) in the Konya plain (water-limited part) had no significant trend of *PET* ($p<0.1$). Similarly, the combined distribution of *ET* and *P* trends in Figure 5.11b shows that, especially in the Konya plain part, neither the increasing nor the decreasing trends of *ET* had relation with the changes in *P* because there was no significant trend of *P* in any direction in these areas. The only part *P* and *ET* trends had correlation was around lake Beysehir in the west (brown colour), where both *ET* and *P* had decreasing trends, where *ET* had been depicted as relatively moisture-limited (i.e. positively correlated with precipitation) in Figures 11a and b. More

specifically, Figures 5.11c-d show the histograms of *ET*, *PET*, and *P* trends in the areas with significant *ET* trend for energy and water-limited regions separately. Based on these histograms, Table 5.2 presents the quantitative summary of attributing and partitioning of *ET* trends in the energy- and water-limited parts. According to Table 5.2, in the water-limited part, for a total *ET* increase of about 135 MCM $y^{-1}$ (mainly croplands, Figure 5.3c), only about 21 MCM $y^{-1}$, which corresponds to about 16% of total *ET* increasing trend, can be attributed to the increasing trend of *PET* in these areas, while the rest cannot be explained by *PET* or *P* trends. With respect to the decreasing trend areas of *ET*, neither *PET* nor *P* trend can explain any of the *ET* decrease, which is totally about -25 MCM $y^{-1}$ (mainly in the wetlands and water bodies, Figure 5.3d) in the water-limited part. On the other hand, in the energy limited part, the whole of the *ET* increasing trend (i.e. about 25 MCM $y^{-1}$) can be explained by the increasing *PET* trend of totally 44 MCM $y^{-1}$. While for the decreasing portion of *ET* in the energy limited part (i.e. about -13 MCM $y^{-1}$), 65% of it can be explained by the decreasing trend of *P* (i.e. about -9 MCM $y^{-1}$).

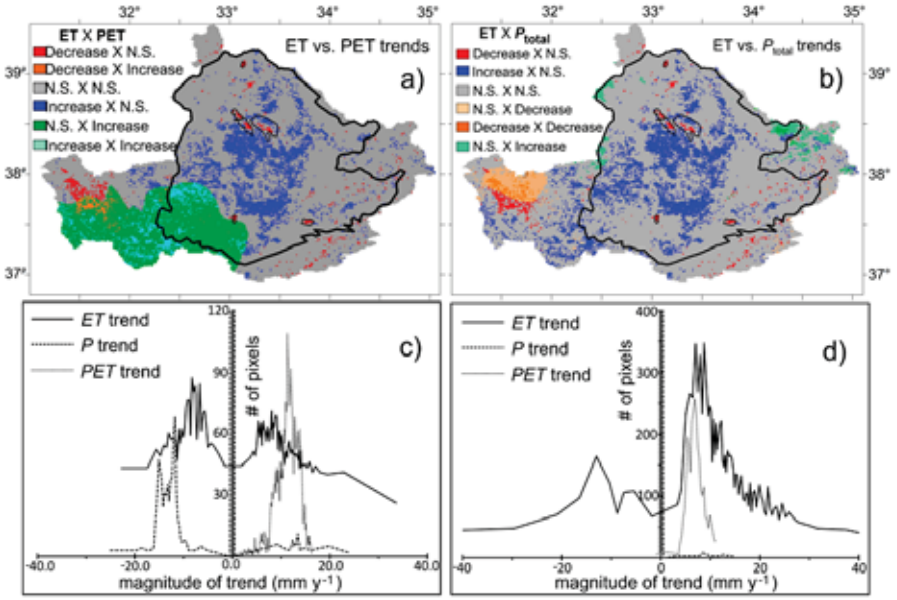


**Figure 5.11a** The cross-relation between *ET* vs. *PET* trends, **b)** cross-relation between *ET* vs. *PET* trends (Note that "N.S." represent "Not significant trend" in the legends of Figs.5.11a and 11b), **c)** histograms of *ET*, *PET* and *P* trends for the energy-limited part (outside Konya-plain polygon), **d)** histograms of *ET*, *PET* and *P* trends for the water-limited part (inside Konya-plain polygon). Note that the histograms of all the three variables represents the represents the areas with significant *ET* trend ($p<0.25$) both in the energy- and water limited parts.

**Table 5.2** The quantitative summary of *ET*, *PET* and *P* trends for the areas with significant *ET* trend (p<0.25) in the energy- and water-limited parts, separately.

| | | | ET | PET | $P_{total}$ |
|---|---|---|---|---|---|
| Water limited part | Increase | Avg. (mm $y^{-1}$) | 13,6 | 6.8 | 10,9 |
| | | Total (MCM $y^{-1}$) | **135,8** | **21.3** | **0,5** |
| | Decrease | Avg. (mm $y^{-1}$) | -13,8 | -0,3 | 0,0 |
| | | Total (MCM $y^{-1}$) | **-12,2** | **-0,006** | **0,0** |
| Energy limited part | Increase | Avg. (mm $y^{-1}$) | 7.9 | 8.4 | 13,4 |
| | | Total (MCM $y^{-1}$) | **24,8** | **44.3** | **1,1** |
| | Decrease | Avg. (mm $y^{-1}$) | -6,3 | 0,0 | -13,2 |
| | | Total (MCM $y^{-1}$) | **-13.3** | **0,0** | **-8,6** |

Based on Figures 5.10, 5.11 and Table 5.2, we can conclude that the *ET* trends that occurred in the Konya plain, where moisture supply controls the *ET* regime, are mostly (about 84% of the increase and 100% of the decrease) not related to the changes in the climate variables such as *P* and *PET*. Hence, the *ET* trends in the plain can mainly be attributed to the anthropogenic effects such as land and water use changes (i.e. conversion of lands to the irrigated croplands and intensification of groundwater irrigation), which is also supported by *NDVI* trends of these land cover types (Figure 5.6b and Figure 5.7a). On the other hand, the *ET* trends that occurred in the mountainous part, especially in the southwest, are mainly related to the climate-related *PET* and *P* trends.

### *5.3.4 Interactions between the water use (irrigation) and ecosystems (wetlands) health*

In the Konya basin, groundwater is the main source of water for irrigation (about 80% according to Chapter 4), because it can be accessed almost anywhere in the flat areas of the basin (Bayari et al., 2009). The conceptual diagram in Chapter 2 (Figure 2.3), shows that the regional groundwater flow, from the mountains in the south towards the terminal Tuz Lake in the north, discharges at some wetlands and water bodies around the basin and sustains

these ecosystems. As these groundwater-dependent ecosystems are highly sensitive to groundwater level changes, they are also directly affected by the agricultural activities that utilize groundwater as a source for irrigation.

Figs. 5.12a and b show the changes in the aerial average and the total volume of *ET* per year for different land cover classes in the water-limited Konya plain, which experienced mainly human-induced trends as shown in section 5.3.3. According to Figure 5.12a, irrigated croplands had the highest average increase of *ET* with 6.4 mm $y^{-1}$, while the only decrease of *ET* was for wetland, with a rate of -2.8 mm $y^{-1}$. With respect to the changes in the total volumes of water evaporated in the areas having significant trends, irrigated croplands was again leading with a totally 47.1 MCM $y^{-1}$ increase of *ET* (which means more than 500 MCM increase of *ET* overall during the 2000 - 2010 study period), followed by non-irrigated croplands with a total increasing volume of 15.6 MCM $y^{-1}$. On the other hand, wetlands had a total decreasing volume of 2.1 MCM $y^{-1}$, which adds up to about 23 MCM overall during the 2000 - 2010 study period.

Moreover, by the histogram of changes in the yearly average *NDVI* for different land covers, Figure 5.12c indicates with a similar distribution to Figure 5.12a that the highest increasing rate of *NDVI* was observed for irrigated croplands (0.004 NDVI $y^{-1}$), while the only decreasing rate was observed for wetlands again (-0.001 NDVI $y^{-1}$). Finally, Figure 5.12d shows the overlaid spatial distributions of *ET* and *NDVI* to analyse if their trends also spatially correspond to each other. Figure 5.12d indicates that there is generally a good agreement for both significantly increasing (purple colour) and decreasing (dark brown colour) trend areas, which suggests that the drying trend of wetlands in the Konya plain is the direct result of the increasing rate of evapotranspiration from the croplands because the increasing irrigation water use is depleting the groundwater resources, upon which the wetlands are dependent.

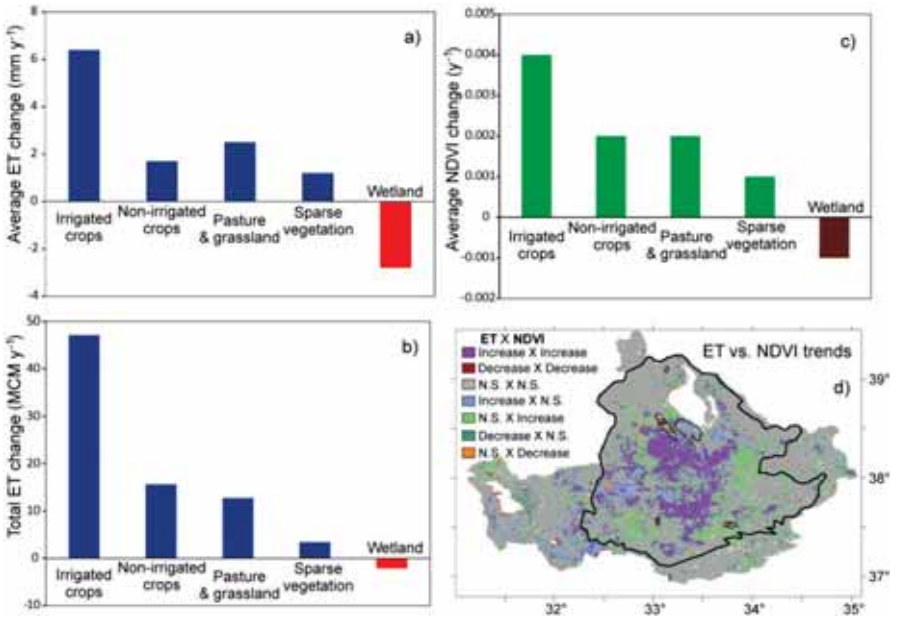


**Figure 5.12** The histograms of **a)** average, **b)** total *ET* changes and **c)** average *NDVI* changes in the areas having significant trend, **d)** the spatial distribution of the overlaid trends of *ET* and *NDVI* in the Konya plain during the study period (2000 - 2010).

## 5.4 Discussion

Putting forward a regional perspective on the trends in evaporation, (Teuling et al., 2009) stated that identifying the trends in evapotranspiration (and hence runoff) can only be understood regionally (and temporally) because the controlling factors of *ET* (i.e. energy demand and moisture supply) vary from region to region. In addition, (Douville et al., 2012) state that, among the water cycle components, changes in *ET* are easier to detect and attribute than changes in precipitation or runoff, due to their stronger "signal-to-noise ratio", because precipitation and runoff are intermittent and non-linear processes, whereas *ET* occurs every day and is a much better time integrator of regional change. Therefore, following a regional perspective, we used the time series of RS-based *ET* estimations as the key variable to assess the spatial distribution of the eco-hydrological changes in the semi-arid Konya basin.

Detection of trends and their significance generally requires consistent and long term records of the variables considered, especially in the case of detecting climate change driven trends. In this respect, the 11 years period (2000 - 2010) of this study, which was mainly limited by the availability of one

of the core data sets (i.e. MODIS), was relatively short, especially for assessing the climate-related trends. However, some human-induced trends such as land-use changes are likely to have an important role regionally (Jung et al., 2010) and can be detected in relatively short periods, as revealed by a previous study by Rodell et al. (2009) about the satellite based estimates of groundwater depletion in India during a six years study period. Similarly, by presenting a striking example of a semi-arid region where anthropogenic factors (i.e. land use changes and non-sustainable groundwater use) strongly affect the hydrological fluxes and ecosystems health, our study could reveal the human-induced trends in the eco-hydrology of the region over a relatively short period of about a decade. However, in case of applying such a framework for regions not subjected to strong human influences, one must pay special care on the length of data that allow the detection of trends with high statistical confidence (i.e. detection time). As stated by Leroy et al. (2008), it is obvious that the longer the time series, the easier it should be to distinguish a trend from natural variability (and measurement uncertainty), because shorter periods of record generally have small signal-to-noise (S/N) ratios (Allen et al., 1994). The strong timescale dependence of S/N ratios arises primarily because of the large decrease in noise amplitude as the period used for trend fitting increases (Santer et al., 2011). Based on a hypothetical dataset with certain statistical characteristics, Leroy et al. (2008) determined the minimum detection time as about 33 years for detecting a global warming signal of 0.2 K decade$^{-1}$. Similarly, assessing the trend consistency over a range of timescales (from 10 to 32 years), Santer et al., 2011 states that multi-decadal records are required for identifying the human effect on the climate variables (e.g. temperature) with high statistical confidence.

To ensure a reliable assessment of the eco-hydrological trends during the relatively short study period in the region, we employed an integrated trend analysis of the *ET* time series along with the time series of *NDVI* as the indicator of vegetation greenness, and *P* and *PET* as representatives of climate-related changes, so that we could evaluate the consistencies between hydrological and vegetation trends and attribute the observed trends to climate and/or anthropogenic effects. Assessing the multi-decadal changes in surface soil moisture globally, (Dorigo et al. 2012) not only merged different soil moisture products from different satellite sensors, but also compared the observed trends with trends in a precipitation dataset and a vegetation dataset, in order to identify consistencies and potential shortcomings. Our

combined assessment of the trends in *ET* and *NDVI* time series (2000 - 2010) revealed that hydrological and vegetation trends were consistent with each other: significant ($p < 0.1$) increasing trends were mainly found for the croplands (Figs. 5.3c and 5.7a), while significant decreasing trends ($p < 0.1$) were mostly found in wetlands (Figs. 5.3d and 5.7b). Furthermore, according to the comparison with the trends in climate-related *P* and *PET* time series it was revealed that the observed eco-hydrological trends (i.e. *ET* and *NDVI*) in the basin, especially in the water-limited plain part, were not related to the climate-related variables (Figs. 5.10 and 5.11) except for only about 16% of the increasing *ET* trend being explained by the increasing trend of *PET* (Table 5.2). The emerging picture suggests that the greening trend of the vegetation in the Konya plain is mostly related to land cover changes (i.e. conversion into irrigated croplands) and to the intensification of the irrigated agricultural activities, which in turn caused a drying out of some of the wetlands and the natural vegetation, which mostly depend on groundwater, the main source of irrigation water as well. These findings are in agreement with the previous study by (Bayari et al., 2009), who reported groundwater depletion due to supplementary irrigation to sustain the agricultural activities in the region.

With respect to the possible sources of error in the analysis, it should be noted that the CORINE land cover map (Figure 2.2a) used in analysing the distribution of trends among different land cover types was from the year 2006 (source: Ministry of Environment and Forestry of Turkey), rasterized from originally a polygon map (with a smallest mapping unit of about 0.001 $km^2$) and resampled to 1 $km^2$ resolution. Such a rasterization procedure can result in errors in the lower resolution output map due to the heterogeneity of the input data at the higher resolution (a kind of mixed-pixel effect) and can cause related errors in the land cover based analysis of the trends. For example, although irrigated croplands can be clearly identified by their increasing *ET* and *NDVI* trends in the Konya plain (Figure 5.3c, Figure 5.7a and Figs. 5.12a-c), some considerable increasing trends were also observed for pixels indicated on the maps as non-irrigated croplands and pasture/grassland, mostly on the edges of irrigated regions. Since no climate-related trends were observed in the plain during the study period, the increasing *ET* and *NDVI* in these land cover types can be partly explained by the mixed-pixel effect, i.e. there are patches of irrigated lands within non-irrigated pixels. Secondly, as the land cover map is only representative for the

year 2006, it is not fully representative for up-to-date changes of land cover (up to 2010 for this study) that have occurred in the Konya plain. Hence, although shown as increasing trends in non-irrigated croplands and pasture in the figures (Figure 5.3c, Figure 5.7a and Figures 5.12a-c), it is likely that parts of these areas were already fully converted into irrigated croplands.

In addition, as the distribution of potential evapotranspiration (*PET*) was obtained from the point-base pan-A evaporation data of 18 meteorology stations (Figure 2.1), there is certain errors attached to the interpolation of the point-based data. According to the inter-comparison of the results by the original point-base data and the interpolated map, the significance/signs of trends agreed on all the stations except two (i.e. Konya and Nigde stations in Figure 2.1), and quantitatively, the spatial average of the *PET* increasing trend by the interpolated map was about 4.5 mm lower than the average of the stations that had significant increasing trend. In overall, such a difference of *PET* would cause an additional total *PET* of about 15 MCM in the significant change areas (in both energy- and water-limited parts), which would still correspond to less than 10% the total *ET* increase in these areas (Table 5.2)"

## *5.4 Conclusions*

In this study, we analysed the recent trends in evapotranspiration, vegetation greenness (i.e. *NDVI*) and precipitation, using satellite-based observations to assess the human-induced changes in the hydrology and the associated ecological health of the semi-arid Konya closed basin, where both human activities (agriculture) and natural ecosystems are highly groundwater dependent.

Based on our relatively finer scale (1 km) analysis of the spatiotemporal trends we conclude that the controlling factors of *ET* even vary spatially inside the region. Therefore, for a better assessment of the trends, it is necessary to analyse the spatial distribution of the controlling regimes together with trends of *ET*, also at sub-regional scale.

In arid and semi-arid regions, *ET* is the main and frequently also the only outflow from the hydrological system, hence it can be considered one of the key variables to understand the regional eco-hydrological changes and trends, especially when driven by anthropogenic causes. We showed that an integrated trend analysis of consistently established *ET* time series, along

with vegetation (*NDVI*) and climate variables (i.e. *PET*, *P*), is effective to reveal the distribution and quantity of human-induced changes in the hydrology and the ecology of the semi-arid Konya basin, where previous studies (Chapter 4, and Bayari et al., 2009) had also indicated huge non-renewable groundwater abstraction for irrigation, with corresponding groundwater head declines. The integrated assessment of hydrological (*ET*), vegetation (*NDVI*) and climate (*P* and *PET*) variables not only enabled to identify the consistencies among them, but also allowed a better separation of climate-driven and human-induced trends.

In addition, this study showed how the human-induced trends in the hydrological fluxes (*ET* in this case) directly influence the health of the ecosystems when both agricultural activities and ecosystems compete for the same groundwater resources. Based on our findings we conclude that the depletion of the limited groundwater resources and the associated degradation of the ecosystems will continue if the business-as-usual practices, especially the current rates of water extraction, continue in the semi-arid Konya basin. As highlighted by Grafton et al. (2012), this conclusion does not imply that climate change is no longer a threat, but it does support the view that the most effective adaptation option is to reduce consumptive water uses.

Finally, our study presented an example of the utility of spatially and temporally continuous RS data for assessing the regional trends in hydrological and ecological variables and their interactions in a spatially distributed manner in a semi-arid region, which methodology can also be adapted to other regions. Such spatiotemporally distributed analyses at the basin and regional level is particularly important considering that most of the water management interventions also take place at these scales.

# Chapter 6

## Determining the sustainable water resources & ecological water demand

**Abstract**: We present a quantitative framework that uses RS-based seasonal and yearly *P*, *ET* and *P* - *ET* estimates over a decade period for assessing the limits and variations of the sustainable water resources. The method considers that the sustainable yield from a basin is the portion of the total yield remaining after the demands by the ecosystems. Additionally, the spatiotemporal trends in the *P* - *ET* balance were used for assessing the impacts of changes in the water use for irrigation on natural groundwater discharges and thereby on the health of ecosystems

## 6.1 Introduction

Water resources cannot be developed without altering the natural environment (Alley and Leake, 2004). However, in the past it was common practice to assume a "safe yield" term with respect to groundwater resources, which was firstly introduced by Lee (1915) as the quantity of water that can be pumped "regularly and permanently without dangerous depletion of the storage reserve", and later on broadly defined as "the amount of water which can be withdrawn from a groundwater basin annually without producing an undesired result" (Todd, 1959). In practice, the quantity of "safe yield" used to be taken equal to the volume of recharge to an aquifer (Sophocleous, 2000). The concept of "safe yield" ignores the fact that over the long term under natural or equilibrium conditions, natural recharge is balanced by discharge from the aquifer by evapotranspiration or into streams, springs, wetlands, or seeps. Consequently, if pumping equals recharge, eventually streams, marshes, and springs may dry up, and if it is continued in excess of recharge it may also eventually deplete the aquifer. We now understand that the sustainable yield of an aquifer must be considerably less than recharge, if adequate amounts of water continue to be available to sustain both the quantity and quality of streams, springs, wetlands, and groundwater-dependent ecosystems (Sophocleous, 2000). Along with the changing view from the "safe yield" to "sustainable yield", regulations such as Water Framework Directive by the European Union also adopted new approaches to redefine sustainable use of groundwater resources, stating that for good management, only that portion of the overall recharge that is not needed by the ecology can be abstracted - that is the sustainable resource, and the Directive limits abstraction to that quantity (http://ec.europa.eu/environment/water/water-framework/info/intro_en.htm).

The trade-off between the water used for consumption and the effects of withdrawals on the environment is increasingly the driving force in determining the sustainability of many groundwater systems (Alley et al., 1999). In addition, a holistic view is needed on the relationships between ground and surface waters because groundwater cannot be managed separately from surface waters without considering their interdependence.

A wise management of water resources needs to recognize that yield should vary over time as environmental conditions vary (Sophocleous, 2000). Because of uncertainties and spatio-temporal variabilities of key controlling variables (such as recharge and other water budget components), sustainability assessment should be understood as a dynamic and iterative process, requiring continued monitoring, analysis, prioritization, and revision (Sophocleous, 2000). For example, even small changes in precipitation may lead to large changes in recharge in semi-arid and arid regions (Woldeamlak et al., 2007), because these regions are highly vulnerable to anthropogenic and climate effects due to their scarce water resources. Sandstrom (1995) showed that a 15% reduction in precipitation, with no change in temperature, resulted in a 40 - 50 % reduction in recharge in semi-arid Tanzania. On the other hand, due to a high evaporative demand (i.e. potential evapotranspiration, *PET*), the total actual evapotranspiration is usually the largest component of the water balance, when additional water resources (e. g. groundwater or surface runoff) are available.

To ensure sustainability of aquifers (and other water resources), it is imperative that water limits be established based on hydrologic principles of the mass balance. In connection with determining the sustainable water limits and their variations, quantifying environmental provisions and ecological water demands forms also an urgent research need (Sophocleous, 2000). Therefore, the accurate knowledge of both *P* and *ET* and their spatiotemporal distribution is necessary to support the wise management of scarce water resources, not only for determining the volume of water available for sustainable use, but also for assessing the impact of groundwater exploitation on the natural environment. The difference between *P* and *ET* provides information regarding the net exchange of water between the atmosphere and the land surface (Swenson and Wahr, 2006). As defined by (Contreras et al., 2011), a surplus of *P* over *ET* in the water balance is proportional to the fraction of precipitation that recharges to the aquifer and/or generates surface runoff, while excess of *ET* over *P* in the water balance is related to the actual consumption of supplementary water resources (i.e. direct use of phreatic groundwater, groundwater discharge to a wetland, natural surface water contributions, water withdrawal for irrigation). As a result, the spatiotemporal distribution of *P* - *ET* can be effectively used to obtain the limits and the variability of sustainable water

resources (i.e. a portion of the overall recharge and surface water generated) and the ecological water demands for sustaining the health of ecosystems.

In this chapter, we present a quantitative framework that uses RS-based seasonal and yearly *P*, *ET* and *P* - *ET* estimates for assessing the seasonal dynamics, the limits and variations of water availability for sustainable use, and the quantities and variations of natural groundwater discharges upon which the ecosystems depend, to obtain a better understanding of sustainable water resources in water-limited regions. The methodology is tested and applied for the semi-arid Konya basin, which is a characteristic example of groundwater resources under strong anthropogenic influence, where i) both human activities (agriculture) and natural ecosystems are highly groundwater dependent and ii) the limited surface runoff is managed through man-made reservoirs for supplying additional irrigation. More specifically this chapter aims at:

1) Quantifying the seasonal variations of *P* and *ET* over a decade to assess the dynamics and limits of potential water availability.
2) Quantifying the yearly distributions of the *P* - *ET* balance over a decade to assess the limits and variations of the net yearly sustainable water resources (i.e. as a portion of natural recharge and surface water generation) and the quantities and variations of natural groundwater discharges to wetlands and water bodies.
3) Quantifying the spatiotemporal trends in the *P* - *ET* balance for assessing the changes in the water availability, water use for irrigation and their impacts on natural groundwater discharges and thereby on the health of ecosystems

## 6.2 Materials and methods

### 6.2.1 Conceptual model

Figures 6.1a & b present the conceptual model of the hydrological fluxes in the Konya basin. The Taurus Mountains in the south and southwest are the main water source areas, where high rainfall and snowmelt feed the ephemeral rivers and recharge the aquifer. Due to a well-developed karst geology, the (semi-)arid climate and the huge plain areas in the mid- and downstream parts, the Konya basin has no well-established drainage network. The water from the ephemeral rivers is either stored in reservoirs to

facilitate irrigation, or feeds the groundwater along the foot-slopes of the mountains. The basin is hydrologically closed, meaning that the horizontal fluxes of surface and groundwater are retained in the basin, terminating at the hyper-saline Tuz Lake in the north (Bayari et al., 2009). The evapotranspiration is the only out-flux from the basin and controls salinization of surface water bodies such as the hyper-saline Tuz Lake (Bayari et al., 2009).

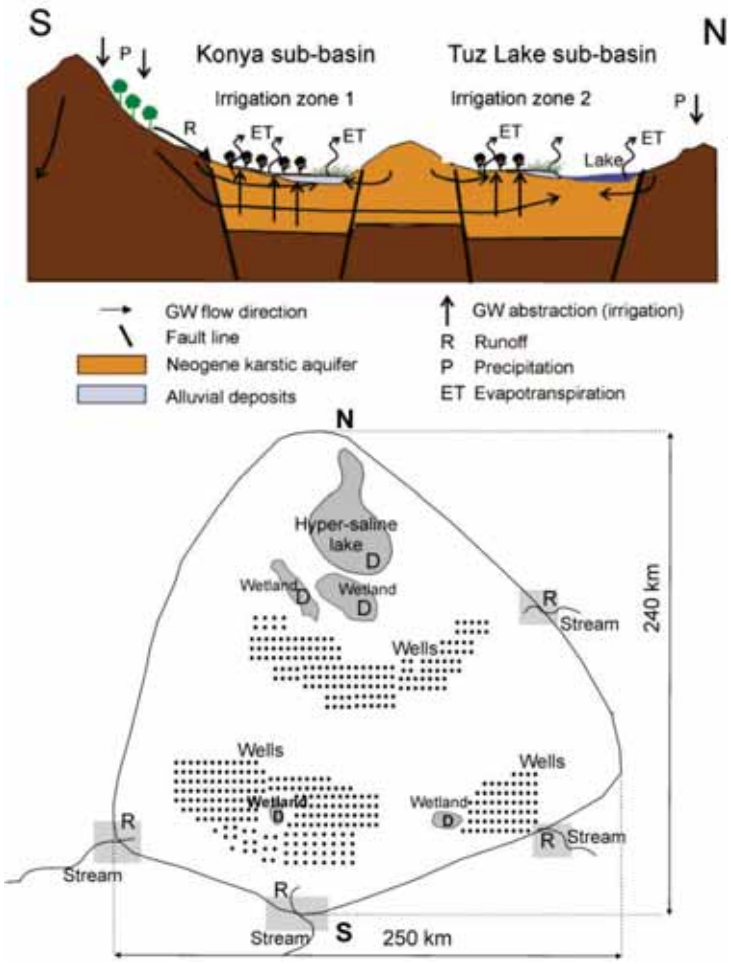


**Figure 6.1a)** A cross-section of the Konya basin and hydrological fluxes (modified after Bayari et al., 2009; Naing, 2011), **b)** Conceptual model of the GW recharge (R) /discharges (D) and GW-dependent systems in the basin

There are extensive plains in the central and downstream areas of the basin, which make the Konya basin one of the most important agricultural regions of Turkey. Although surface water is also utilized, groundwater is the main source of water for irrigation. It can be accessed almost anywhere in the flat areas of the basin by means of 50 to 250 m deep wells (Bayari et al., 2009) abstracting from the Neogene aquifer. According to an unpublished inventory conducted by the regional water authority (DSI), there are more than 90,000 groundwater abstraction wells, around 75% of which are unregistered wells, in the Konya basin. Besides providing irrigation water to sustain agriculture in the region, most of the wetlands and the water bodies in the region can also be classified as groundwater-dependent ecosystems. Figure 6.1b illustrates the spatial setup of groundwater system (i.e. the areas of the GW recharge (R)/discharges (D) and GW abstraction wells).

### *6.2.2 Method*

We used RS-based spatiotemporal estimates of *P* and *ET* between the years 2000 and 2010 in determining the boundaries and the dynamics of sustainable water resources and the water demand for sustaining the health of ecosystems in the semi-arid, groundwater-dependent and hydrologically closed Konya basin.

Figure 6.2 presents the flowchart of assessing the sustainable water availability and ecological water demand. As the first step, the seasonal dynamics and the potential limits of water availability (i.e. spatial and temporal variations of water excess and losses) were analysed using the monthly distributions of *P* and *ET* over the eleven-year period (2000 - 2010). Afterwards, for assessing the net sustainable water availability in the yearly water balance and the demands by the ecosystems, the yearly *P* and *ET* distributions and the difference between them were obtained from the monthly *P*, *ET* data. Using the spatiotemporal *P* - *ET* distributions, the average and the variations of net sustainable water resources (i.e. sustainable yield of both groundwater and surface water resources) and the ecological water demand by the ecosystems (i.e. surface and groundwater discharges to the wetlands and water bodies) were analysed. Finally, we applied the Mann-Kendall trend test (Kendall, 1975; Mann, 1945) to the time series of yearly *P* - *ET* over the period 2000 - 2010 for assessing the trends and changes in the water consumption (mainly for irrigation) and its impacts on the ecosystems.

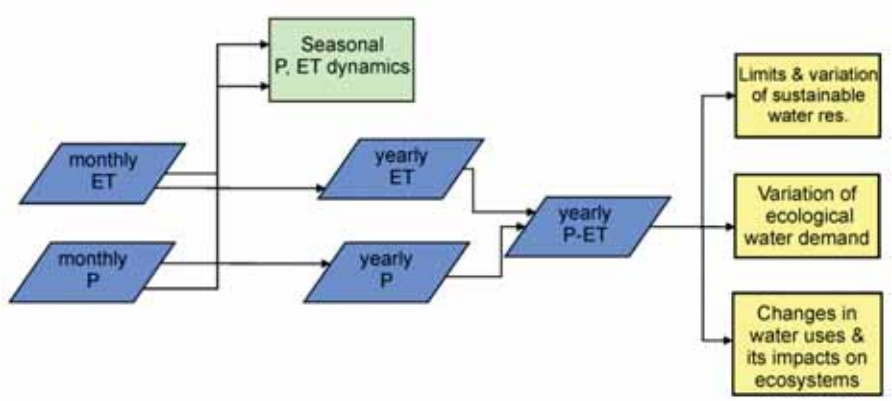


**Figure 6.2** Flow chart of determining sustainable yield and ecological water demand.

To define the sustainable water resources yield in the basin, we followed the concept laid down by (Sophocleous, 2000) who stated that the sustainable yield of an aquifer (with respect to groundwater resources) must be considerably less than recharge (i.e. conventional safe yield) if adequate amounts of water are to be available to sustain both the quantity and quality of streams, springs, wetlands, and groundwater-dependent ecosystems. In this regard, we first estimated the variation of the conventional safe yield through assessing the variations of the yearly *P* - *ET* surplus. This indicated the limit of the additional total water availability both in the form of net recharge to groundwater resources (i.e. aquifers) and surface water flow. Next, we subtracted the amount of ecological water demand (determined from yearly *P* - *ET* distributions over wetlands and water bodies) from the total (conventional "safe") yield to obtain the net sustainable yield available for other water consumptions (mainly for agriculture).

### *6.2.3 Data*

In our study, we used monthly and yearly *P*, *ET* data that covered the period between 2000 and 2010. Details of the data used are described below.

#### a. Evapotranspiration data

In this chapter, we used the monthly and yearly *ET* estimated in Chapter 5 that used SEBS-SM (Chapter 3) to obtain spatiotemporal *ET* distribution. The monthly and yearly *ET* data used in this study had 1 km spatial resolution.

The input data, model description and the method for upscaling the daily *ET* model outputs to monthly and yearly *ET* are provided in Chapters 3 and 4 in detail.

**b. Precipitation data**

To quantify distributions of monthly and yearly precipitation, we used the sums of separately estimated rainfall and snow water equivalent (*SWE*) estimations, because the RS-based rainfall products and the rain gauge observations (as they are not located at higher altitudes) do not sufficiently capture the snowfall contribution to the total precipitation.

To estimate the rainfall distribution, we used the monthly product of the Tropical Rainfall Measuring Mission (TRMM-3B43). The TRMM 25 $\times$ 25 $km^2$ gridded estimates extend from 50 degrees south to 50 degrees north and have a temporal resolution corresponding to a calendar month. We resampled the original 25 km spatial resolution to 1 km grid cells using bi-cubic interpolation in order to match it with the resolution of *ET* flux.

With respect to the snowfall contribution to total precipitation, we used the *SWE* data described in Chapter 4, which was based on a multivariate linear regression approach that used the ground measurements from snow gauges, the total amount of snow cover days from the 8-daily snow cover product of MODIS (MOD10A2) and the elevation data from the digital elevation model as inputs. Finally, monthly and yearly total precipitation (*P*) distributions were obtained by summing the rainfall and *SWE* data.

## *6.3 Results*

### *6.3.1 Seasonal dynamics of water availability*

As natural groundwater recharge and surface water generation processes occur mainly in wet periods when *P* is mostly higher than *ET*, Figure 6.3a shows the spatial distribution of average *P* - *ET* in the wet period (OCT-APR) between 2000 and 2010. According to Figure 6.3a, there is a clear separation between the potential source and consumptive areas for water resources: the mountainous parts in the southwest, south and east of the basin (the areas between the basin border and the inner polygon indicating the plain part) have a considerable surplus of *P* over *ET* up to 750 mm (bluish coloured areas) in wet periods. While in the plain parts (inside the polygon), there is

either a balance of *P* and *ET* (whitish coloured areas mainly in the midstream part) or a surplus of *ET* over *P* of up to around 250 mm in the downstream part in the north, indicating that there is not even a considerable groundwater recharge in the wet season in the plain part and groundwater/surface water discharges continue to the wetlands and water bodies (smaller polygons inside the plain part) also in the wet seasons.

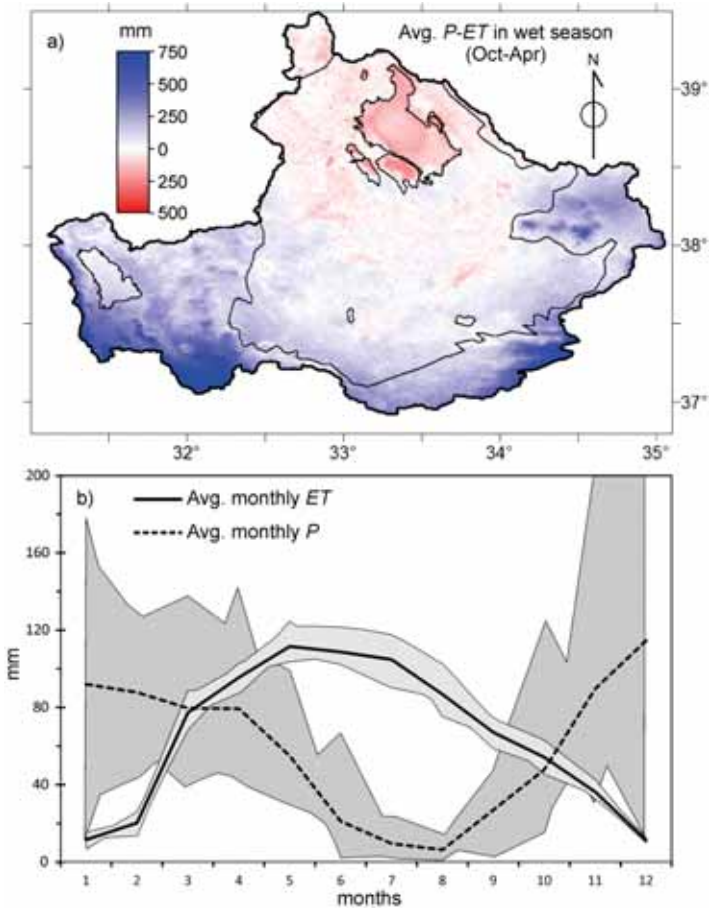


**Figure 6.3a)** Distribution of average *P* - *ET* in the wet season (APR-OCT) during the study period **b)** Monthly changes of *P*, *ET* in the mountainous part of the Konya basin (grey areas indicate year by year variation, and thick lines indicate the average of 11 years)

Although the distribution of *P* - *ET* in wet seasons provides an idea about the potential locations and quantities of water resources, it would be misleading to estimate the real quantity of sustainable water resources using only the data of wet seasons because the water surplus in the wet period is mostly lost

by evaporation from the land and water surfaces in the dry period, only a part of the surplus infiltrates deeper than the rooting depth and recharging the groundwater. Indeed, Figure 6.3b shows the monthly distributions of *P*, *ET* in the mountainous parts (bluish coloured areas in Figure 6.3a), the potential source areas for water resources generation, and exhibit the transition from the *P* - *ET* surplus regime in the wet period (usually from SEP/OCT to MAR/APR) to the *P* - *ET* deficit regime in the dry period. As a result, to estimate the sustainable water resources quantities, it is not sufficient to analyse *P*, *ET* distributions in the wet period but a *P* - *ET* analysis on a yearly basis is necessary. Also, Figure 6.3b shows that the variation of *P* between years (dark grey area) is much larger than the variation of *ET*.

### *6.3.2 Sustainable water resources and the demands by the ecosystems*

Figure 6.4a shows the histogram of average yearly *P* - *ET* over the period 2000 - 2010. The histogram reveals that there is an imbalance between the yearly *P* and *ET* towards a negative balance (mean: -140 mm $y^{-1}$), which indicates a loss of water from the storage during the 11 years study period in the Konya basin. Indeed, representing the distribution of the negative balance part (left hand side of the histogram) among the different land covers, the pie-chart in Figure 6.4a shows that more than half of the negative *P* - *ET* values are from croplands, implying supplementary water consumption from storage. Besides, a considerable portion of negative *P* - *ET* values corresponds to water bodies, wetlands and heathland in the downstream area, implying considerable groundwater and/or surface water discharges to these ecosystems as sources of the excess *ET* over *P* in these areas. Also, the spatial distribution of average yearly *P* - *ET* in Figure 6.4b confirms the widespread and varying degree of negative *P* - *ET* balance, which goes as high as -600 mm, especially in the downstream wetlands in the north and the water bodies.

In spite of the widespread negative *P* - *ET* values, there is still a considerable portion in the histogram where yearly *P* - *ET* values are positive. In fact, it is the total area under this portion (*P* - *ET* > 0) which indicates the average total yield per year during study period. For the 2000 - 2010 period, the volume of average total (*P* - *ET* > 0) surplus was 1,385 MCM, which indicates the total net yearly source for surface runoff and groundwater recharge. These source areas are shown in bluish colours in Figure 6.4b where the magnitude of the yearly *P* - *ET* surplus goes up as high as 400 mm, and these areas correspond to the mountainous upstream parts in the basin.

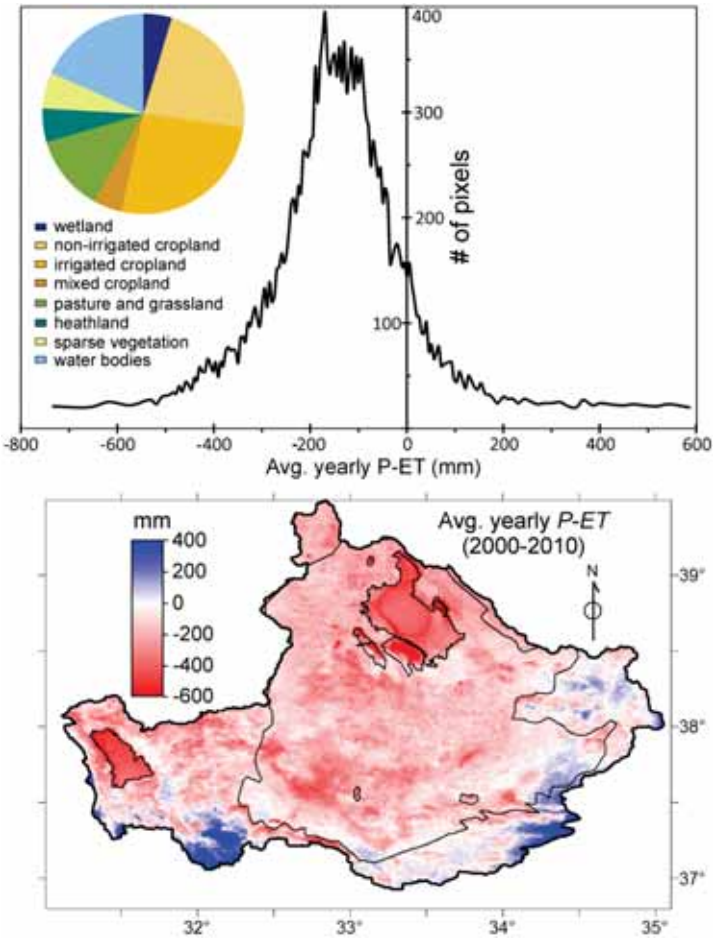


**Figure 6.4a)** *P-ET* yearly average histogram **b)** *P - ET* yearly average map

Yet, the average total water yield (2000 - 2010) obtained from the histogram in Figure 6.4a is not representative of sustainable water yield in the basin, because the total yield also includes the portion discharging to the wetlands and lakes (i.e. ecological water demand), which is sustaining the health of these ecosystems.

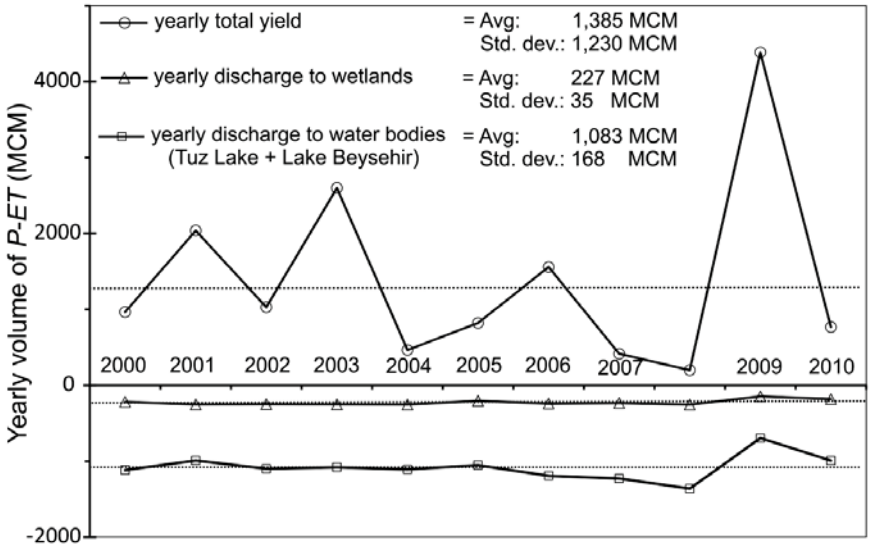


**Figure 6.5** Year by year *P-ET* distributions graph

To further partition the yearly available water resources between sustainable yield and the ecological water demands, Figure 6.5 shows the year by year distributions of total yield and discharges to wetlands and the water bodies. According to Figure 6.5, firstly it is observed that the yearly total yield varies greatly between the years (i.e. standard deviation is almost as high as the average total yield), which can mainly be attributed to the variation of precipitation as shown in Figure 6.3b. For the wetlands and water bodies the total yearly discharge values are rather stable between the years, with standard deviation values of about 10% of the average values. Adding up the average yearly discharges to wetlands and water bodies, the total ecological water demand is found as 1,310 MCM $y^{-1}$, which is almost equal to the yearly average total yield (1,385 MCM $y^{-1}$). This finding confirms that the water balance of the Konya closed basin system is approaching a dynamic balance in the long term, where the inflow (i.e. recharge) balances out the discharges. As a result, on average, only a negligible amount of 75 MCM $y^{-1}$ sustainable yield is found for the Konya closed basin over the 11 years study period, assuming long-term average conditions of the water bodies (i.e. lake levels) and wetlands are maintained. On the other hand, if a dynamic approach is followed for the determination of the sustainable yield on a yearly basis, the sustainable yield reaches up from around 700 MCM $y^{-1}$ (year 2001) to 4,000 MCM $y^{-1}$ (year 2009) in wet years, while it is highly in deficit up to -

1,200 MCM $y^{-1}$ in dry years such as the year 2008. However, following such a dynamic approach for determining the sustainable yield would lead to lower lake levels and/or drying of wetlands and springs, as the higher amounts of yield in wet years would not be able to compensate the deficits in dry years, but instead be consumed for other uses.

### *6.3.3 Consumptive water uses and their effects on the ecosystems*

Although the yearly discharges to wetlands and water bodies are quite stable (Figure 6.5) and the average water yield (i.e. recharge) and discharges are balanced over the 11 years study period in the Konya closed basin, this does not necessarily mean that there are no disturbances (e.g. water consumptions for irrigation) to the system, because the results of such disturbances might take long periods to be reflected in the groundwater discharges to wetlands, due to the very slow lateral movement and very long residence times of groundwater systems. Indeed, according to Table 6.1, a total volume of on average -3,000 MCM $y^{-1}$ balance ($P$ - $ET$) is indicated for the cropland areas, which is more than twice the average yearly total yield in the basin.

To further reveal the spatiotemporal changes that have occurred in the consumptive water uses (i.e. irrigation) and their impacts on the health of ecosystems, we assessed the trends in the yearly $P$ - $ET$ distributions from 2000 to 2010 (Figure 6.6). In the trend analysis, an increasing trend indicates that the $P$ - $ET$ difference gets larger (in the negative direction as $ET$ is generally larger than $P$ in the Konya basin), while a decreasing trend indicates that $P$ - $ET$ gets smaller (i.e. approaching to zero). According to Figure 6.6a, it is clearly shown that the significant increasing trends ($p < 0.1$, dark green areas) of yearly $P$ - $ET$ have mainly occurred in the irrigated croplands (indicated by the polygons with a green colour), meaning a shift of the evapotranspiration regime from water-limited to energy-limited (e.g. intensification of supplementary irrigation due to crop type and pattern changes). Among the sub-regions of irrigated croplands, the majority of the increasing trends occurred in the zone around Altinekin and south of Tuz Lake, while there was only limited change in the Cumra sub-region, which is the oldest irrigation project in the Konya basin. On the other hand, the significant decreasing trend of $P$ - $ET$ ($p < 0.1$, dark brown areas) has mainly occurred in the wetlands (dark blue polygons) and in the Tuz Lake, besides the areas in the north of the basin (Figure 6.6a). The decreasing trend of $P$ - $ET$ (i.e. smaller $P$ - $ET$ differences) in these areas indicates a shift of the

evapotranspiration regime from energy-limited to water-limited. Therefore, although the yearly average values in Figure 6.5 showed a quite stable quantity of discharges to wetlands, Figure 6.6a shows that the drying of wetlands already started, and advanced with varying degree in all the wetlands in the Konya basin, which is the result of decreasing GW discharges to wetlands due to lowering of the GW table in the basin through extractions for irrigation.

**Table 6.1** Distributions of the average yearly *P-ET* fluxes, volumes and their standard deviations (2000-2010) per different land covers in the Konya plain.

| | ***Area (%)*** | **Avg. P-ET [mm]** | **Volume of P-ET [MCM]** | **Std. Dev. [MCM]** |
|---|---|---|---|---|
| *Wetland* | 2.4 | -343.5 | -257 | 39.3 |
| *Non-irrigated cropland* | 29.4 | -141.9 | -1,283 | 506.1 |
| *Irrigated cropland* | 24 | -201.2 | -1,484 | 488.4 |
| *Mixed cropland* | 5.9 | -142.8 | -258 | 106.3 |
| *Pasture and grassland* | 17.3 | -130 | -697 | 301.7 |
| *Heathland* | 3.7 | -269.9 | -307 | 54 |
| *Sparse vegetation* | 9.2 | -116.2 | -329 | 148 |
| *Water bodies* | 8.1 | -412.3 | -1,033 | 129.8 |

In terms of rates of change, Figure 6.6b shows that both the rates of decreasing and increasing trends reached up to -25 and 25 mm $y^{-1}$, which would be equivalent to a total decrease and increase of -275 and 275 mm between 2000 and 2010, respectively.

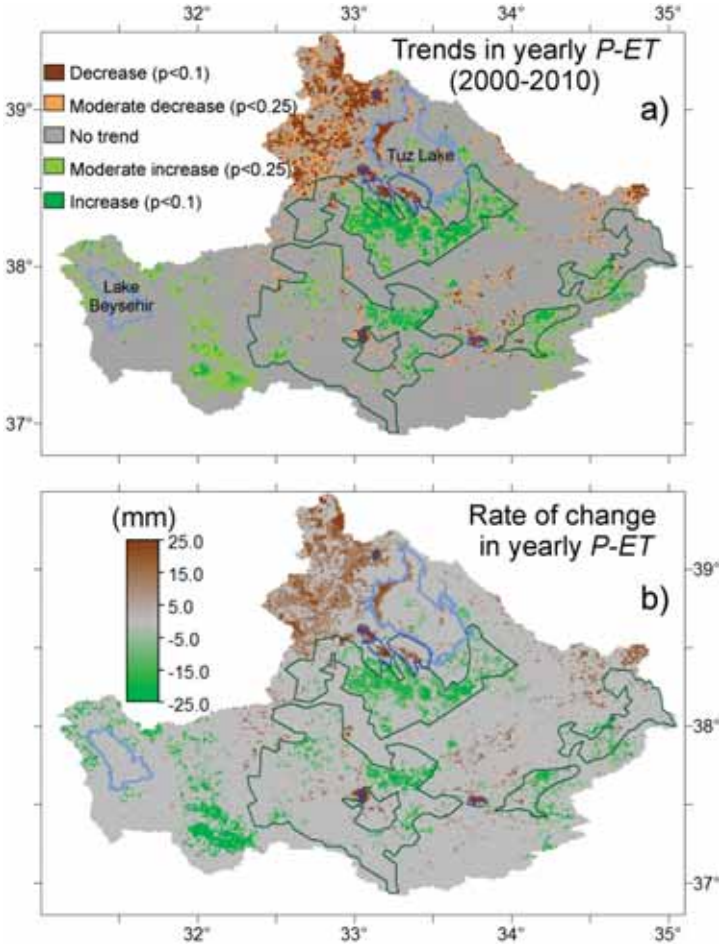


**Figure 6.6a)** Significance/direction of *P-ET* yearly trend **b)** Slope of *P-ET* yearly trend

## *6.4 Discussion and conclusions*

In this chapter, our first aim was to assess the seasonal dynamics and limits of potential water availability through seasonal and spatial distributions of the *P* and *ET* over a decade period. Mapping of the average wet season (OCT-APR) distribution of *P - ET* (Figure 6.3a) enabled to identify the potential source areas and quantities for water resources. However, as it was shown in the seasonal dynamics of *P* and *ET* throughout the year in Figure 6.3b, water surplus in the wet period is mostly lost by evapotranspiration in the dry period. Therefore, a *P - ET* analysis on a yearly basis is necessary to estimate the sustainable water resources quantities (i.e. yearly net recharge and

surface water). Besides, Figure 6.3b showed a large variation of *P* compared to a relatively smaller variation of *ET* between years during the study period, implying that the yield would vary over time due to the large spatiotemporal variation of *P*, as also reported by other studies, including Woldeamlak et al. (2007) and Sandstrom (1995).

Secondly, we assessed the limits and variations of the net yearly sustainable water resources (i.e. a portion of natural recharge and surface water generation) and the ecological water demand through yearly distributions of the *P - ET* balance over a decade period. Under natural conditions, prior to the development of water resources (groundwater and/or surface water), it would be expected in a closed basin system that the water balance approaches a state of dynamic equilibrium: over hundreds of years, wet years in which inflow (i.e. recharge) exceeds discharge would offset dry years when discharge exceeds recharge (Sophocleous 2000). However, the histogram in Figure 6.4a indicates an overall negative water balance in the Konya basin (with a mean *P-ET* value of -140 mm $y^{-1}$ over the 11 years study period), which is mainly caused by the supplementary water consumptions for irrigation in the croplands. Despite such a disturbance by water consumption for irrigation, a comparison of the average yearly total yield (1,385 MCM $y^{-1}$) estimated from the area under the positive side of *P-ET* histogram (Figure 6.4a) with the total average yearly discharges (1,310 MCM $y^{-1}$) to wetlands and water bodies (Figure 6.5) still revealed a near balance between inflow (i.e. the recharge as the yield) and discharges in the closed basin system. This can be mainly explained by the fact that the results of such disturbances might take a long period before they are reflected in groundwater discharges to wetlands due to the very slow lateral movement and very high residence times of groundwater systems (Gleeson et al., 2012).

Considering that the sustainable yield from a basin is the portion of the total yield remaining after the demands by the ecosystems, we can conclude that the average sustainable yield in the Konya closed basin over the 11 years study period has been only a negligible amount of 75 MCM $y^{-1}$, which is as expected for the semi-arid Konya basin that has been depicted as highly water-limited except for the mountainous upstream parts (Figure 4.11a in Chapter 4). On the other hand, as the total yields vary largely between the years (Figure 6.5) due to the high variation of precipitation input (Figure 6.3b), the yearly sustainable yield (or deficits in dry years) from the

basin also varied largely accordingly (reaching up to 4,000 MCM $y^{-1}$ in wet years such as 2009, while large deficits up to -1,200 MCM $y^{-1}$ occurred in dry years such as year 2008). Sophocleous (2000) highlights that a wise management of water resources needs to recognize that yield should vary over time as environmental conditions vary because of the uncertainties and spatiotemporal variabilities in key controlling variables (such as recharge and other water budget components). However, it should be borne in mind that following such a dynamic approach for the sustainable yield could still have significant and undesirable impacts if the higher amounts of yield generated in wet years are allocated for consumptive uses (e.g. for irrigation) and do not compensate the deficits in dry years. Eventually, a new equilibrium state could still be reached, in which the extraction is balanced by re-arrangement of the water table (also called capture, (Bredehoeft and Durbin, 2009). Although physically sustainable, the changes in the hydrologic system in this new state (e.g. lowered groundwater table) may result in significant environmental, social or economic impacts (Scanlon et al., 2012; Zhou, 2009). If the stress (i.e. perturbation) applied to a groundwater system is too large, that is, if capture cannot ultimately compensate for extraction, a new equilibrium is impossible and the system has a finite life (Bredehoeft and Durbin, 2009; Zhou, 2009). Therefore, as highlighted by (Sophocleous, 2000), sustainability assessment is a management issue as well as a scientific problem, and should be understood as a dynamic and iterative process, requiring continued monitoring, analysis, prioritization, and revision.

Lastly, we analysed the changes in the consumptive water uses and their impacts on the health of ecosystems in the Konya basin through the assessment of spatiotemporal trends in yearly $P - ET$ between 2000 and 2010. The analysis of the spatiotemporal trends (Figs. 6.6a and 6.6b) revealed that there has been a widening gap of $P - ET$ (an increase up to about 250 mm totally during the 11 years period, Figure 6.6b) concentrating in the irrigated croplands (mostly in the Altinekin sub-region). This growing trend of the $P - ET$ difference can be mainly attributed to the increase of $ET$ from the increased supplementary irrigation due to crop type and pattern changes, because no significant trends had been detected for $P$ in the same period in the Konya basin (Chapter 5). On the contrary, we detected significant trends of a narrowing $P - ET$ difference (a decrease up to about 250 mm totally during the 11 years period, Figure 6.6b) mainly in the wetlands and in the Tuz Lake (Figure 6.6a), indicating a shift from an energy-limited (i.e. plenty

groundwater discharges to wetlands) to a water-limited (i.e. precipitation-limited) evapotranspiration regime in these areas. According to the emerging picture we can conclude that the increases in consumptive water uses (i.e. irrigation) have already caused significant impacts on the health of ecosystems because both of them depend mainly on groundwater resources in the Konya basin. This finding was not depicted by the overall average values in Figure 6.5, but could be revealed by the distribution of spatiotemporal trends in Figure 6.6. In addition, the spatial distributions of the trends show that the closer parts of the wetlands are affected first by irrigated croplands (Figure 6.6), because extraction of groundwater from wells initially reduces storage and causes a depression of the hydraulic head (i.e. water table) that spreads outward from the wells (Theis, 1940). Examining the influence of the dynamics of a ground-water system in response to differently located development schemes, (Bredehoeft et al., 1982) also illustrated that the placement of pumping wells changes the dynamic response.

In this Chapter, we assessed the effects of groundwater extraction on the wetlands and water bodies, while the effects of groundwater depletion, which strongly depends on irrigation patterns, methods and efficiencies (Scanlon et al., 2007; Siebert et al., 2010), are complex and numerous. Groundwater depletion, and thereby the lowering of water tables, leads to i) increased cost of pumping or the drying up of wells, thus affecting users (Fishman et al., 2011; Shah, 2007); ii) reduced groundwater discharge to streams, springs and wetlands, affecting the ecosystems (Sophocleous, 2000); iii) land subsidence, irreversibly reducing storage and potentially damaging the infrastructure (Giordano 2009); and iv) land degradation such as salinization (Aeschbach-Hertig and Gleeson, 2012). Groundwater depletion also depends on the availability of water to replenish groundwater reserves, suggesting that arid regions are more vulnerable to the effects of extraction (Aeschbach-Hertig and Gleeson, 2012). To tackle groundwater depletion, water management strategies can be classified as demand-side strategies that aim at decreasing groundwater extraction and supply-side strategies that try to increase the water supply in general and specifically the groundwater recharge. Improved irrigation efficiency is often suggested (Giordano, 2009; Kendy, 2003) as a way to reduce water demand and thus extraction. But for agricultural areas with shallow aquifers, groundwater depletion is largely controlled by the rate of evapotranspiration rather than the rate of extraction per se, because excess

extracted groundwater returns to the aquifer (Kendy, 2003). Ultimately, groundwater depletion is inevitable if irrigation based on groundwater raises crop evapotranspiration to levels above water inputs to the region through precipitation and inflow (Kendy, 2003). Instead, rates of groundwater depletion can be decreased by growing less crops or irrigating less area, although this is typically not as politically attractive as using technology to increase irrigation efficiency (Kendy, 2003). One option to reduce groundwater depletion while maintaining agricultural production could be to optimize conjunctive use of ground and surface water for irrigation (Konikow and Kendy, 2005; Shah, 2007), although groundwater irrigation is generally more productive (Giordano, 2009; Shah, 2007), and conjunctive use is of limited value in regions with little surface water, such as the southern High Plains (Scanlon et al., 2012). In the Konya basin, the average ratio of surface water irrigation for 2005 - 2009 was found to be about 20% of total irrigation (Chapter 4), which ranges between 15 - 30% according to the figures of the regional water authority (unpublished data of DSI). Supply-side management options aim at increasing groundwater recharge by technical measures (e.g. artificial recharge). A "hard path" (Gleick, 2003) measure to increase water supply is large-scale water diversions, as realized in the Central Valley (Scanlon et al., 2012), or even a bigger scheme in China (Stone and Jia, 2006). But even such a gigantic project might not suffice to close the gap between precipitation and evapotranspiration (Liu et al., 2008), and the social, economic and ecological costs of such projects are high (Gleick, 2003). Similarly in the Konya basin, an inter-basin water diversion project (i.e. Blue tunnel project) was realized in 2012, which is planned to provide an additional 414 MCM $y^{-1}$ surface water resources mainly for irrigation purposes (http://www.konya.gov.tr/goster.asp?baslik=Konya%20Ovalar%FD%20Projesi%20(KOP). However, it should be noted that such an additional water resource would only contribute about 14% to the average total irrigation water consumption of 3,000 MCM $y^{-1}$ that occurred for the croplands in the Konya plain over the 2000 - 2010 study period (Table 6.1).

# Chapter 7

## Synthesis

## 7.1 Introduction

This chapter summarizes the main achievements and results of chapters 3 to 6 and discusses these results with respect to the specific research objectives. The aim of this thesis was to effectively utilize and integrate earth observation methods in assessing the spatially and temporally the hydrological fluxes and ecosystem's health and the inter-relations between them in a closed, semi-arid basin with good accuracy.

The specific research objectives of this thesis were:

- to contribute in developing improved models for a better estimation of energy and water fluxes in continuously or seasonally water-stressed regions (section 7.2),
- to construct and validate a spatiotemporally distributed water balance for assessing the water availability (i.e. surface runoff), consumptive water uses (i.e. irrigation), *GW* storage changes and *GW* discharges at large basin scale (section 7.3),
- to develop and implement a framework for a RS-based and integrated assessment of eco-hydrological trends and their causes at regional scale (section 7.4),
- to develop a quantitative framework for assessing the limits and variations of sustainable water resources along with the ecological water demands

Each of the following sections discusses the achievements obtained for one of the objectives. The final section gives recommendations on future research.

## 7.2 Improved estimation of water fluxes in water-stressed regions

Remote sensing models that obtain evapotranspiration, *ET*, from the energy balance do not take below-ground processes explicitly into account. The effects of soil evaporation, soil moisture redistribution, stomatal regulation and related transpiration, and interception storage are all implicitly incorporated in the resulting land surface temperature. This simplification is usually adequate where available energy is the limiting factor for *ET*, but problems appear when water availability becomes limiting for *ET*, which will often be the case in semi-arid regions.

In Chapter 3, we introduced a modified surface energy balance model (i.e. SEBS-SM) that integrated soil moisture data explicitly in the calculation of sensible heat flux by introducing a soil moisture dependent scaling factor in the parameter $kB^{-1}$ that plays a role in the aerodynamic resistance. The new approach was tested by comparing it with observations from BR stations. The results indicated not only a clear improvement for the case of sparse non-irrigated vegetation, with a large reduction in RMSE (and 40% reduction in rRMSE), but also a slight improvement for the agricultural crops, while keeping the good results (low RMSE values) for the wetland areas.

Further validation of the SEBS-SM was carried out in Chapter 4 through quantifying the yearly water fluxes and analysing the closure of the water balance in the region. The assessment confirmed the advantage of SEBS-SM over the standard SEBS by its better accounting for the water stress conditions (i.e. soil moisture limitation on *ET*), which was reflected by estimating a lower yearly *ET* compared to SEBS with varying magnitude.

The proposed integration of soil moisture into SEBS required the tuning of the parameters of the S-curve function through which the level of water stress is incorporated in the sensible heat calculation. Nevertheless, the new approach can also be applied in other regions, or for regional, continental or global mapping of ET. Such an improved mapping of regional *ET* by SEBS-SM has a large potential in providing a more accurate estimation of energy and water fluxes in continuously or seasonally water-stressed regions.

With respect to obtaining an improved estimation of the precipitation distribution, in Chapter 4, we assessed the RS-based monthly Tropical Rainfall Measuring Mission (TRMM) rainfall product. Important aspects in the assessment of *P* were: i) the correction of the TRMM rainfall product with ground based rainfall estimates in gauges and ii) an estimate of the snowfall contribution to precipitation from the *SWE* of the snowpack based on RS and field measurements.

## 7.3 Quantifying and validating a spatially distributed water balance in a managed and semi-arid basin

In Chapter 4, we developed a conceptual water balance model that was implemented based on the integrated (i.e. RS and ground based) estimations of yearly *P*, *ET* and *R* water fluxes for evaluation of the storage changes in the

water limited Konya basin in a distributed manner. For assessing the effectiveness of the methodology, we compared the results with groundwater storage changes estimated from water table decline in boreholes.

According to Chapter 4, the quantity of supplementary irrigation from the irrigated croplands was found to be 308 ± 132 mm $y^{-1}$ (the maximum reaching up to 500 mm $y^{-1}$) with the source of about 80% from groundwater and 20% from surface water. These fluxes correspond to an average total volume change of -2,270 MCM $y^{-1}$ from the groundwater storage in the irrigated croplands (totally -4,700 MCM $y^{-1}$ for all croplands including mixed and non-irrigated) during the study period (2005 - 2009). Besides the croplands, the large $P$ - $ET$ differences in the wetlands (-422 ± 209 mm $y^{-1}$) and water bodies (avg. -495 ± 76 mm $y^{-1}$) indicate that they receive large groundwater and/or surface water inputs to sustain such excess $ET$.

To validate the spatially distributed water balance, $\Delta S_{RS}$ estimated from RS ($P \pm R - ET$) were compared with the $\Delta S_{GW}$ calculated based on yearly groundwater decline at the locations (pixels) of GW observation wells. The results showed that the average yearly $\Delta S_{RS}$ values were within the ranges of $\Delta S_{GW}$ for 4 out of 5 wells estimated, assuming $S_y$ ranging between 0.05 and 0.20. These findings suggest that that RS-based estimate of $\Delta S_{RS}$ was capable of obtaining the magnitude and distribution of the groundwater storage depletion in the semi-arid Konya basin, which had also been reported by (Bayari et al., 2009). A similar approach was also documented by Sheffield et al. (2009) and Tang et al. (2010), but our study differs from those in that we validated the spatially distributed water balance also in a spatially distributed manner comparing with the distributed GW level observations, while those studies validated their satellite-based water balance against the streamflow data at the outlet of the river basins.

The proposed method can also be applied in other large basins, especially in semi-arid and arid regions, where there are higher potentials for obtaining long time series of frequent optical remote sensing data. Still, the individual assessments of the water balance components can be improved further in several ways such as (but not limited to):

- Through improved methods for filling the data gaps in daily *ET* (e.g. extrapolating the relation of *ET* with daily in situ estimates of *PET* or solar radiation over missing data);
- Longer time horizon for the water balance (e.g. 10 years period instead of 5 years) for further minimizing the effects of horizontal fluxes and the variations in soil moisture;
- Multiple model/data integration for assessing the individual water balance components of *ET*, rainfall, snow water equivalent, and storage changes (i.e. soil moisture and groundwater) with the advancements in data products and models.

## *7.4 An integrated framework for monitoring ecohydrology*

To achieve the specific objectives of this research, we aimed at developing an integrated approach combining different methods (e.g. RS, ground, models and time series analysis) and different sources of data with different spatial, spectral and temporal resolution to improve the accuracy and reliability of the analyses. Here we will shortly describe each component of this integrated approach with respect to the chapters:

### a. Integration of different spatial resolution data

The integration of different spatial resolution data was not only necessary for establishing a consistent dataset for the models (i.e. SEBS) and analysis (i.e. spatiotemporal water balance and trend analysis) but also for the assessment of the accuracy of the results through comparing grid-based model outputs against point-based ground measurements.

In Chapter 3, for estimating the daily *ET* by soil moisture integrated SEBS-SM, we integrated the land surface parameters obtained from MODIS level 1B data (visible and near infrared bands 1 to 7 with 250–500 m spatial resolution and thermal emissive bands 31 and 32 with 1 km spatial resolution) with the point-based meteorological data from the 18 stations distributed in the basin and with the field and remotely sensed (~ 25 km spatial resolution) data of soil moisture. For harmonizing the input dataset for the model, the point-based meteorological data were spatially interpolated, while the remote sensing data of different spatial resolution were up/downscaled to the same resolution through appropriate resampling. Besides building a harmonized dataset, grid-based SEBS-SM outputs were validated using the ground

measurements from the Bowen ratio stations, taking into account foot print analysis and assessing the error sources due to the difference in spatial representativeness.

Similarly, in Chapter 4, to obtain an improved precipitation distribution, firstly the monthly TRMM rainfall product (~ 25 km spatial resolution) was assessed and bias-removed comparing with the ground based rainfall measurements in gauges. After the bias removal, we combined it with the snow water equivalent estimated by a multivariate analysis using point-based snow gauge observations, the MODIS snow cover product (1 km spatial resolution) and the digital elevation model (90 m spatial resolution). Also, we resampled the originally 25 km spatial resolution to 1 km resolution using bi-cubic interpolation in order to match it with the resolution of *ET* flux for the spatially distributed water balance analysis.

Lastly in Chapter 5, we conducted an integrated trend analysis of different variables (i.e. *ET*, *PET*, *NDVI* and *P*) that had different spatial resolutions from point base (i.e. PET) to 250 m (i.e. *NDVI*), 1 km (i.e. *ET*) and 25 km (i.e. *P*). To enable a consistent and combined assessment of the spatiotemporal trends, these variables were standardized at a spatial resolution of 1 km through spatial interpolation and up/downscaling so that the distribution and quantity of human-induced changes in the hydrology and the ecology of the semi-arid Konya basin could be revealed.

On the other hand, each of the steps in spatial integration are prone to different sources of error related with spatial interpolation, up/down scaling and validating the grid-based estimations with ground-based estimations. For example, in Chapter 3, in validating the *ET* estimations by SEBS-SM, the spatial representativeness of the BR measurements and the SEBS calculations were different. Considering the fetch guidelines by Brutsaert (1982) and Shuttleworth (1992), a BR station has a source area up to approximately 200 m (top sensor was at 2 m height), which was confirmed by our foot print analysis (Hsieh et al., 2000) which indicated that 80% of the total flux measured by both BR-3 and 4 originated from a source area ranging between 80 and 220 m in the wind direction during the study period. However, due to the use of MODIS thermal band data in quantifying land surface temperature, SEBS had a fixed output pixel size of 1 $km^2$, which is much larger than the source area of a BR station. Due to this large grid size, SEBS outputs represent

a different source area in terms of spatial dimensions, which will contain more heterogeneity in land cover compared to the BR stations. Therefore, there was a certain amount of error due to the difference in terms of spatial coverage of the two methods and the heterogeneity in the large grid output provided by SEBS. To increase the reliability of the assessments, such uncertainties due to spatial integration were tackled through integrating additional variables in the analysis (e.g. field measurements of soil moisture in Chapter 3, Figs. 3.7 and 3.8). While field measurements of soil moisture were used to support the validation of the proposed method for integrating *SM* into the SEBS, passive microwave measurements of SM were used in the final mapping of the regional daily *ET* to achieve operational application. The passive microwave *SM* data has a coarser spatial resolution (~25 km) compared to the MODIS thermal bands with 1 km resolution. However, despite this coarser scale, the regional *ET* output map from SEBS (Figure 3.10b) hardly reflects any deterioration in the continuity of *ET* spatial distribution. This is mainly due to the fact that *H* is obtained solving a set of non-linear equations in SEBS. Therefore, while the explicit integration of soil moisture data into SEBS affects greatly the daily *ET* output map, the influence is not linear.

**b. Integration of different temporal resolution data**

Besides the integration of different spatial resolutions, this research also dealt with integration at the temporal scale due to handling of data with different resolutions (i.e. instantaneous, daily, bi-weekly or monthly) and analyses conducted at different temporal terms.

In Chapter 3, SEBS model was used for the calculation of daily *ET*. The model solves the surface energy balance instantaneously at the time of satellite overpass using a combination of instantaneous (e.g. land surface temperature) and daily data (e.g. daily average air temperature), while it upscales the instantaneous solution to daily *ET* by assuming a constant evaporative fraction during the day especially for cloud-free conditions (Crago, 1996; Gentine et al., 2007). Some error can be attributed to the upscaling from the instantaneous to the daily estimations. However, this error was limited since this study was only conducted for cloud-free days, when the evaporative fraction was indeed found to be relatively constant by our half hourly BR measurements (Figure 3.9).

In Chapter 4, a combination of different temporal resolution data were used for establishing the spatiotemporal water balance. For the estimation of spatio-temporal precipitation, the monthly RS-based rainfall data (from TRMM satellite) was firstly assessed for the presence of bias at seasonal scale (i.e. wet and dry seasons) using the daily rain gauge measurements (Figure 4.6). Afterwards, snow water equivalent estimated from a multivariate analysis of snow gauges measurements, snow cover days from the 8-daily product of MODIS (MOD10A2) and the elevation data was integrated with the bias-corrected yearly rainfall to obtain the distribution of total precipitation. For estimating the distribution of yearly ET, the SEBS-SM was run on a daily interval using MODIS input data. However, the model output had some missing days either due to the cloud coverage or unreliable data masked out by the quality control of the MODIS team on the input variables. For filling the ET data gaps, a monthly average compositing was implemented by dividing the sum of the available daily *ET* estimates by the number of days with available *ET* estimates for each pixel. Afterwards, the monthly total *ET* values were calculated by multiplying the average daily *ET* (for the month) by 30 days.

Finally in Chapter 5, as suggested by Burn and Elnur (2002), a systematic framework was established for the assessment of eco-hydrological trends and their causes at regional scale. In this regard, different variables (i.e. *ET*, *PET*, *NDVI* and *P*) that had different temporal resolutions from daily (i.e. *ET* and *PET*), bi-weekly (i.e. *NDVI*) and monthly (i.e. *P*) were assessed on the yearly basis (average and sum) for revealing the distribution and magnitude of the trends in these variables and the inter-relations.

### c. Integration of remote sensing and ground data

To support the main objective of this research, satellite observations had a primary role due to their potential of providing spatially continuous and temporally recurrent estimates over regional to global scales (Alsdorf and Lettenmaier, 2003). Still, to support an improved estimation of the individual fluxes and/or validation of RS-based estimations, ground data were also utilized and integrated to the assessments at different levels. For example, in Chapter 4, for an improved estimation of spatio-temporal precipitation, rain and snow gauge measurements were integrated with the RS-based rainfall (i.e. TRMM product) and snow cover data (i.e. MODIS product) for the purpose of correcting the possible biases in the RS data and estimating the

snow water equivalent contribution to the total precipitation, respectively. One of the main contributions in integrating RS and ground data was that while RS was providing the spatial distribution and scope aspects, ground data provided more the local accuracy and precision.

Besides helping to improve the accuracy, ground data had an indispensable role in validating the results obtained from RS methods. In Chapter 3, the modified SEBS model (i.e. SEBS-SM) was tested by comparing its outputs with field observations from Bowen ratio stations distributed over the Konya basin, and the results confirmed a large improvement when soil moisture is integrated explicitly in the calculation of sensible heat flux by SEBS. In addition, in Chapter 4, to assess the closure of the water budget estimated by the RS-based method (not RS only but integrating RS and ground approaches), $\Delta S_{RS}$ estimates were compared with the $\Delta S_{GW}$ values calculated based on yearly groundwater level observations measured at 5 distributed groundwater wells, and the results indicated about 80% match between RS-based estimations and the range given by ground measurements (Figure 4.13)

**d. An integrated framework for monitoring ecohydrology**

After establishing a consistent (spatially and temporally) time series of the fluxes, one of the last steps of this research was to assess the eco-hydrological trends and their causes at regional scale. In Chapter 5, we showed that an integrated trend analysis of consistently established *ET* time series along with vegetation (*NDVI*) and climate variables (i.e. *PET*, *P*) is effective to reveal the distribution and quantity of human-induced changes in the hydrology and the ecology of the semi-arid Konya basin, where previous studies (e.g. Bayari et al., 2009) had also indicated huge non-renewable groundwater abstraction for irrigation, and corresponding groundwater head declines. The integrated assessment of hydrological (*ET*), vegetation (*NDVI*) and climate (*P* and *PET*) variables not only enabled to identify the consistencies among them but also a better separation of climate-driven and human-induced trends, spatially over the region. Similarly, Dorigo et al. (2012) not only merged different soil moisture products from different satellite sensors but also compared the observed trends with trends in a precipitation dataset, and a vegetation dataset in order to identify consistencies and potential shortcomings.

## 7.5 Future work

This research presented an example of an integrated use of earth observation methods (remote sensing and ground) for improving the quantitative and spatio-temporal assessment of hydrological fluxes and ecosystem's health and the inter-relations between them in a closed, semi-arid basin. The means used in achieving these goals were mainly developing and implementing improved models (Chapter 3), spatio-temporal water balance (Chapter 4), and establishing harmonized time-series and integrated framework for eco hydrological trends (Chapter 5). Yet, a variety of future research can further complement and advance the steps taken by this thesis. It should be highlighted that both the content of this research and the possible future work could also be adapted to other regions and scales with appropriate adjustments. Some of the possible future works can be listed under the following groups:

### a. Further improvements in the methods

- The spatio-temporal water balance established by the RS-based methods can be coupled with a groundwater model for enabling a dynamic validation of the water balance in a complete spatially distributed manner. Although we also tested the budget closure of the water balance in a distributed way in Chapter 4, the validation was limited with 5 groundwater observation wells distributed in the basin. In addition, through the coupling with a groundwater model, the processes (e.g. ground recharge, discharge and horizontal flow) in the unsaturated and saturated zones could be represented, which were not considered in the current thesis.
- Estimation of the snowmelt contribution to the total precipitation can be further improved, either with advances in the RS-based snow water equivalent and precipitation products, or by implementing snowmelt-runoff models.
- Assessing the uncertainties and alternative methods for filling the data gaps in daily $ET$ to support developing improved methods for the estimation of seasonal and yearly $ET$ distribution. Examples of alternative methods to consider can be the fusing of multi-temporal resolution data (e.g. Anderson et al., 2012, Gao et al., 2006), methods based on the correlation of $ET$ with other variables, among others.

**b. Multi-scale and multi-sensor analyses for enhanced monitoring of ecohydrology**

- In this thesis, the analyses were carried out mostly at a spatial resolution of 1 km due to using MODIS data as the core input data. The medium scale spatial (1 km) and a high temporal (1 day) resolution offered by MODIS provided a valuable base for the basin/regional scale analysis which enabled assessing the eco-hydrological relations between croplands and wetlands at land cover type level. However, such a medium/large scale assessment is not sufficient for the investigations at crop types or species scale, which would be necessary to study water-use by crop types or monitoring irrigation efficiency to support sustainable management of water resources, and studying the adaptations and/or changes of natural vegetation species to the changing hydrological conditions. Therefore, further studies that utilize higher spatial resolution data (e.g. Aster, Landsat) would be needed for investigating eco-hydrological relations at local scales.
- On the other hand, higher spatial resolution RS data suffers from the decrease in temporal frequency, with revisit times of minimum bi-weekly (e.g. Landsat). Therefore, a comprehensive integration of multi-sensor and multi-scale RS observations would be needed for an improved monitoring of the hydrology and ecology from field to basin scale. An example study investigating the scale influences on the RS estimation of evapotranspiration using multiple satellite sensors is provided by (McCabe and Wood, 2006).

**c. Predicting the future**

- In this thesis, we established a harmonized time-series of a set of variables for the eleven years study period (2000 - 2010), which was mainly limited by the availability of one of the core data sets (i.e. MODIS), to assess eco-hydrological trends and their causes. Firstly, a trend analysis covering a longer period would be necessary not only for a detailed assessment of climate-related trends but also to enable the projection of these trends to the future. In this regard, one future work could focus on establishing a long and consistent time-series of variables based on merging multiple source satellite data.
- Based on the assessments of past trends in the hydrology (e.g. groundwater depletion) and ecology (e.g. drying wetlands), several

future studies could focus on the scenario-analysis and predictions of possible future projections for groundwater resources and ecosystems' health based on the current human-induced trends and a variety of climate scenarios from Global/Regional Climate Models (GCMs) predictions and assessments of the Intergovernmental Panel on Climate Change (IPPC).

# Bibliography


Aeschbach-Hertig, W., & Gleeson, T. (2012). Regional strategies for the accelerating global problem of groundwater depletion. *Nature Geosci, 5*, 853-861

Alcaraz-Segura, D., Liras, E., Tabik, S., Paruelo, J., & Cabello, J. (2010). Evaluating the Consistency of the 1982-1999 NDVI Trends in the Iberian Peninsula across Four Time-series Derived from the AVHRR Sensor: LTDR, GIMMS, FASIR, and PAL-II. *Sensors, 10*, 1291-1314

Allen, M. R., Mutlow, C. T., Blumberg, G. M. C., Christy, J. R., McNider, R. T., and Llewellyn - Jones, D. T. (1994). Global change detection, Nature, 370, 24 – 25.

Allen, R.G., Tasumi, M., & Trezza, R. (2007). Satellite-based energy balance for mapping evapotranspiration with internalized calibration (METRIC) - Model. *Journal of Irrigation and Drainage Engineering-Asce, 133*, 380-394

Alley, M., & Leake, S.A. (2004). The journey from safe yield to sustainability. *Ground Water, 42*, 12-16

Alley, W.M., Reilly, T.E., & Franke, O.L. (1999). *Sustainability of Ground-water Resources*. Denver: Geological Survey (U.S.)

Alsdorf, D.E., & Lettenmaier, D.P. (2003). Tracking Fresh Water from Space. *Science, 301*, 1491-1494

Anderson, M.C., Kustas, W.P., & Norman, J.M. (2007). Upscaling flux observations from local to continental scales using thermal remote sensing. *Agronomy Journal, 99*, 240-254

Anderson, M.C., Allen, R.G., Morse, A., & Kustas, W.P. (2012). Use of Landsat thermal imagery in monitoring evapotranspiration and managing water resources. *Remote Sensing of Environment, 122*, 50-65

Armanios, DE and Fisher, JB. (2012). Measuring water availability with limited ground data: assessing the feasibility of an entirely remote-sensing-based hydrologic budget of the Rufiji Basin, Tanzania, using TRMM, GRACE, MODIS, SRB, and AIRS. *Hydrological Processes*, DOI: 10.1002/hyp.9611

Bastiaanssen, W.G.M., Menenti, M., Feddes, R.A., & Holtslag, A.A.M. (1998). A remote sensing surface energy balance algorithm for land (SEBAL) - 1. Formulation. *Journal of Hydrology, 213*, 198-212

Bayari, C.S., Ozyurt, N.N., & Kilani, S. (2009). Radiocarbon age distribution of groundwater in the Konya Closed Basin, central Anatolia, Turkey. *Hydrogeology Journal, 17*, 347-365

Beck, H.E., McVicar, T.R., van Dijk, A., Schellekens, J., de Jeu, R.A.M., & Bruijnzeel, L.A. (2011). Global evaluation of four AVHRR-NDVI data sets: Intercomparison and assessment against Landsat imagery. *Remote Sensing of Environment, 115*, 2547-2563

Beljaars, A.C.M., & Holtslag, A.A.M. (1991). Flux parameterization over land surfaces for atmospheric models. *Journal of Applied Meteorology, 30*, 327-341

Biancamaria, S., Mognard, N.M., Boone, A., Grippa, M., & Josberger, E.G. (2008). A satellite snow depth multi-year average derived from SSM/I for the high latitude regions. *Remote Sensing of Environment, 112*, 2557-2568

Blumel, K. (1999). A simple formula for estimation of the roughness length for heat transfer over partly vegetated surfaces. *Journal of Applied Meteorology, 38*, 814-829

Blyth, E.M., & Dolman, A.J. (1995). The roughness length for heat of sparse vegetation. *Journal of Applied Meteorology, 34*, 583-585

Bolster, C.H., Genereux, D.P., & Saiers, J.E. (2001). Determination of specific yield for the Biscayne Aquifer with a canal-drawdown test. *Ground Water, 39*, 768-777

Bredehoeft, J., & Durbin, T. (2009). Ground Water Development-The Time to Full Capture Problem. *Ground Water, 47*, 506-514

Bredehoeft, J.D., Papadopulos, S.S., & Cooper, H.H. (1982). The water budget myth. *Scientific basis of Water Resources Management, Studies in Geophysics*. Washington D.C. : National Academy Press

Brotzge, J.A., & Crawford, K.C. (2003). Examination of the surface energy budget: A comparison of eddy correlation and Bowen ratio measurement systems. *Journal of Hydrometeorology, 4*, 160-178

Brunner, P., Bauer, P., Eugster, M., & Kinzelbach, W. (2004). Using remote sensing to regionalize local precipitation recharge rates obtained from the Chloride Method. *Journal of Hydrology, 294*, 241-250

Brutsaert, W. (1982). *Evaporation into the Atmosphere: Theory, History and Applications*. Himgham, MA: Springer

Budyko, M.I. (1974). *Climate and life*. New York: Academic Press

Burn, D.H., & Elnur, M.A.H. (2002). Detection of hydrologic trends and variability. *Journal of Hydrology, 255*, 107-122

Carlson, T.N., Capehart, W.J., & Gillies, R.R. (1995). A new look at the simplified method for remote sensing of daily evapotranspiration *Remote Sensing of Environment, 54*, 161-167

Chang, A.T.C., Kelly, R.E.J., Josberger, E.G., Armstrong, R.L., Foster, J.L., & Mognard, N.M. (2005). Analysis of ground-measured and passive-microwave-derived snow depth variations in midwinter across the northern Great Plains. *Journal of Hydrometeorology, 6*, 20-33

Choudhury, B.J., & Monteith, J.L. (1988). A 4-layer model for the heat-budget of homogeneous land surfaces. *Quarterly Journal of the Royal Meteorological Society, 114*, 373-398

Contreras, S., Jobbagy, E.G., Villagra, P.E., Nosetto, M.D., & Puigdefabregas, J. (2011). Remote sensing estimates of supplementary water consumption by arid ecosystems of central Argentina. *Journal of Hydrology, 397*, 10-22

Crago, R.D. (1996). Conservation and variability of the evaporative fraction during the daytime. *Journal of Hydrology, 180*, 173-194

Delogu, E., G. Boulet, A. Olioso, B. Coudert, J. Chirouze, E. Ceschia, V. Le Dantec, O. Marloie, G. Chehbouni, and J.-P. Lagouarde. (2012). Reconstruction of temporal variations of evapotranspiration using instantaneous estimates at

the time of satellite overpass. *Hydrology and Earth System Sciences*, 16, 2995–3010.

Derksen, C., Toose, P., Rees, A., Wang, L., English, M., Walker, A., & Sturm, M. (2010). Development of a tundra-specific snow water equivalent retrieval algorithm for satellite passive microwave data. *Remote Sensing of Environment, 114*, 1699-1709

Dorigo, W., de Jeu, R., Chung, D., Parinussa, R., Liu, Y., Wagner, W., & Fernandez-Prieto, D. (2012). Evaluating global trends (1988-2010) in harmonized multi-satellite surface soil moisture. *Geophysical Research Letters, 39*

Douville, H., Ribes, A., Decharme, B., Alkama, R., & Sheffield, J. (2012). Anthropogenic influence on multidecadal changes in reconstructed global evapotranspiration. *Nature Clim. Change, advance online publication*

Du, J., He, F., Zhang, Z., & Shi, P.J. (2011). Precipitation change and human impacts on hydrologic variables in Zhengshui River Basin, China. *Stochastic Environmental Research and Risk Assessment, 25*, 1013-1025

Elmore, A.J., Mustard, J.F., Manning, S.J., & Lobell, D.B. (2000). Quantifying vegetation change in semiarid environments: Precision and accuracy of spectral mixture analysis and the Normalized Difference Vegetation Index. *Remote Sensing of Environment, 73*, 87-102

Evans, J., & Geerken, R. (2004). Discrimination between climate and human-induced dryland degradation. *Journal of Arid Environments, 57*, 535-554

Famiglietti, J.S., Lo, M., Ho, S.L., Bethune, J., Anderson, K.J., Syed, T.H., Swenson, S.C., de Linage, C.R., & Rodell, M. (2011). Satellites measure recent rates of groundwater depletion in California's Central Valley. *Geophysical Research Letters, 38*

Fan, Y., Li, H., & Miguez-Macho, G. (2013). Global Patterns of Groundwater Table Depth. *Science, 339*, 940-943

Fensholt, R., Langanke, T., Rasmussen, K., Reenberg, A., Prince, S.D., Tucker, C., Scholes, R.J., Le, Q.B., Bondeau, A., Eastman, R., Epstein, H., Gaughan, A.E., Hellden, U., Mbow, C., Olsson, L., Paruelo, J., Schweitzer, C., Seaquist, J., & Wessels, K. (2012). Greenness in semi-arid areas across the globe 1981-2007 - an Earth Observing Satellite based analysis of trends and drivers. *Remote Sensing of Environment, 121*, 144-158

Fensholt, R., & Proud, S.R. (2012). Evaluation of Earth Observation based global long term vegetation trends - Comparing GIMMS and MODIS global NDVI time series. *Remote Sensing of Environment, 119*, 131-147

Fensholt, R., & Rasmussen, K. (2011). Analysis of trends in the Sahelian 'rain-use efficiency' using GIMMS NDVI, RFE and GPCP rainfall data. *Remote Sensing of Environment, 115*, 438-451

Ferguson, C.R., J. Sheffield, E.F. Wood, H.L. Gao. (2010). Quantifying uncertainty in a remote sensing-based estimate of evapotranspiration over continental USA. *International Journal of Remote Sensing*, 31, 3821–3865.

Fishman, R.M., Siegfried, T., Raj, P., Modi, V., & Lall, U. (2011). Over-extraction from shallow bedrock versus deep alluvial aquifers: Reliability versus

sustainability considerations for India's groundwater irrigation. *Water Resources Research, 47*

Flatau, P.J., Walco, R.L., & Cotton, W.R. (1992). Polynomial fits to saturated vapor pressure. *Journal of Applied Meteorology, 31*, 1507-1513

Fontugne, M., Kuzucuoglu, C., Karabiyikoglu, M., Hatte, C., & Pastre, J.F. (1999). From Pleniglacial to Holocene: a C-14 chronostratigraphy of environmental changes in the Konya Plain, Turkey. In (pp. 573-591): Pergamon-Elsevier Science Ltd

French, A.N., Jacob, F., Anderson, M.C., Kustas, W.P., Timmermans, W., Gieske, A., Su, Z., Su, H., McCabe, M.F., Li, F., Prueger, J., & Brunsell, N. (2005). Surface energy fluxes with the Advanced Spaceborne Thermal Emission and Reflection radiometer (ASTER) at the Iowa 2002 SMACEX site (USA). *Remote Sensing of Environment, 99*, 55-65

Gao, H.L., Tang, Q.H., Ferguson, C.R., Wood, E.F., & Lettenmaier, D.P. (2010). Estimating the water budget of major US river basins via remote sensing. *International Journal of Remote Sensing, 31*, 3955-3978

Gao, F., Masek, J., Schwaller, M., & Hall, F. (2006). On the blending of the Landsat and MODIS surface reflectance: Predicting daily Landsat surface reflectance. *IEEE Transactions on GeoScience and Remote Sensing, 44*, 8, 2207-2218

Garratt, J.R., & Hicks, B.B. (1973). Momentum, heat and water-vapor transfer to and from natural and artificial surfaces. *Quarterly Journal of the Royal Meteorological Society, 99*, 680-687

Gentine, P., Entekhabi, D., Chehbouni, A., Boulet, G., & Duchemin, B. (2007). Analysis of evaporative fraction diurnal behaviour. *Agricultural and Forest Meteorology, 143*, 13-29

Ghilain, N., Arboleda, A., & Gellens-Meulenberghs, F. (2011). Evapotranspiration modelling at large scale using near-real time MSG SEVIRI derived data. *Hydrology and Earth System Sciences, 15*, 771-786

Giordano, M. (2009). Global Groundwater? Issues and Solutions. *Annual Review of Environment and Resources* (pp. 153-178). Palo Alto: Annual Reviews

Gleeson, T., VanderSteen, J., Sophocleous, M.A., Taniguchi, M., Alley, W.M., Allen, D.M., & Zhou, Y.X. (2010). Groundwater sustainability strategies. *Nature Geoscience, 3*, 378-379

Gleeson, T., Wada, Y., Bierkens, M.F.P., & van Beek, L.P.H. (2012). Water balance of global aquifers revealed by groundwater footprint. *Nature, 488*, 197-200

Gleick, P.H. (2003). Global freshwater resources: Soft-path solutions for the 21st century. *Science, 302*, 1524-1528

Gowda, P.H., Chavez, J.L., Colaizzi, P.D., Evett, S.R., Howell, T.A., & Tolk, J.A. (2007). Remote sensing based energy balance algorithms for mapping ET. *Transactions of the Asabe, 50*, 1639-1644

Grafton, R.Q., Pittock, J., Davis, R., Williams, J., Fu, G., Warburton, M., Udall, B., McKenzie, R., Yu, X., Che, N., Connell, D., Jiang, Q., Kompas, T., Lynch, A., Norris, R., Possingham, H., & Quiggin, J. (2012). Global insights into water resources, climate change and governance. *Nature Clim. Change, advance online publication*

Green, T.R., Taniguchi, M., Kooi, H., Gurdak, J.J., Allen, D.M., Hiscock, K.M., Treidel, H., & Aureli, A. (2011). Beneath the surface of global change: Impacts of climate change on groundwater. *Journal of Hydrology, 405*, 532-560

Hall, D.K., Riggs, G.A., Salomonson, V.V., DiGirolamo, N.E., & Bayr, K.J. (2002). MODIS snow-cover products. *Remote Sensing of Environment, 83*, 181-194

Hall, F.G., Huemmrich, K.F., Goetz, S.J., Sellers, P.J., & Nickeson, J.E. (1992). Satellite Remote Sensing of Surface Energy Balance: Success, Failures, and Unresolved Issues in FIFE. *J. Geophys. Res., 97*, 19061-19089

Hamed, K.H. (2008). Trend detection in hydrologic data: The Mann–Kendall trend test under the scaling hypothesis. *Journal of Hydrology, 349*, 350-363

Hatzianastassiou, N., Katsoulis, B., Pnevmatikos, J., & Antakis, V. (2008). Spatial and temporal variation of precipitation in Greece and surrounding regions based on global precipitation climatology project data. *Journal of Climate, 21*, 1349-1370

Heumann, B.W., Seaquist, J.W., Eklundh, L., & Jonsson, P. (2007). AVHRR derived phenological change in the Sahel and Soudan, Africa, 1982-2005. *Remote Sensing of Environment, 108*, 385-392

Hinckley, T.M., Brooks, J.R., Cermák, J., Ceulemans, R., Kuèera, J., Meinzer, F.C., & Roberts, D.A. (1994). Water flux in a hybrid popular stand. *Tree Physiology, 14*, 1005-1018

Hsieh, C.-I., Katul, G., & Chi, T.-w. (2000). An approximate analytical model for footprint estimation of scalar fluxes in thermally stratified atmospheric flows. *Advances in Water Resources, 23*, 765-772

Huffman, G.J., Adler, R.F., Bolvin, D.T., Gu, G.J., Nelkin, E.J., Bowman, K.P., Hong, Y., Stocker, E.F., & Wolff, D.B. (2007). The TRMM multisatellite precipitation analysis (TMPA): Quasi-global, multiyear, combined-sensor precipitation estimates at fine scales. *Journal of Hydrometeorology, 8*, 38-55

Huffman, G.J., & Bolvin, D.T. (2012). TRMM and other data precipitation data set documentation. In (p. 11): Laboratory for Atmospheres, NASA Goddard Space Flight Center and Science Systems and Applications

Jia, L., Su, Z.B., van den Hurk, B., Menenti, M., Moene, A., De Bruin, H.A.R., Yrisarry, J.J.B., Ibanez, M., & Cuesta, A. (2003). Estimation of sensible heat flux using the Surface Energy Balance System (SEBS) and ATSR measurements. In (pp. 75-88): Pergamon-Elsevier Science Ltd

Jiang, L., & Islam, S. (2001). Estimation of surface evaporation map over southern Great Plains using remote sensing data. *Water Resources Research, 37*, 329-340

Jin, X.M., Schaepman, M.E., Clevers, J., & Su, Z.B. (2009). Impact and consequences of ET changes on water resources availability in the arid Zhangye Basin, China. *International Journal of Remote Sensing, 30*, 3223-3238

Johnson, A.I. (1967). Specific yield — compilation of specific yields for various materials. In, *Water Supply Paper 1662-D* (p. 74 p.). U.S. Geological Survey

Joyce, R.J., Janowiak, J.E., Arkin, P.A., & Xie, P.P. (2004). CMORPH: A method that produces global precipitation estimates from passive microwave and

infrared data at high spatial and temporal resolution. *Journal of Hydrometeorology, 5*, 487-503

Julien, Y., Sobrino, J.A., & Verhoef, W. (2006). Changes in land surface temperatures and NDVI values over Europe between 1982 and 1999. *Remote Sensing of Environment, 103*, 43-55

Jung, M., Reichstein, M., Ciais, P., Seneviratne, S.I., Sheffield, J., Goulden, M.L., Bonan, G., Cescatti, A., Chen, J.Q., de Jeu, R., Dolman, A.J., Eugster, W., Gerten, D., Gianelle, D., Gobron, N., Heinke, J., Kimball, J., Law, B.E., Montagnani, L., Mu, Q.Z., Mueller, B., Oleson, K., Papale, D., Richardson, A.D., Roupsard, O., Running, S., Tomelleri, E., Viovy, N., Weber, U., Williams, C., Wood, E., Zaehle, S., & Zhang, K. (2010). Recent decline in the global land evapotranspiration trend due to limited moisture supply. *Nature, 467*, 951-954

Kahler, D. M., and Brutsaert W. (2006). Complementary relationship between daily evaporation in the environment and pan evaporation. *Water Resources Research*, 42, DOI: 10.1029/2005wr004541.

Kalma, J.D., McVicar, T.R., & McCabe, M.F. (2008). Estimating Land Surface Evaporation: A Review of Methods Using Remotely Sensed Surface Temperature Data. *Surveys in Geophysics, 29*, 421-469

Karami, E., & Hayati, D. (2005). Rural Poverty and Sustainability: The Case of Groundwater Depletion in Iran. *Asian Journal of Water, Environment and Pollution, 2*, 51-61

Kelly, R.E., Chang, A.T., Tsang, L., & Foster, J.L. (2003). A prototype AMSR-E global snow area and snow depth algorithm. *Ieee Transactions on Geoscience and Remote Sensing, 41*, 230-242

Kendall, M.G. (1975). *Rank Correlation Methods*. London

Kendy, E. (2003). The false promise of sustainable pumping rates. *Ground Water, 41*, 2-4

Konikow, L.F. (2011). Contribution of global groundwater depletion since 1900 to sea-level rise. *Geophysical Research Letters, 38*, L17401

Konikow, L.F., & Kendy, E. (2005). Groundwater depletion: A global problem. *Hydrogeology Journal, 13*, 317-320

Koster, R.D., Schubert, S.D., & Suarez, M.J. (2009). Analyzing the Concurrence of Meteorological Droughts and Warm Periods, with Implications for the Determination of Evaporative Regime. *Journal of Climate, 22*, 3331-3341

Kustas, W., & Anderson, M. (2009). Advances in thermal infrared remote sensing for land surface modeling. *Agricultural and Forest Meteorology, 149*, 2071-2081

Kustas, W., Anderson, M., Norman, J., & Li, F. (2007). Utility of Radiometric–aerodynamic Temperature Relations for Heat Flux Estimation. *Boundary-Layer Meteorology, 122*, 167-187

Kustas, W.P., Choudhury, B.J., Moran, M.S., Reginato, R.J., Jackson, R.D., Gay, L.W., & Weaver, H.L. (1989). Determination of sensible heat-flux over sparse canopy using thermal infrared data. *Agricultural and Forest Meteorology, 44*, 197-216

Kustas, W.P., & Norman, J.M. (1997). A two-source approach for estimating turbulent fluxes using multiple angle thermal infrared observations. *Water Resources Research, 33*, 1495-1508

Kustas, W.P., & Norman, J.M. (2000). A two-source energy balance approach using directional radiometric temperature observations for sparse canopy covered surfaces. *Agronomy Journal, 92*, 847-854

Kustas, W.P., Perry, E.M., Doraiswamy, P.C., & Moran, M.S. (1994). Using satellite remote sensing to extrapolate evapotranspiration estimates in time and space over a semiarid rangeland basin *Remote Sensing of Environment, 49*, 275-286

Lebel, T., & Ali, A. (2009). Recent trends in the Central and Western Sahel rainfall regime (1990-2007). *Journal of Hydrology, 375*, 52-64

Lee, C.H. (1915). The Determination of Safe Yields of Underground Reservoirs of the Closedbasin Type. *Transactions of the American Society of Civil Engineers, LXXIX*, 148-218

Leroy, S. S., Anderson, J. G., and Ohring, G. (2008) Climate Signal Detection Times and Constraints on Climate Benchmark Accuracy Requirements. J. Climate, 21, 841–846, doi: http://dx.doi.org/10.1175/2007JCLI1946.1.

Liang, S. (2001). Narrowband to broadband conversions of land surface albedo I: Algorithms. *Remote Sensing of Environment, 76*, 213-238

Liu, J., Zheng, C.M., Zheng, L., & Lei, Y.P. (2008). Ground Water Sustainability: Methodology and Application to the North China Plain. *Ground Water, 46*, 897-909

Liu, Y.Y., van Dijk, A., McCabe, M.F., Evans, J.P., & de Jeu, R.A.M. (2013). Global vegetation biomass change (1988-2008) and attribution to environmental and human drivers. *Global Ecology and Biogeography, 22*, 692-705

Lubczynski, M.W., & Gurwin, J. (2005). Integration of various data sources for transient groundwater modeling with spatio - temporally variable fluxes : Sardon study case, Spain. *Journal of Hydrology, 306*

Lunetta, R.S., Knight, J.F., Ediriwickrema, J., Lyon, J.G., & Worthy, L.D. (2006). Land-cover change detection using multi-temporal MODIS NDVI data. *Remote Sensing of Environment, 105*, 142-154

Ma, W.Q., Hafeez, M., Rabbani, U., Ishikawa, H., & Ma, Y.M. (2012). Retrieved actual ET using SEBS model from Landsat-5 TM data for irrigation area of Australia. *Atmospheric Environment, 59*, 408-414

Ma, Y.M., Song, M.H., Ishikawa, H., Yang, K., Koike, T., Jia, L., Meneti, M., & Su, Z.B. (2007). Estimation of the regional evaporative fraction over the Tibetan Plateau area by using Landsat-7 ETM data and the field observations. *Journal of the Meteorological Society of Japan, 85A*, 295-309

Mann, H.B. (1945). Nonparametric Tests against Trend. *Econometrica, 13*, 245-259

Massman, W.J., & Weil, J.C. (1999). An analytical one-dimensional second-order closure model of turbulence statistics and the Lagrangian time scale within and above plant canopies of arbitrary structure. *Boundary-Layer Meteorology, 91*, 81-107

McCabe, M.F., & Wood, E.F. (2006). Scale influences on the remote estimation of evapotranspiration using multiple satellite sensors. *Remote Sensing of Environment, 105*, 271-285

McCabe, M.F., Wood, E.F., Wójcik, R., Pan, M., Sheffield, J., Gao, H., & Su, H. (2008). Hydrological consistency using multi-sensor remote sensing data for water and energy cycle studies. *Remote Sensing of Environment, 112*, 430-444

McGuire, V. (2009). Changes in water levels and storage in the High Plains aquifer, predevelopment to 2007. In (pp. 2009–3005): USGS Fact Sheet

Meijerink, A.M.J., Gieske, A.S.M., & Vekerdy, Z. (2005). Surface energy balance using satellite data for the water balance of a traditional irrigation—wetland system in SW Iran. *Irrigation and Drainage Systems, 19*, 89-105

Menenti, M. and Choudhury, B.J. (1993). Parametrization of land surface evapotranspiration using a location-dependent potential evapotranspiration and surface temperature range. In: *Exchange processes at the land surface for a range of space and time scales*, Bolle, H.J. et al. (Eds.). I AHS Publ. no. 212: 561–568.

Milliman, J.D., Farnsworth, K.L., Jones, P.D., Xu, K.H., & Smith, L.C. (2008). Climatic and anthropogenic factors affecting river discharge to the global ocean, 1951-2000. *Global and Planetary Change, 62*, 187-194

Miralles, D.G., Holmes, T.R.H., De Jeu, R.A.M., Gash, J.H., Meesters, A., & Dolman, A.J. (2011). Global land-surface evaporation estimated from satellite-based observations. *Hydrology and Earth System Sciences, 15*, 453-469

Monteith, J.L. (1965). Evaporation and environment. *Sym. Soc. Exp. Biol., 19*, 205-234

Morrow, E., Mitrovica, J.X., & Fotopoulos, G. (2011). Water Storage, Net Precipitation, and Evapotranspiration in the Mackenzie River Basin from October 2002 to September 2009 Inferred from GRACE Satellite Gravity Data. *Journal of Hydrometeorology, 12*, 467-473

Muskett, R. (2012). Multi-Satellite and Sensor Derived Trends and Variation of Snow Water Equivalent on the High-Latitudes of the Northern Hemisphere. *International Journal of Geosciences, 3*, 1-13

Naing, Z.W. (2011). Groundwater Fluxes in the Konya Closed Basin, Turkey. In, *Water Resources Department* (p. 55). Enschede: University of Twente

New, M., Todd, M., Hulme, M., & Jones, P. (2001). Precipitation measurements and trends in the twentieth century. *International Journal of Climatology, 21*, 1899-

Newman, B.D., Wilcox, B.P., Archer, S.R., Breshears, D.D., Dahm, C.N., Duffy, C.J., McDowell, N.G., Phillips, F.M., Scanlon, B.R., & Vivoni, E.R. (2006). Ecohydrology of water-limited environments: A scientific vision. *Water Resources Research, 42*, 15

Niinemets, U., Sober, A., Kull, O., Hartung, W., Tenhunen, & D., J. (1999). Apparent controls on leaf conductance by soil water availability and via light-acclimation of foliage structural and physiological properties in a

mixed deciduous, temperate forest *International Journal of Plant Sciences, 160*, 707-721

Norman, J.M., Anderson, M.C., & Kustas, W.P. (2006). Are Single-Source, Remote-Sensing Surface-Flux Models Too Simple? In, *Earth Observation for Vegetation Monitoring and Water Management. AIP Conference Proceedings* (pp. 170-177)

Ohmura, A. (1982). Objective criteria for rejecting data for BR flux calculations *J. Appl. Meteor., 21*, 595-598

Oku, Y., Ishikawa, H., & Su, Z. (2007). Estimation of land surface heat fluxes over the Tibetan plateau using GMS data. *In: Journal of applied meteorology and climatology, 46(2007)2, pp. 183-195*

Owe, M., de Jeu, R., & Holmes, T. (2008). Multisensor historical climatology of satellite-derived global land surface moisture. *Journal of Geophysical Research-Earth Surface, 113*, 17

Owen, P.R., & Thomson, W.R. (1963). Heat transfer across rough surfaces
*Journal of Fluid Mechanics, 15*, 321-334

Pagano, T.C., & Sorooshian, S. (2006). Global Water Cycle (Fundamental, Theory, Mechanisms). *Encyclopedia of Hydrological Sciences, 5*, 2697-2711

Pan, M., Sahoo, A.K., Troy, T.J., Vinukollu, R.K., Sheffield, J., & Wood, E.F. (2012). Multisource Estimation of Long-Term Terrestrial Water Budget for Major Global River Basins. *Journal of Climate, 25*, 3191-3206

Pan, M., Wood, E.F., Wojcik, R., & McCabe, M.F. (2008). Estimation of regional terrestrial water cycle using multi-sensor remote sensing observations and data assimilation. *Remote Sensing of Environment, 112*, 1282-1294

Parlange, M.B., & Albertson, J.D. (1995). Regional scale evaporation and the atmospheric boundary layer. *Reviews of Geophysics, 33*, 99-124

Parsons, A.J., & Abrahams, A.D. (Eds.) (1994). *Geomorphology of desert environments* CRC Press

Pauwels, V.R.N., & Samson, R. (2006). Comparison of different methods to measure and model actual evapotranspiration rates for a wet sloping grassland. *Agricultural Water Management, 82*, 1-24

Penck, A. (1896). Unterschungen über Verbunstung und Abfluss von grösseren Landflächen. *Geogr. Abh., 5*, 5

Perez, P.J., Castellvi, F., Ibanez, M., & Rosell, J.I. (1999). Assessment of reliability of Bowen ratio method for partitioning fluxes. *Agricultural and Forest Meteorology, 97*, 141-150

Pettorelli, N., Vik, J.O., Mysterud, A., Gaillard, J.M., Tucker, C.J., & Stenseth, N.C. (2005). Using the satellite-derived NDVI to assess ecological responses to environmental change. *Trends in Ecology & Evolution, 20*, 503-510

Priestley, C.H.B., & Taylor, R.J. (1972). On the assessment of surface heat flux and evaporation using large-scale parameters. *Mon. Weather Rev., 100*, 81-92

Prigent, C., Chevallier, F., Karbou, F., Bauer, P., & Kelly, G. (2005). AMSU-A Land Surface Emissivity Estimation for Numerical Weather Prediction Assimilation Schemes. *Journal of Applied Meteorology, 44*, 416-426

Rahman, H., & Dedieu, G. (1994). SMAC - A simplified method for the atmospheric correction of satellite measurements in the solar spectrum *International Journal of Remote Sensing, 15*, 123-143

Ramsay, B.H. (1998). The interactive multisensor snow and ice mapping system. *Hydrological Processes, 12*, 1537-1546

Raupach, M.R. (1994). Simplified expressions for vegetation roughness length and zero-plane displacement as functions of canopy height and area index. *Boundary-Layer Meteorology, 71*, 211-216

Rivas, R., & Caselles, V. (2004). A simplified equation to estimate spatial reference evaporation from remote sensing-based surface temperature and local meteorological data. *Remote Sensing of Environment, 93*, 68-76

Rodell, M., Chen, J.L., Kato, H., Famiglietti, J.S., Nigro, J., & Wilson, C.R. (2007). Estimating groundwater storage changes in the Mississippi River basin (USA) using GRACE. *Hydrogeology Journal, 15*, 159-166

Rodell, M., Velicogna, I., & Famiglietti, J.S. (2009). Satellite-based estimates of groundwater depletion in India. *Nature, 460*, 999-U980

Roerink, G.J., Su, Z., & Menenti, M. (2000). S - SEBI : a simple remote sensing algorithm to estimate the surface energy balance. *In: Physics and chemistry of the earth. Part B: Hydrology, oceans and atmosphere, 25(2000)2, pp. 147-157*

Ryu, Y., Baldocchi, D.D., Ma, S., & Hehn, T. (2008). Interannual variability of evapotranspiration and energy exchange over an annual grassland in California. *Journal of Geophysical Research-Atmospheres, 113*

Sahoo, A.K., Pan, M., Troy, T.J., Vinukollu, R.K., Sheffield, J., & Wood, E.F. (2011). Reconciling the global terrestrial water budget using satellite remote sensing. *Remote Sensing of Environment, 115*, 1850-1865

Sandstrom, K. (1995). *Modeling the effects of rainfall variability on groundwater recharge in semi-arid Tanzania*. Lyngby, DANEMARK: Nordic Association for Hydrology

Santer, B. D., Mears, C., Doutriaux, C., Caldwell, P., Gleckler, P. J., Wigley, T. M. L., Solomon, S., Gillett, N. P., Ivanova1, D., Karl, T. R., Lanzante, J. R., Meehl, G. A., Stott, P. A., Taylor, K. E., Thorne, P. W., Wehner, M. F., Wentz, F. J. (2011). Separating signal and noise in atmospheric temperature changes: The importance of timescale, J. Geophys. Res., 116, D22105, doi:10.1029/2011JD016263.

Scanlon, B.R., Faunt, C.C., Longuevergne, L., Reedy, R.C., Alley, W.M., McGuire, V.L., & McMahon, P.B. (2012). Groundwater depletion and sustainability of irrigation in the US High Plains and Central Valley. *Proceedings of the National Academy of Sciences of the United States of America, 109*, 9320-9325

Scanlon, B.R., Jolly, I., Sophocleous, M., & Zhang, L. (2007). Global impacts of conversions from natural to agricultural ecosystems on water resources: Quantity versus quality. *Water Resources Research, 43*

Scanlon, B.R., Reedy, R.C., & Gates, J.B. (2010). Effects of irrigated agroecosystems: 1. Quantity of soil water and groundwater in the southern High Plains, Texas. *Water Resources Research, 46*

Seneviratne, S.I., Corti, T., Davin, E.L., Hirschi, M., Jaeger, E.B., Lehner, I., Orlowsky, B., & Teuling, A.J. (2010). Investigating soil moisture–climate interactions in a changing climate: A review. *Earth-Science Reviews, 99*, 125-161

Seneviratne, S.I., Luthi, D., Litschi, M., & Schar, C. (2006). Land-atmosphere coupling and climate change in Europe. *Nature, 443*, 205-209

Serreze, M.C., Clark, M.P., Armstrong, R.L., McGinnis, D.A., & Pulwarty, R.S. (1999). Characteristics of the western United States snowpack from snowpack telemetry (SNOTEL) data. *Water Resources Research, 35*, 2145-2160

Shah, T. (2007). The Agricultural Groundwater Revolution: Opportunities and Threats to Development. In M. Giordano & K.G. Villholth (Eds.), *CABI, 2007* (pp. 7–36)

Sharma, K.P., Moore, B., & Vorosmarty, C.J. (2000). Anthropogenic, climatic, and hydrologic trends in the Kosi Basin, Himalaya. *Climatic Change, 47*, 141-165

Sheffield, J., Ferguson, C.R., Troy, T.J., Wood, E.F., & McCabe, M.F. (2009). Closing the terrestrial water budget from satellite remote sensing. *Geophysical Research Letters, 36*, 5

Shuttleworth, W.J. (1992). *Evaporation (Chapter 4.), Handbook of Hydrology*: Mc Graw Hill

Siebert, S., Burke, J., Faures, J.M., Frenken, K., Hoogeveen, J., Döll, P., & Portmann, F.T. (2010). Groundwater use for irrigation – a global inventory. *Hydrol. Earth Syst. Sci. Discuss., 7*, 3977-4021

Snyder, R.L., Orang, M., Matyac, S., & Grismer, M.E. (2005). Simplified estimation of reference evapotranspiration from pan evaporation data in California. *Journal of Irrigation and Drainage Engineering-Asce, 131*, 249-253

Sobrino, J.A., Kharraz, J.E., & Li, Z.L. (2003). Surface temperature and water vapour retrieval from MODIS data. *International Journal of Remote Sensing, 24*, 5161-5182

Sobrino, J.A., & Raissouni, N. (2000). Toward remote sensing methods for land cover dynamic monitoring: Application to Morocco. *International Journal of Remote Sensing, 21*, 353 - 366

Sophocleous, M. (2000). From safe yield to sustainable development of water resources - the Kansas experience. *Journal of Hydrology, 235*, 27-43

Stewart, J.B., & Thom, A.S. (1973). Energy budgets in pine forest. *Quarterly Journal of the Royal Meteorological Society, 99*, 154-170

Stone, R., & Jia, H. (2006). Hydroengineering - Going against the flow. *Science, 313*, 1034-1037

Strassberg, G., Scanlon, B.R., & Rodell, M. (2007). Comparison of seasonal terrestrial water storage variations from GRACE with groundwater-level measurements from the High Plains Aquifer (USA). *Geophysical Research Letters, 34*

Su, H., McCabe, M.F., Wood, E.F., Su, Z., & ... (2005). Modeling evapotranspiration during SMACEX : comparing two approaches for local - and regional - scale prediction. *In: Journal of hydrometeorology, 6(2005)6, pp. 910-922*

Su, Z. (2002). The Surface Energy Balance System (SEBS) for estimation of turbulent heat fluxes. *Hydrology and Earth System Sciences, 6*, 85-99

Su, Z., Dorigo, W., Fernandez-Prieto, D., Van Helvoirt, M., Hungershoefer, K., de Jeu, R., Parinussa, R., Timmermans, J., Roebeling, R., Schröder, M., Schulz, J., Van der Tol, C., Stammes, P., Wagner, W., Wang, L., Wang, P., & Wolters, E. (2010). Earth observation Water Cycle Multi-Mission Observation Strategy (WACMOS). *Hydrol. Earth Syst. Sci. Discuss., 7*, 7899-7956

Su, Z., Pelgrum, H., & Menenti, M. (1999). Aggregation effects of surface heterogeneity in land surface processes. *Hydrology and Earth System Sciences, 3*, 549-563

Su, Z., Schmugge, T., Kustas, W.P., & Massman, W.J. (2001). An evaluation of two models for estimation of the roughness height for heat transfer between the land surface and the atmosphere. *Journal of Applied Meteorology, 40*, 1933-1951

Swenson, S., Famiglietti, J., Basara, J., & Wahr, J. (2008). Estimating profile soil moisture and groundwater variations using GRACE and Oklahoma Mesonet soil moisture data. *Water Resources Research, 44*

Swenson, S., & Wahr, J. (2002). Methods for inferring regional surface-mass anomalies from Gravity Recovery and Climate Experiment (GRACE) measurements of time-variable gravity. *Journal of Geophysical Research-Solid Earth, 107*

Swenson, S., & Wahr, J. (2006). Estimating large-scale precipitation minus evapotranspiration from GRACE satellite gravity measurements. *Journal of Hydrometeorology, 7*, 252-270

Tang, Q.H., Gao, H.L., Yeh, P., Oki, T., Su, F.G., & Lettenmaier, D.P. (2010). Dynamics of Terrestrial Water Storage Change from Satellite and Surface Observations and Modeling. *Journal of Hydrometeorology, 11*, 156-170

Taylor, R.G., Scanlon, B., Doll, P., Rodell, M., van Beek, R., Wada, Y., Longuevergne, L., Leblanc, M., Famiglietti, J.S., Edmunds, M., Konikow, L., Green, T.R., Chen, J., Taniguchi, M., Bierkens, M.F.P., MacDonald, A., Fan, Y., Maxwell, R.M., Yechieli, Y., Gurdak, J.J., Allen, D.M., Shamsudduha, M., Hiscock, K., Yeh, P.J.F., Holman, I., & Treidel, H. (2012). Ground water and climate change. *Nature Clim. Change, advance online publication*

Teuling, A.J., Hirschi, M., Ohmura, A., Wild, M., Reichstein, M., Ciais, P., Buchmann, N., Ammann, C., Montagnani, L., Richardson, A.D., Wohlfahrt, G., & Seneviratne, S.I. (2009). A regional perspective on trends in continental evaporation. *Geophysical Research Letters, 36*

Teuling, A.J., Seneviratne, S.I., Williams, C., & Troch, P.A. (2006). Observed timescales of evapotranspiration response to soil moisture. *Geophysical Research Letters, 33*, 5

Theis, C.V. (1940). The source of water derived from wells: Essential factors controlling the response of an aquifer to development. *Civil Engineer, 10*, 277-280

Thom, A.S. (1972). Momentum, mass and heat-exchange of vegetation *Quarterly Journal of the Royal Meteorological Society, 98*, 124

Timmermans, W.J., Kustas, W.P., Anderson, M.C., & French, A.N. (2007). An intercomparison of the surface energy balance algorithm for land (SEBAL) and the two-source energy balance (TSEB) modeling schemes. *Remote Sensing of Environment, 108*, 369-384

Timmermans, W.J., & Meijerink, A.M.J. (1999). Remotely sensed actual evapotranspiration: implications for groundwater management in Botswana. *International Journal of Applied Earth Observation and Geoinformation, 1*, 222-233

Tiwari, V.M., Wahr, J., & Swenson, S. (2009). Dwindling groundwater resources in northern India, from satellite gravity observations. *Geophysical Research Letters, 36*

Todd, D.K. (1959). *Groundwater hydrology*. New York: J. Willey and Sons

Troufleau, D., Lhomme, J.P., Monteny, B., & Vidal, A. (1997). Sensible heat flux and radiometric surface temperature over sparse Sahelian vegetation .1. An experimental analysis of the $kB^{-1}$ parameter. *Journal of Hydrology, 189*, 815-838

Van der Kwast, J., Timmermans, W., Gieske, A., Su, Z., Olioso, A., Jia, L., Elbers, J., Karssenberg, D., & de Jong, S. (2009). Evaluation of the Surface Energy Balance System (SEBS) applied to ASTER imagery with flux-measurements at the SPARC 2004 site (Barrax, Spain). *Hydrology and Earth System Sciences, 13*, 1337-1347

Verhoef, A., DeBruin, H.A.R., & VandenHurk, B. (1997a). Some practical notes on the parameter $kB^{-1}$ for sparse vegetation. *Journal of Applied Meteorology, 36*, 560-572

Verhoef, A., McNaughton, K.G., & Jacobs, A.F.G. (1997b). A parameterization of momentum roughness length and displacement height for a wide range of canopy densities. *Hydrology and Earth System Sciences, 1*, 81-91

Verhoef, W., Menenti, M., & Azzali, S. (1996). A colour composite of NOAA-AVHRR-NDVI based on time series analysis (1981-1992). *International Journal of Remote Sensing, 17*, 231-235

Vinukollu, R.K., Wood, E.F., Ferguson, C.R., & Fisher, J.B. (2011). Global estimates of evapotranspiration for climate studies using multi-sensor remote sensing data: Evaluation of three process-based approaches. *Remote Sensing of Environment, 115*, 801-823

Wada, Y., van Beek, L.P.H., & Bierkens, M.F.P. (2012). Nonsustainable groundwater sustaining irrigation: A global assessment. *Water Resources Research, 48*

Wada, Y., van Beek, L.P.H., van Kempen, C.M., Reckman, J.W.T.M., Vasak, S., & Bierkens, M.F.P. (2010). Global depletion of groundwater resources. *Geophysical Research Letters, 37*, L20402

Wagner, W., Hahn, S., Kidd, R., Melzer, T., Bartalis, Z., Hasenauer, S., Figa-Saldana, J., de Rosnay, P., Jann, A., Schneider, S., Komma, J., Kubu, G., Brugger, K., Aubrecht, C., Zuger, J., Gangkofner, U., Kienberger, S., Brocca, L., Wang, Y., Bloschl, G., Eitzinger, J., Steinnocher, K., Zeil, P., & Rubel, F. (2013). The ASCAT Soil Moisture Product: A Review of its Specifications,

Validation Results, and Emerging Applications. *Meteorologische Zeitschrift, 22*, 5-33

Wagner, W., Scipal, K., Pathe, C., Gerten, D., Lucht, W., & Rudolf, B. (2003). Evaluation of the agreement between the first global remotely sensed soil moisture data with model and precipitation data. *Journal of Geophysical Research-Atmospheres, 108*

Wahr, J., Swenson, S., & Velicogna, I. (2006). Accuracy of GRACE mass estimates. *Geophysical Research Letters, 33*, L06401

Wang, K.C., Wang, P., Li, Z.Q., Cribb, M., & Sparrow, M. (2007). A simple method to estimate actual evapotranspiration from a combination of net radiation, vegetation index, and temperature. *Journal of Geophysical Research-Atmospheres, 112*, 14

Woldeamlak, S.T., Batelaan, O., & De Smedt, F. (2007). Effects of climate change on the groundwater system in the Grote-Nete catchment, Belgium. *Hydrogeology Journal, 15*, 891-901

Yang, D.W., Sun, F.B., Liu, Z.Y., Cong, Z.T., Ni, G.H., & Lei, Z.D. (2007). Analyzing spatial and temporal variability of annual water-energy balance in nonhumid regions of China using the Budyko hypothesis. *Water Resources Research, 43*

Yeh, P.J.F., Swenson, S.C., Famiglietti, J.S., & Rodell, M. (2006). Remote sensing of groundwater storage changes in Illinois using the Gravity Recovery and Climate Experiment (GRACE). *Water Resources Research, 42*

Zhang, K., Kimball, J.S., Mu, Q.Z., Jones, L.A., Goetz, S.J., & Running, S.W. (2009). Satellite based analysis of northern ET trends and associated changes in the regional water balance from 1983 to 2005. *Journal of Hydrology, 379*, 92-110

Zhang, L., Dawes, W.R., & Walker, G.R. (2001). Response of mean annual evapotranspiration to vegetation changes at catchment scale. *Water Resources Research, 37*, 701-708

Zhang, Q., Jiang, T., Gemmer, M., & Becker, S. (2005). Precipitation, temperature and runoff analysis from 1950 to 2002 in the Yangtze basin, China. *Hydrological Sciences Journal-Journal Des Sciences Hydrologiques, 50*, 65-80

Zhang, X.B., Zwiers, F.W., Hegerl, G.C., Lambert, F.H., Gillett, N.P., Solomon, S., Stott, P.A., & Nozawa, T. (2007a). Detection of human influence on twentieth-century precipitation trends. *Nature, 448*, 461-U464

Zhang, Y.Q., Leuning, R., Chiew, F.H.S., Wang, E.L., Zhang, L., Liu, C.M., Sun, F.B., Peel, M.C., Shen, Y.J., & Jung, M. (2012). Decadal Trends in Evaporation from Global Energy and Water Balances. *Journal of Hydrometeorology, 13*, 379-391

Zhang, Y.Q., Liu, C.M., Tang, Y.H., & Yang, Y.H. (2007b). Trends in pan evaporation and reference and actual evapotranspiration across the Tibetan Plateau. *Journal of Geophysical Research-Atmospheres, 112*

Zhou, Y.X. (2009). A critical review of groundwater budget myth, safe yield and sustainability. *Journal of Hydrology, 370*, 207-213

# Summary

Arid and semi-arid regions are highly vulnerable to anthropogenic and climate effects due to their scarce water resources, usually with a clear imbalance and a widening gap between the demand and the availability of water, mainly due to agricultural activities. Furthermore, when supplementary groundwater or surface water is used for irrigation, the increased evapotranspiration by crops may largely exceed the input from precipitation, causing large deficits in the regional water balance. Therefore, acquiring accurate knowledge of both precipitation and evapotranspiration and their spatial distribution in arid and semi-arid regions are both considered important challenges in the scientific community and essential for a sustainable water/land resources management and preventing the degradation of ecosystems.

Main objective of the research presented in this thesis is to effectively utilize and integrate earth observation methods to improve the spatio-temporal assessment of the hydrological fluxes and the ecosystem's health and their inter-relations at a large semi-arid basin scale through taking a prominent example of a semi-arid region, namely The Konya basin in central Anatolia (Turkey).

As the first step, this research focused on improving estimation of the spatio-temporal fluxes (i.e. evapotranspiration and precipitation) through developing enhanced models and/or integrating different data/methods. In Chapter 3, an updated version of the SEBS model (i.e. SEBS-SM), that explicitly includes the effect of soil moisture availability on evapotranspiration, is introduced. The results indicated a better accounting for the water stress conditions by the updated SEBS-SM, with an overall accuracy improvement of about 70 W $m^{-2}$ in the estimation of heat fluxes for the sparse vegetation land cover. With respect to obtaining an improved estimation of the precipitation distribution, the RS-based monthly Tropical Rainfall Measuring Mission (TRMM) rainfall product was firstly bias-removed based on rain-gauge measurements and then integrated with an explicit estimate of the snowfall contribution to precipitation based on RS and field measurements (Chapter 4).

In the next step, Chapter 4, the focus was quantifying and validating a spatially distributed water balance through developing a simplified conceptual model and using improved estimations of evapotranspiration and precipitation. According to the spatially distributed water balance, the average quantity of supplementary irrigation from the irrigated croplands was 308 ± 132 mm $y^{-1}$ (the maximum reaching up to 500 mm $y^{-1}$) with the source of about 80% from groundwater and 20% from surface water. These fluxes correspond to an average total volume change of about -4,700 MCM $y^{-1}$ from the groundwater storage in the croplands (including irrigated, mixed and non-irrigated) during the study period (2005 - 2009). Besides the croplands, the large *P* - *ET* differences in the wetlands (-422 ± 209 mm $y^{-1}$) and water bodies (avg. -495 ± 76 mm $y^{-1}$) indicate that they receive large groundwater and/or surface water inputs to sustain such excess *ET*. For assessing the effectiveness of the methodology, we validated the spatially distributed water balance also in a spatially distributed manner comparing with the distributed GW level observations, which differs from other studies that validated their satellite-based water balance against the streamflow data at the outlet of the river basins.

In the following Chapter 5, an integrated framework was implemented for assessing the recent spatio-temporal trends (from 2000 to 2010) and inter-relations in the ecohydrology of the region. The combined assessment of the trends in *ET* and *NDVI* revealed that: significant ($p<0.1$) increasing trends were mainly in the croplands (totally about 63 MCM $y^{-1}$ *ET* increase; a mean increase of 0.004 *NDVI* $y^{-1}$ in irrigated croplands) while the significant decreasing trends ($p<0.1$) were mostly in wetlands (totally about -2.1 MCM $y^{-1}$ *ET* decrease; a mean decrease of -0.001 *NDVI* $y^{-1}$). Furthermore, according to the comparison with the trends in climate-related *P* and *PET*, the observed eco-hydrological trends (i.e. *ET* and *NDVI*) in the basin, especially in the water-limited plain part, were not related to the climate-related variables except for only about 16% of the increasing *ET* trend being explained by the increasing trend of *PET*. The emerging picture suggest that the greening trend of the vegetation in the Konya plain is mostly related to land cover changes (i.e. conversion into irrigated croplands) and to the intensification of the irrigation, which in turn caused drying out of the some of the wetlands and the natural vegetation which mostly depend on the groundwater, the main source of irrigation water as well.

Lastly, the limits and variations of the sustainable water resources were assessed considering that the sustainable yield from a basin is the portion of the total yield remaining after the demands by the ecosystems. Based on the yearly distributions of the *P - ET* balance over a decade period we found that the average sustainable yield in the Konya closed basin has been only a negligible amount of 75 MCM $y^{-1}$, because 1,310 MCM $y^{-1}$ of the totally 1,385 MCM $y^{-1}$ average yearly yield constituted the ecological water demand (i.e. discharges to wetlands and water bodies). However, the sustainable varied largely between the years (from 4,000 MCM $y^{-1}$ in the wet 2009 to -1,200 MCM $y^{-1}$ in the dry 2008) due to the high variation of precipitation input. It should be borne in mind that sustainability assessment is a management issue as well as a scientific problem, and should be understood as a dynamic and iterative process, requiring continued monitoring, analysis, prioritization, and revision. To tackle groundwater depletion, water management strategies can be classified as demand-side strategies that aim at decreasing groundwater extraction and supply-side strategies that try to increase the water supply in general. A "hard path" measure to increase water supply is large-scale water diversions, as realized in the Central Valley in the U.S., or even a bigger schemes in China. Similarly in the Konya basin, an inter-basin water diversion project (i.e. Blue tunnel project) was realized in 2012, which is planned to provide an additional 414 MCM $y^{-1}$ surface water resources mainly for irrigation purpose (http://www.konya.gov.tr/goster.asp?baslik=Konya%20Ovalar%FD%20Projesi%20(KOP). However, such an additional water resource would only contribute about 14% to the average total irrigation water consumption of 3,000 MCM $y^{-1}$ that occurred for the croplands in the Konya plain over the 2000 - 2010 period.

# Samenvatting

Aride and semi-aride gebieden zijn vanwege hun schaarse watervoorraden zeer kwetsbaar voor antropogene and klimaatgerelateerde effecten, veelal met een duidelijke onbalans en een toenemende kloof tussen de vraag en de beschikbaarheid van water, voornamelijk door het gebruik in de landbouw. Bovendien, wanneer bij watertekorten grond- of oppervlaktewater wordt gebruikt voor irrigatie, kan de toegenomen gewasverdamping de neerslag ruimschoots overschrijden, waardoor grote tekorten in de regionale waterbalans kunnen ontstaan. Daarom vormt het verkrijgen van nauwkeurige informatie over de hoeveelheid en de ruimtelijke verdeling van zowel de neerslag als de verdamping in deze gebieden een belangrijke uitdaging voor de wetenschappelijke gemeenschap, hetgeen essentieel is voor een duurzaam water- en landbeheer en het in stand houden van ecosystemen.

De belangrijkste doelstelling van het in deze dissertatie gepresenteerde onderzoek is vast te stellen hoe door het effectief toepassen en integreren van aardobservatiemethoden de ruimtelijke verdeling en het dynamisch gedrag van de hydrologische stromen en hun onderlinge verbanden beter in kaart kunnen worden gebracht. Voor het onderzoek is als voorbeeld genomen het semi-aride Konya bekken in centraal Anatolië in Turkije.

De eerste stap in het onderzoek was gericht op het verbeteren van de bepaling van de spatio-temporele fluxen (d.w.z. verdamping en neerslag) door het ontwikkelen van verfijnde modellen en het integreren van diverse gegevens en methoden. In Hoofdstuk 3 wordt een aangepaste versie van het model SEBS geïntroduceerd. Dit model heet SEBS-SM en bevat een expliciete beschrijving van het effect van de beschikbaarheid van bodemvocht op de verdamping. De resultaten geven aan dat het model het optreden van water stress in het gewas beter kan weergeven, met als gevolg een globale verbetering van de nauwkeurigheid met ca. 70 $W/m^2$ in de bepaling van de warmtefluxen voor dun begroeide gebieden. Voor de neerslagverdeling is gebruik gemaakt van het neerslagproduct van de TRMM (Tropical Rainfall Measuring Mission) missie, geijkt aan de hand van regenmeter metingen op de grond en vervolgens samengevoegd met expliciete schattingen van de bijdrage door sneeuwval bepaald uit RS opnamen en veldwaarnemingen (Hoofdstuk 4).

In de volgende stap, beschreven in Hoofdstuk 4, was het doel het kwantificeren en valideren van de ruimtelijk verdeelde waterbalans door het ontwikkelen van een versimpeld conceptueel model en het gebruiken van de verbeterde schattingen van gewasverdamping en neerslag. De ruimtelijk verdeelde waterbalans geeft aan dat de gemiddelde hoeveelheid aanvullende irrigatie in het geïrrigeerde landbouwgebied 308 ± 132 mm/jaar bedroeg (met een maximum van 500 mm/jaar, waarbij ca. 80% afkomstig is uit het grondwater en 20% uit oppervlaktewater. Deze fluxen komen overeen met een gemiddelde totale volumeflux van ca. 4700 $Mm^3$/jaar in de grondwatervoorraad in de landbouwgebieden (incl. geïrrigeerd, gemengd en ongeïrrigeerd) gedurende de periode 2005-2009. Buiten het landbouwgebied geven de grote neerslag - verdamping saldo's in de wetlands (-422 ± 209 mm/jaar) en de oppervlaktewateren (gem. -495 ± 76 mm/jaar) aan dat ook deze grote instromen ontvangen uit het grondwater en het oppervlaktewater om deze excessieve gewasverdamping te kunnen volhouden. Om de effectiviteit van de methode te kunnen bepalen hebben we de ruimtelijke verdeelde waterbalans ook op een ruimtelijke verdeelde manier gevalideerd door vergelijking met metingen van het grondwaterpeil, hetgeen verschilt met andere studies waarbij de met satellieten vastgestelde waterbalans werd gevalideerd aan de hand van stroomgegevens bij de uitlaten van de waterbekkens.

Vervolgens beschrijft Hoofdstuk 5 de implementatie van een geïntegreerd raamwerk voor de bepaling van spatio-temporele trends (van 2010 tot 2010) en hun interrelaties in de eco-hydrologie van het gebied. Uit de gecombineerde bepaling van de trends in verdamping en de NDVI kwam naar voren: significant toenemende trends ($p < 0.1$) vooral in de landbouwgebieden (totale verdampingstoename ca. 63 $Mm^3$/jaar; een gemiddelde toename van 0.004 in de NDVI per jaar in geïrrigeerde landbouwgebieden) terwijl significant dalende trends ($p < 0.1$) meestal plaatsvonden in de wetlands (totale afname ca. 2.1 $Mm^3$/jaar in de gewasverdamping; een gemiddelde afname in de NDVI van 0.001 per jaar). Bovendien bleek uit vergelijking met de klimaatgebonden trends in neerslag en potentiële verdamping dat de waargenomen eco-hydrologische trends (d.w.z. in verdamping en NDVI) in het bekken, met name in het watergelimiteerde vlakke deel, geen relatie hadden met de klimaatgebonden variabelen, behalve dan dat ca. 16% van de toenemende trend in de gewasverdamping kan worden verklaard uit de positieve trend in de

potentiële verdamping. Het beeld dat naar boven komt suggereert dat de vergroenende trend van de vegetatie in de Konya vlakte meestal is te relateren aan veranderingen in het landgebruik (d.w.z. conversie naar geïrrigeerde landbouw) en aan de intensivering van de irrigatie, die op zijn beurt leidt tot uitdroging van sommige wetlands en de natuurlijke vegetatie welke vooral afhankelijk zijn van grondwater, tevens de voornaamste bron van irrigatiewater.

Tenslotte zijn de grenzen en de variaties van de duurzame waterbronnen bepaald, waarbij is aangenomen dat de duurzame opbrengst uit een bekken gelijk is aan het deel van de totale opbrengst dat overblijft nadat voldaan is aan de vraag afkomstig van de ecosystemen. Gebaseerd op de jaarlijkse verdelingen van de neerslag - verdamping balans per decennium hebben we vastgesteld dat de gemiddelde duurzame opbrengst in het afgesloten Konya bekken slechts een verwaarloosbare hoeveelheid van 75 $Mm^3$/jaar bedroeg, omdat 1310 $Mm^3$/jaar van het totaal van 1385 $Mm^3$/jaar aan gemiddelde jaarlijkse opbrengst bestond uit de vraag naar ecologisch vereist water (d.w.z. voor afvoer naar wetlands en oppervlaktewater). Echter, de duurzame opbrengst varieerde sterk van jaar tot jaar (van 4000 $Mm^3$/jaar in het natte jaar 2009 tot -1200 $Mm^3$/jaar in het droge jaar 2008) door de grote variatie in de aanvoer door neerslag. Beseft moet worden dat het bepalen van de duurzaamheid zowel een beheervraagstuk is als een wetenschappelijk probleem, en dat dit moet worden gezien als een dynamisch en iteratief proces dat voortdurende bewaking, analyse, prioriteitsstelling en heroverweging vereist. Om grondwateruitputting te bestrijden kunnen in het waterbeheer vraaggestuurde strategieën worden geïdentificeerd, die zijn gericht op het verminderen van de grondwateronttrekking, en aanbodgestuurde strategieën, die het wateraanbod in het algemeen proberen te verhogen. Een rigoreuze maatregel om het wateraanbod te verhogen is het op grote schaal ombuigen van waterlopen, zoals is gerealiseerd in de Centrale Vallei in de VS, of zoals bij nog grotere ingrepen in China. Op soortgelijke wijze is in 2012 voor het Konya bekken een inter-bekken waterloop ombuigingsproject (het Blauwe tunnel project) gerealiseerd, dat moet voorzien in een extra hoeveelheid van 414 $Mm^3$/jaar aanbod van oppervlaktewater dat voornamelijk bedoeld is voor irrigatiedoeleinden (http://www.konya.gov.tr/goster.asp?baslik=Konya%20Ovalar%FD%20Projesi%20(KOP). Echter, zo'n extra waterhulpbron zou slechts ca. 14% bijdragen van de gemiddelde totale consumptie aan irrigatiewater van de 3000

$Mm^3$/jaar die plaatsvond voor de landbouwgebieden in de Konya vlakte gedurende de periode 2000 – 2010.

# Özet

Kurak ve yarı-kurak bölgeler, kısıtlı su kaynaklarına sahip olmaları ve buna karşın özellikle tarım faaliyetlerine bağlı olarak eldeki su miktarı ve talep arasındaki belirgin dengesizlik nedeniyle, iklim ve insan etkilerine karşı çok hassastır. Özellikle sulama amaçlı olarak ilave yeraltı ve yüzey sularının kullanılması durumunda, sulu tarım bitkilerinden kaynaklı buharlaşma (buharlaşma terimi buharlaşma ve terlemeyi ifade etmektedir) artışı nedeniyle bölgedeki toplam buharlaşma yoluyla su kaybı, toplam yağış girdisini büyük miktarda aşarak havzanın su dengesinde büyük bir açığa yol açabilir. Bu nedenle, kurak ve yarı-kurak bölgelerde, hem yağışın hem de buharlaşmanın miktarı ve mekânsal dağılımının doğru biçimde hesaplanması yalnızca önemli bir bilimsel problem değil aynı zamanda doğal kaynakların sürdürülebilir yönetimi ve ekosistem tahribatının engellenmesi için gereklidir.

Bu tezde sunulan araştırmanın ana amacı yer gözlem yöntemlerini etkin bir şekilde kullanarak ve entegre ederek, yarı-kurak ve su-kısıtlı Konya kapalı havzası örneği yoluyla, havza bazında su girdi/çıktıları, ekosistemlerinin sağlığı ve bunlar arasındaki ilişkilerin mekânsal ve zamansal dağılımının değerlendirilmesini iyileştirmektir.

İlk aşama olarak bu araştırma, su girdi-çıktılarının (yağış ve buharlaşma) mekansal-zamansal dağılımının hesaplanmasını iyileştirmek için daha iyi modeller geliştirmeyi ve/ya da farklı model ve verileri entegre etmeyi amaçlamıştır. Bölüm 3'te, buharlaşmanın hesaplanmasında kullanılan önemli bir model olan SEBS modeli performansının yarı-kurak bölge koşullarında iyileştirmesi amacıyla geliştirilen, ve bu amaçla modele toprak nemi miktarının buharlaşma üzerindeki etkisini entegre eden SEBS-SM modeli sunulmuştur. Elde edilen sonuçlar geliştirilen SEBS-SM modeli ile su-stresinin buharlaşma üzerindeki etkisinin daha iyi ifade edildiğini, böylece özellikle seyrek vejetasyona sahip arazi örtüsü alanlarında buharlaşma miktarı hesabının doğruluk derecesinin arttırıldığını ortaya koymuştur.

Yağış dağılımının daha doğru biçimde hesaplanmasına ilişkin olarak ise, uzaktan algılama (RS) tabanlı aylık yağmur verisi sağlayan TRMM (Tropical Rainfall Measuring Mission) verisi öncelikle yağış-ölçüm istasyonlarının ölçümleri ile kıyaslanarak RS-tabanlı tahminlerdeki bias ortadan kaldırılmış

olup, ardından kar-suyunun toplam yağışa katkısı arazi ölçümleri ve RS verilerinin multi-regresyon analizi ile hesaplanarak yağmur hesabına entegre edilmiştir (Bölüm 4).

Bir sonraki aşamada (Bölüm 4), doğruluk derecesi arttırılarak elde edilen buharlaşma ve yağış hesaplarını kullanarak ve basit bir kavramsal model geliştirilerek, havza-bazında su dengesinin mekânsal ve zamansal dağılımı hesaplandı ve doğrulandı. Su dengesi mekânsal dağılımı sonuçlarına göre, sulu tarım arazi örtüsüne sahip alanlarda yağışa ilave ortalama sulama miktarı $308 \pm 132$ mm $y^{-1}$ (maksimum olarak 500 mm $y^{-1}$ ye kadar) olarak belirlenmiş olup, söz konusu sulama %80 oranında yeraltı suyundan ve %20 yüzey suyundan gerçekleşmiştir. Konya havzasındaki toplam tarım arazileri (sulu, karışık ve kuru tarım arazileri dahil olmak üzere) dikkate alındığında, 2005-2009 dönemi boyunca hesaplanan su kullanımı dağılımı yeraltı suyu kaynaklarında hacimsel olarak -4,700 MCM $yıl^{-1}$ miktarında bir azalmaya karşılık gelmektedir. Tarım alanlarının yanı sıra en büyük $P - ET$ farkı sulak alanlarda(ort. $-422 \pm 209$ mm $y^{-1}$) ve sucul ortamlarda (ort. $-495 \pm 76$ mm $y^{-1}$) gözlenmiş olup, söz konusu alanlarda buharlaşmanın yağıştan çok daha fazla olması bu alanlara büyük miktarda yeraltı suyu ve/ ya da yüzey suyu deşarjları olduğunu göstermektedir. Söz konusu su dengesi hesabının doğruluk derecesini test etmek amacıyla, RS yöntemleri temel alınarak hesaplanan su bütçesinin havza içindeki dağılımı Devlet Su İşleri (DSİ) Genel Müdürlüğü tarafından ölçümleri gerçekleştirilen yeraltı suyu seviyesi değişimleri ile 5 farklı kuyu noktasında kıyaslanmış olup, RS-tabanlı su bütçesinden hesaplanan yeraltı suyu değişimi ile kuyu ölçümleri büyük oranda örtüşmüştür.

Bölüm 5'te ise, bölgede 2000-2010 yılları arasında hidrolojik ve ekolojik değişkenlerde gözlenen trendlerin konumsal-zamansal dağılımı ve bu değişkenler arasındaki ilişkiler RS-tabanlı entegre bir yöntem uygulanarak incelenmiştir. Buharlaşma (ET) ve yeşillik derecesini gösteren vejetasyon indeksi (NDVI – Normalized Difference Vegetation Index) değişkenlerindeki trendlere göre, tarım arazileri için bu değişkenlerde istatistiksel olarak önemli derecede ($p<0.1$) bir artış trendi (toplam olarak yaklaşık 63 MCM $yıl^{-1}$ $ET$ artışı, ve yeşillik derecesinde ise ortalama 0.004 $NDVI$ $yıl^{-1}$ oranında bir artış) gözlenirken, sulak alanlar için ise aynı değişkenlerde önemli derecede ($p<0.1$) bir azalış trendi (toplam olarak yaklaşık 2.1 MCM $yıl^{-1}$ $ET$ azalışı, ve yeşillik derecesinde ise ortalama 0.001 $NDVI$ $yıl^{-1}$ oranında bir azalış) tespit

edilmiştir. Dahası, söz konusu trendlerin iklim ile bağlantılı yağış (P) ve potansiyel buharlaşma (PET) değişkenlerindeki trendler ile karşılaştırılması sonucunda, eko-hidrolojik değişkenler için (ET ve NDVI) havzada gözlenen trendlerin, iklim değişkenlerindeki (P ve PET) değişimler ile bağlantılı olmadığı, toplam buharlaşma artış trendinin yalnızca %16'sının PET değişkenindeki artış ile açıklanabileceği ortaya konulmuştur. Bu sonuçlar ışığında ortaya çıkan resim, özellikle Konya ovasında vejetasyonun yeşillenme trendinin genel olarak arazi örtüsündeki değişiklikler (ör. arazilerin sulu tarım sahalarına dönüştürülmesi) ve sulamanın yoğunlaşması sonucunda gerçekleştiğini, ve buna bağlı olarak gerçekleşen yeraltı suyu seviyesindeki düşmenin ise sulak alanlar ve doğal vejetasyonda gözlenen kuruma trendine yol açtığını önermektedir.

Son bölümde ise (Bölüm 6), bir havzadaki sürdürülebilir su veriminin toplam verimden ekosistemlerin ihtiyacı olan su miktarının çıkarılmasından sonra geriye kalan kısım olduğu prensibi dikkate alınarak, Konya havzasındaki sürdürülebilir su kaynaklarının limiti ve değişimleri incelenmiştir. 2000-2010 yılları arasında P – ET dengesindeki yıllık dağılımlara göre, Konya havzasında ortalama toplam su verimi 1,385 MCM $y^{-1}$, ortalama toplam ekolojik su ihtiyacı (sulak alanlara ve sucul ortamlara su deşarjları) 1,310 MCM $y^{-1}$ olarak hesaplanmış olup, bu değerlere göre yıllık ortalama sürdürülebilir su verimi ise sadece 75 MCM $y^{-1}$ mertebesinde olmaktadır. Buna karşın, özellikle yağış girdisinde gözlenen yıllar arasındaki büyük değişimlerden dolayı, sürdürülebilir su verimi de yıllar arasında büyük değişim göstermiştir (yağışlı 2009'da 4,000 MCM $y^{-1}$'a ulaşırken, kurak 2008'de -1,200 MCM $y^{-1}$ ile "0" altına düşmüştür). Diğer taraftan, sürdürülebilirlik ile ilgili değerlendirmelerin bilimsel bir problem olduğu kadar bir yönetim konusu olduğu dikkate alındığında, bu tür değerlendirmelerin devamlı gözlem, analiz, önceliklendirme ve revizyon gerektiren dinamik ve iteratif bir süreç olarak anlaşılması gerekir. Yeraltı suyu rezervlerinin tükenmesi problemi ile mücadele etmek için geliştirilen su yönetim stratejileri iki ana grupta toplanabilir: yeraltı suyu çekimlerini azaltmayı hedefleyen "talep-odaklı stratejiler" ve genel olarak su teminini arttırmayı hedefleyen "arz-temin odaklı stratejiler". "Arz-temin stratejisi" olarak Amerika Birleşik Devletleri'nde Merkezi Vadi bölgesinde, ya da daha büyük ölçeklerde Çin'de gerçekleştirilen zorlu bir çözüm yöntemi ise havzalar arası büyük ölçekli su transferi projeleridir. Benzer şekilde, Konya havzasına özellikle sulama amaçlı olmak üzere ilave olarak 414 MCM $y^{-1}$ yüzey suyu taşıması planlanan "Mavi

Tünel" projesi 2012 yılında faaliyete geçmiştir (http://www.konya.gov.tr/goster.asp?baslik=Konya%20Ovalar%FD%20Projesi%20(KOP). Ancak, Konya ovasında 2000-2010 yılları arasında tarım arazilerinde ortalama toplam sulama amaçlı su tüketiminin 3,000 MCM $y^{-1}$ mertebesinde gerçekleştiği göz önüne alınırsa, söz konusu proje yıllık toplam sulama suyu tüketiminin ancak %14'ünü karşılayabilecektir.

## Biography

Mustafa Gökmen was born on 19th February 1978 in Ankara, Turkey. He obtained his bachelor degree in Environmental Engineering (2000), and MSc. Degree in Biology (Freshwater Ecology), both at the Middle East Technical University (2003) in Ankara. In 2005, he was awarded Jean Monnet scholarship by European Commission and obtained Master degree in GIS and Remote Sensing for Integrated Catchment and Water Resources Management in Faculty of Geo-Information Science and Earth Observation of the University of Twente (ITC), in the Netherlands. In 2008, he was awarded HUYGENS scholarship by Netherlands Organization for International Cooperation in Higher Education (NUFFIC) to pursue PhD research at ITC Faculty of University of Twente. He has published the results from those MSc and PhD researches in a range of articles in international journals, and presented at various conferences. His main research interests are applying spatial earth observation techniques for water cycle, ecohydrology, drought monitoring and water resources management.

# Author's publications

1. **Gokmen, M.**, Vekerdy, Z., Lubczynski, M. W., Timmermans, J., Batelaan, O., and Verhoef, W., (2013), Assessing groundwater storage changes using RS-based evapotranspiration and precipitation at a large semi-arid basin scale, *Journal of Hydrometeorology*, doi:10.1175/JHM-D-12-0156.1.

2. **Gokmen, M.**, Vekerdy, Z., Verhoef, W. and Batelaan, O., (2013) Satellite based analysis of recent trends in the ecohydrology of a semi-arid region, *Hydrol. Earth Syst. Sci. Discuss.*, 10, 6193-6235.

3. **Gokmen, M.**, Vekerdy, Z., Verhoef, A., Verhoef, W., Batelaan, O., and van der Tol, C., (2012), Integration of soil moisture in SEBS for improving evapotranspiration estimation under water stress conditions, *Remote Sensing of Environment*, 121, 261-274.

4. **Gokmen**, **M.**, van der Tol, C., Vekerdy, Z., Verhoef, W., Batelaan, O., (2012), Towards an improved mapping of evapotranspiration in semi - arid regions. In: *Remote Sensing and Hydrology, Proceedings of the 2010 Symposium* held at Jackson Hole, Wyoming, 27-30 September 2010 / ed. by C.M.U. Neale and M.H. Cosh. Wallingford: IAHS, 2012. ISBN 978-1-907161-27-8. (IAHS Publication 352), 149-153.

5. Timmermans, J., **Gokmen, M.**, Eden, U., Abou Ali, M., Vekerdy, Z., Su, Z., 2012. Drought monitoring over the Horn of Africa using remotely sensed evapotranspiration, soil moisture and vegetation parameters. *EGU General Assembly 2012*, held 22-27 April, 2012 in Vienna, Austria., p.2717.

6. **Gökmen**, M., Win Naing, Z., Vekerdy, Z., Verhoef, W., Batelaan, O., 2011. Remote sensing estimates of evapotranspiration to analyze the groundwater influx and ecological water demand for a groundwater-dependent wetland. *HydroEco 2011 – 3rd Int. Conference*, held 2-5 May, 2011 in Vienna, Austria, p.5318.

7. **Gokmen, M.**, Vekerdy, Z., Verhoef, W., 2009. Water budget of a shallow lake and the eco-hydrological interactions in its semi-arid catchment. *EGU General Assembly 2009*, held 19-24 April, 2009 in Vienna, Austria, Abstract-301.

**8.** **Gökmen**, M., Strobl, R.O., Mannaerts, C.M., (2007), Evaluation of the SWAT Model Setup Process Through A Case Study in Roxo Catchment, Portugal. In: *Proceedings of the 4th International SWAT Conference*, held 4-6 July 2007 in Delft, Netherlands, ed. by Raghavan Srinivasan

**9.** Al-Khaier, F., Mutiga, J.K., Abkar, A.A., Kanwar, R., Dost, R.J.J., Chiluba, M., **Gökmen, M.**, Hunde, M., Ndhlovu, G.Z., Saila, M., Sanga, H.S., Sarr, M. and Parodi, G.N. (2007) EAGLE 2006 : soil moisture field observations over the Cabauw grassland : abstract. Presented at *AgriSAR and EAGLE Campaigns Final Workshop*, 15-16 October 2007, ESA, ESTEC, Noordwijk.

# ITC Dissertation List

http://www.itc.nl/research/phd/phd_graduates.aspx